

**INFLUENCE OF
RARE EARTH METALS ON
THE NUCLEATION AND
PRECIPITATION OF SLAG
INCLUSIONS DURING
SOLIDIFICATION OF
MOLTEN STEEL**

DR. TO DUY CA



NATIONAL METALLURGICAL LABORATORY
(Council of Scientific & Industrial Research)
JAMSHEDPUR - 831 007, BIHAR
INDIA

1999

INTRODUCTION

During the last 50 years many studies on the various aspects of the application of rare earth metals (RE) in the field of metallurgy had been done by metallurgists all over the world. Because of their strong chemical affinity for oxygen and sulphur, REs are considered as suitable deoxidizers and desulphurizers in liquid steel [1-30]. The group of RE comprises the lanthanide elements atomic numbers 57 to 71 as shown in Table 1 [31-35]

Among these elements, La, Ce, Nd and Pr are commercially available in a concentrated form as commercial alloys such as cerium mischmetal (50-55%Ce, 25-30%La, 10-15%Nd, 4-6%Pr) or neodymium metal (70-75%Nd, 15-19%Pr).

In recent years REs have attracted a considerable amount of attention from steelmakers, because of the beneficial effects resulting from their use in steels. First REs can modify the shape of sulphide inclusions and improve the hotworkability of steel [36-38]. Second REs can reduce the degree of undercooling for nucleation, refine the as-cast structure and limit solidification segregation in steels [39-41]. Much research work concerning the thermodynamic and phase equilibria had been reported for the first effect and the mechanism is now well understood [42-45]. There are few reports on the mechanisms of the second effect. Two contradictory mechanisms proposed by different researchers, are given below:

(1) Dissolved RE reduces the surface tension of liquid iron and steel; thus in principle, reduces the solid-liquid interfacial tension and decrease

CONTENTS

Page No.

ACKNOWLEDGMENT

INTRODUCTION.....1

CHAPTER I

THERMODYNAMICS OF NUCLEATION AND PRECIPITATION OF INCLUSIONS IN MOLTEN STEEL

- 1.1. Thermodynamic condition for the formation of non-metallic
inclusions during addition of RE and Al into molten steel,
system Fe-Me-E at 1600°C.....4
- 1.2. Oxygen reaction with liquid steel.....6
- 1.3. Thermodynamics of the system Fe-RE-O.....11
- 1.4. Thermodynamics of the system Fe-RE-S.....17
- 1.5. Thermodynamics of the system Fe-RE-O-S.....20

CHAPTER II

NUCLEATION STUDIES ON RARE EARTH METAL INCLUSION

- 2.1. Initial formation of inclusions.....26

2.2. Kinetics of Nucleation of non-metallic inclusions	
in molten steel	28

CHAPTER III

THEORETICAL CONDITION FOR INCLUSION PRECIPITATION

3.1. Precipitation studies.....	42
3.2. Precipitation condition of inclusions.....	48
3.3. The inclusion precipitation diagram of RE-O-S system	
in liquid iron.....	55
3.4. Prediction of the precipitated inclusion size.....	65
1. Morphology of inclusions	65
2. Inclusion size.....	68

CHAPTER IV

STUDIES ON ELIMINATION OF INCLUSION OF MOLTEN STEEL

4.1. The growth of inclusions.....	73
------------------------------------	----

4.2. Floatation of inclusion.....	78
4.3. Separation of RE inclusions by floatation.....	84

CHAPTER V

EXPERIMENTAL METHODS

5.1. Ingot casting experiments.....	87
5.2. Tammann melted examples.....	89
5.3. Thermal analysis.....	92
5.4. Determination of equilibrium between RE and Sulphur in molten iron.....	99
5.5. Determination of Gibbs energies for formation of RE oxysulphides.....	103
5.6. Measurement on supersaturation activities of oxygen in Fe-Al-RE.....	107
5.7. Measurement on solidification microstructure of ingot treating RE.....	109
5.8. Determination of equilibrium between the RE, oxygen and sulphur in molten steel.....	110

5.9. Phase analysis of sulphides of RE elements in steel..... 113

5.10. Measurement of surface tension.....118

CHAPTER VI

EXPERIMENTAL

INFLUENCE OF RARE EARTH METALS ON NUCLEATION

PRECIPITATION OF INCLUSION IN MOLTEN STEEL

6.1. Experimental procedure..... 123

6.1.1. Ingot casting experiments in induction furnace.....123

6.1.2. A study of superheating and supercooling samples.....126

6.2. Analytical processes.....128

6.3. Results and discussions.....132

6.3.1. Chemical compositions of steel samples.....132

6.3.2. The results of supercooling.....136

6.3.3. The interaction relationship143

6.3.4. Effect of cerium on macrostructure of steel.....154

6.3.5. Effect of rare earth metals on morphology of
inclusions in steel.....158

6.3.6. SEM and EDX analytical results of inclusion in steel.....162

CONCLUSIONS.....192

REFERENCES

APPENDIX

ANNEXES

ACKNOWLEDGMENT

The author wish to thank Dr. R.K. Bhandari, Head of International S&T Affairs Directorate CSIR, Mr. A. Chakraborty, Deputy Adviser ISTAD/CSIR for invitation and providing enabling conditions to author for pursuing Post-Doctoral work in India.

The author gratefully thank Professor P. Ramachandra Rao, Director of National Metallurgical Laboratory Jamshedpur (NML) for his interest, valuable encouragement and support for all time at NML.

The author expresses his gratitude to all the peer groups at NMI for hearty co-operation, more specifically for the helps and support received from Dr. C.S. Sivaramakrishnan, Deputy Director NML and his MTP Division, Mr. G. V.Ram Iyer, Dr. A.K Ray, scientists of melting and casting unit. Special mention must be made of Dr. P.K. Biswas for helping in drafting the manuscript.

The author is grateful to Mr. P.R. Sastry and his staff for more valuable, enthusiastic and effective helps, also to Dr. K.K. Mishra Deputy Director and Head Division, Mr. H.Patnaik, Dr. D.K. Biswas, Dr. N.G. Goswami of IRM Division of NML.

His thanks are also to Dr. S. Srikant of NFP Division, Dr. N. Parida NDT, Mr. S.K. Das and metallography Lab of MTC Division and Scientists of CAP Division of NML for their timely help in author research work.

decrease the activation energy for formation of nuclei to refine the grain structure [46].

Table 1. Rare earth metals and oxides

at. No	metal	melting temperature, (°C)	density (g/cm ³)	metals oxides	melting temperature, (°C)	density (g/cm ³)
58	Cerium	798	6.77	Ce ₂ O ₃	1687	6.86
57	Lanthanum	920	6.17	La ₂ O ₃	2315	6.51
59	Praseodymium	931	6.78	Pr ₂ O ₃	2200	6.88
60	Neodymium	1016	7.00	Nd ₂ O ₃	2272	7.24
61	Promethium	-	-	Pm ₂ O ₃	-	-
62	Samarium	1072	7.54	Sm ₂ O ₃	2325	7.43
63	Europium	826	5.26	Eu ₂ O ₃	2320	7.42
64	Gadolum	1312	7.90	Gd ₂ O ₃	2330	7.41
65	Terbium	1356	8.27	Tb ₂ O ₃	2387	8.77
66	Dysposium	1409	8.54	Dy ₂ O ₃	2340	7.81
67	Holmium	1461	8.80	Ho ₂ O ₃	2390	-
68	Erbium	1522	9.05	Er ₂ O ₃	2400	8.64
69	Thulium	1545	9.33	Tm ₂ O ₃	2341	8.77
70	Ytterbium	825	6.98	Yb ₂ O ₃	2346	9.17
71	Luterium	1652	9.84	Lu ₂ O ₃	2375	9.42

(2) RE oxide inclusions act as effective nucleants to refine the as-cast structure of iron [47].

With RE addition for deoxidizing in steel, some authors [48] have also made theoretical predictions from the available thermodynamic data which qualitatively confirm the observed order of formation for the different inclusions. However, from a theoretical point of view a certain RE content or a RE/S ratio is not a sufficient condition for the precipitation of a RE inclusion. In order to get precipitation an equilibrium composition must be exceeded [49,50] As condition of the same kind exists also for the other RE inclusions, empirical relations of the types discussed above are only meaning ful if the O,S and Al contents are fixed.

The present work aims at establishing mechanism of influence of RE with Al as deoxidizer on nucleation during solidification of molten steel and precipitation of slag inclusions. The aim is also to develop relations between chemical composition and inclusion type, which can be used for steels with arbitrary chemical compositions. Special attention has been paid to the precipitation of different oxide types during solidification, and also to the differences in morphologies between these inclusions. In this work further attention was paid to investigate the predictability of the floatation behaviour of RE inclusions in molten steel.

Special mention must be made of Dr. O. N. Mohanty, Director of R & D of Tata Steel Co. and his R & D colleagues for their input in the author's work, Dr. Subrahmanyam, Head LD-2 Lab for his help in analyzing of research samples.

CHAPTER I.

THERMODYNAMICS OF NUCLEATION AND PRECIPITATION OF INCLUSIONS IN MOLTEN STEEL.

1.1. Thermodynamic condition for the formation of non-metallic inclusions during addition of RE and Al into in molten steel. system Fe-Me-E at 1600°C

Considering the system Fe-Me-E under isothermal and isobaric condition:

$$/Me_xE_y/ = x /Me/ + y/E/ \quad (1)$$

The Gibbs free energy of dissolution of Me into liquid iron is given by the following equation [34,35,50-52].

$$\Delta G = -RT \ln K + RT \ln \frac{a_{Me}^x \cdot a_E^y}{a_{Me_xE_y}} \quad (2)$$

where R...is the gas constant ($8.3143 \text{ J} \cdot \text{K}^{-1} \cdot \text{mol}^{-1}$),

$a_{Me}, a_E, a_{Me_xE_y}$...are activities of metal Me, non-metal E and production reaction (1) Me_xE_y ,

T...is the temperature in °K

For forming only oxides or sulphides $a_{Me_xE_y}$ is equal to one [34,35,50] then ΔG can be calculated as follows:

$$\Delta G = -RT \ln K + RT \ln a_{Me}^x \cdot a_E^y \quad (3)$$

and
$$\Delta G = \Delta G^\circ + RT \ln a_{Me}^x \cdot a_E^y \quad (4)$$

The following equilibrium constant of reaction (1) was obtained at 1600°C

$$\log K = \log \alpha_{Me}^x \cdot \alpha_E^y \quad (5)$$

where $\alpha_{Me}^x = f_{Me}^x \cdot \%Me^x$ and $\alpha_E^y = f_E^y \cdot \%E^y$ (6)

where f_{Me} , f_E are activity coefficients of metals Me and non-metal E added into the system Fe-Me-E when their concentration is calculated in wt%.

$\%E/$...is weight percentage of dissolution metals.

Then equilibrium constant can be obtained as follows [35,53,54]:

$$\log K = \log f_{Me}^x \cdot \%Me^x \cdot f_E^y \cdot \%E^y \quad (7)$$

or $\log K = \log K^+ + x \log f_{Me} + y \log f_E$ (8)

where $K^+ = \%Me^x \cdot \%E^y$ (9)

$$f_{Me} = f_{Me}^{Me} \cdot f_{Me}^E \cdot f_E^E \cdot f_E^{Me} \quad (10)$$

The commonly used simplification is that f_{Me}^{Me} and f_E^E also equals one the can be written:

$$\log K = \log K^+ + x \log f_{Me}^E + y \log f_E^{Me} \quad (11)$$

Using interaction parameters in the system [21,35,53]:

$$\log f_i = e_i^j \cdot \%j/ \quad (12)$$

Then equation (11) is as follows:

$$\log K = \log K^+ + x \{e_{Me}^E \cdot \%E/\} + y \{e_E^{Me} \cdot \%Me/\} \quad (13)$$

where e_{Me}^E , e_E^{Me} are interaction parameters expressing influence of element E on metal Me and influence of metal Me on element E respectively. According to Wagner [21,35,53] can be obtained as the following:

$$e_{Me}^E = \frac{M_{Me}}{M_E} \cdot e_{E}^{Me} \quad (14)$$

where M_{Me} , M_E are molecular weight of element of Me and E.

Using above reaction in equation (13),

$$\log K = \log K^+ + x \left\{ e_{E}^{Me} \cdot \frac{M_{Me}}{M_E} \cdot \%E \right\} + y \left\{ e_{E}^{Me} \cdot \%Me \right\} \quad (15)$$

Finally the general equation of interaction parameter of reaction (1) is:

$$e_{E}^{Me} = \frac{\frac{1}{y} (\log K - \log K^+)}{\%Me + \frac{x}{y} \cdot \frac{M_{Me}}{M_E} \cdot \%E} \quad (16)$$

Now the values of equilibrium constant of reaction (1) can be calculated by following reaction:

$$\log K = \frac{\Delta G}{2.302RT} \quad (17)$$

1.2. Oxygen reaction with liquid steel

In spite of utmost care all steels may contain oxide inclusions of some kind at least in small quantities [31]. Such inclusions are inevitable as a consequence of the physical chemistry of liquid steel. They influence the mechanical properties and machinability of steel depending upon their volume and which essentially dependent upon their size,

shape and distribution. It is therefore important to understand the reasons for their occurrence and estimate the extent to which their influence on the properties of various kinds of steels may be controlled.

The origin of the problem is that elemental oxygen is soluble in liquid iron to the extent of 0.168%wt at the monotectic temperature and above 0.2wt% at usual steel refining temperature. The solubility of oxygen simplifies the refining of steel by selective oxidation of carbon and other elements.

The lanthanide elements form highly stable oxygen compounds preferentially of the Me_2O type [55-60]. The Gibbs free energies of formation of selected lanthanide oxides and their temperature dependence are listed in Table 2 [15,21,58,60,61]. The thermodynamic stability of these oxides slightly increases with increasing atomic number of the elements.

Table 2. Standard free energies of formation of RE oxides[15,21,35,58,60,61].

reaction	$\Delta G = \Delta H - \Delta S.T$ kJ/mol	temperature range °C	$\Delta G_{1600^\circ C}$ kJ/molO ₂
$2La_{(l)} + 3/2O_{2(g)} = La_2O_{3(s)}$	$-1792.369+0.28265T$	920 to 2040	841.977
$2Ce_{(l)} + 3/2O_{2(g)} = Ce_2O_{3(s)}$	$-1776.627+0.27193T$	798 to 1687	844.868
$2Nd_{(l)} + 3/2O_{2(g)} = Nd_2O_{3(s)}$	$-1814.559+0.28952T$	1016 to 2100	848.192
$2Gd_{(l)} + 3/2O_{2(g)} = Gd_2O_{3(s)}$	$-1836.623+0.28973T$	1312 to 2150	862.693
$2Dy_{(l)} + 3/2O_{2(g)} = Dy_2O_{3(s)}$	$-1878.868+0.29014T$	1409 to 2200	890.291
$2Er_{(l)} + 3/2O_{2(g)} = Er_2O_{3(s)}$	$-1913.074+0.29362T$	1522 to 2280	908.749

It should be noted that the absolute Gibbs free energy of formation of La_2O_3 (841 977kJ/molO₂) for instance, is still remarkably higher than that of Al_2O_3 (723629kJ/molO₂). This leads to the conclusion that lanthanide elements could probably exert a stronger deoxidation effect in steel melts than aluminum. The density of the lanthanide oxides which form hexagonal monoclinic or cubic crystal structures also increases with increasing atomic number of the elements (Tab.1). The densities of the oxides La_2O_3 , Ce_2O_3 , Pr_2O_3 and Nd_2O_3 are slightly lower or the same as the density of liquid iron the value of which is 6.96 g/cm³ at 1600°C [21,55]. In sulphur containing steel melts treated with lanthanide elements inclusions of the type $\text{Me}_2\text{O}_2\text{S}$ rather than Me_2O_3 can be detected. The oxysulphides of the lanthanide elements exhibit a high thermochemical stability similar to that of the pure oxides [21,25,62,63].

Some authors [64] have determined nearly stability data about physical properties of RE with oxygen and sulphur (Table 3) [15,21,64]. As the name implies a deoxidizer [65-67] is an element which has the capability of reacting with dissolved oxygen in liquid steel and removing it as an insoluble compound.

A generalized reaction is:



The solubility product for equation (18) [68] must be small enough to enable the removal of O to residual concentration low enough to control as desired. Examples are silicon or aluminum, which ordinarily form

Table3. Physical properties of RE oxides and sulphides [21]

compounds of metaloxide	melt.temperat °C	density kg/m ³	- ΔH° kJ/mol	molecular mass
CeO	2599	7.300	1026	156.13
CeO ₂	1950	-	1089	172.13
Ce ₂ O ₃	1691	6.870	1821	328.26
La ₂ O ₃	2315	6.500	1792	325.84
Nd ₂ O ₃	2271	7.300	1809	336.54
Pr ₂ O ₃	2199	7.067	1842	329.84
Al ₂ O ₃	2030	2.820	1676	101.96
FeO	1420	5.700	268	71.84
CaO	2600	3.400	636	56.08
CeS	2099	5.900	557	172.196
Ce ₂ S ₃	2149	5.200	1453	376.458
LaS	2200	5.660	508	170.986
La ₂ S ₃	2099	5.000	1432	374.038
NdS	2138	6.200	-	176.336
Nd ₂ S ₃	2199	5.400	1093	384.738
Pr ₂ S ₃	1795	6.600	500	378.038
MnS	1530	4.00	205	87.006
FeS	1193	2.600	117	87.840
Ce ₂ O ₂ S	1949	6.000	1339	344.326
La ₂ O ₂ S	1993	5.800	1709	341.906
Nd ₂ O ₂ S	1988	6.300	-	352.606
Pr ₂ O ₂ S	-	6.200	-	345.906

$\text{SiO}_{2(s)}$ or $\text{Al}_2\text{O}_{3(s)}$ respectively. Under some circumstances, the reaction product may include iron oxide or a compound containing more than one reactive element.

Particles of deoxidation products, that fail to float out, become trapped in the steel during solidification, are known as indigenous or endogenous inclusions resulting from the entrapment of refractory materials..., which might have been attained more or less extensively by reaction with the steel before solidification. Large inclusions may also result from reoxidation of the deoxidized steel by air during tapping or teeming.

The fundamental starting point for studying inclusion formation is Gibbs's phase rule [69-73]

$$F = C + 2 - p \quad (19)$$

where F ...is the variability or degrees of freedom of a system comprising

C ...is the number of dependent components

p ...is the number of coexisting phase

A phase diagram is a graphic representation of phase relations in a particular system as observed experimentally and prescribed by the phase rule [74-76].

The simplest example of deoxidation and formation of inclusion is that the reaction product is a pure, stoichiometric oxide, as implied by equation (18).

A ternary Fe-O-A system having two condensed phases (namely liquid metal and solid oxide) has bivariant solidification for a given

temperature and concentration of deoxidizing element. The concentration of dissolved oxygen is predetermined when equilibrium is reached. This consequence of the phase rule is expressed quantitatively by the thermodynamic equilibrium constant K of reaction (18):

$$K = \frac{a_{Me_x} \cdot a_{O_y}}{a_{Me_xO_y}} \quad (20)$$

where: a_{Me} and a_O ...are the activities of the reacting elements

$a_{Me_xO_y}$...is the activity of the formed constituent

On the assumption, that the oxide is of constant composition having an activity of unity, a deoxidation constant or solubility product can be commonly defined as the reciprocal of the above equilibrium constant K

$$K = \{f_{Me} \cdot \%Me/\}^x \cdot \{f_O \cdot \%O/\}^y \quad (21)$$

where: f_{Me} and f_O ...are activity coefficients (defined below);

$\%Me/$, $\%O/$ are weight percentages of metal Me and oxygen O respectively

1.3. Thermodynamics of the system Fe-RE-O

When RE are dissolved in liquid iron the reaction between RE and oxygen take place as follows;



and
$$K_{RE} = \{f_{Re} \cdot \%RE/\}^x \cdot \{f_O \cdot \%O/\}^y \quad (23)$$

The following equilibrium constants of reaction (22) are obtained at 1600°C:

$$\log K = \log \{f_{RE} \cdot \%RE\}^x \cdot \{f_O \cdot \%O\}^y \quad (24)$$

where: f_{RE} , f_O .. are the activity coefficients of RE and O in the system Fe-RE-O, when concentration of dissolution of RE and O in melts is expressed by wt%.

$\%RE\}$ and $\%O\}$.. are the weight percentages dissolution of RE and O.

Then equation (24) can be written as:

$$\log K = \log (f_{RE}^x \cdot \%RE^x \cdot f_O^y \cdot \%O^y) \quad (25)$$

$$\text{or} \quad \log K = \log K^+ + x \log f_{RE} + y \log f_O \quad (26)$$

$$\text{where} \quad K^+ = \%RE^x \cdot \%O^y \quad (27)$$

$$f_{RE} = f_{RE}^{RE} \cdot f_{RE}^O \quad (28)$$

$$f_O = f_O^O \cdot f_O^{RE} \quad (29)$$

The values of f_O^O , f_{RE}^{RE} can be given to equal to one at 1600°C:

$$\log K = \log K^+ + x \log f_{RE}^O + y \log f_O^{RE} \quad (30)$$

Selected data obtained under the suitable condition mentioned above were used to evaluate equilibrium constants and interaction parameters in the system according to equation (12) [21,35,58]:

$$\log K = \log K^+ + x \{e_{RE}^O \cdot \%O\} + y \{e_O^{RE} \cdot \%RE\} \quad (31)$$

where: e_{RE}^O , e_O^{RE} .. are the interaction parameters expressing influence of O on RE and RE on O.

According to Wagner 's equation (14):

$$e_{RE}^O = \frac{M_{RE}}{M_O} \cdot e_{O}^{RE} \quad (32)$$

Combining equation (31) and equation (32) the following equilibrium constants were obtained:

$$\log K = \log K^+ + x\{e_{O}^{RE} \cdot \%O\} + y\{e_{O}^{RE} \cdot \%RE\} \quad (33)$$

Then the interaction parameter was obtained at 1600°C as follows:

$$e_{O}^{RE} = \frac{\frac{1}{y}(\log K - \log K^+)}{\%RE + \frac{x}{y} \cdot \frac{M_{RE}}{M_O} \cdot \%O} \quad (34)$$

where : M_{RE} and M_O are molecular weight of elements RE and O in the system Fe-RE-O. and the values of $\log K$ can be calculated using equation (17) as follows:

$$\log K = \frac{-\Delta G^\circ}{2.302RT} \quad (35)$$

In the system Fe-RE-O, most of the lanthanide elements form only one stable oxide, the sesquioxide of type RE_2O_3 . But cerium is able to exist as Ce_2O_3 or CeO_2 . $Ce_2O_3 - CeO_2$ [77,78] seems to be stable at higher oxygen activities [21] potential representing the coexistence of Ce_2O_3 and CeO_2 .

The values of standard free energy of formation of RE_2O_3 are given in Table 4.

Table 4. Standard free energy of formation of RE₂O₃, REO₂ and CaO, Al₂O₃, MnO[11, 21]

reaction	temperat. range to	$\Delta G^\circ = \Delta H - \Delta ST$ - ΔH , (kJ/mol)	ΔS° - ΔS , (kJ/Kmol)
2Ce + 3O = /Ce ₂ O ₃ /	1960	1437.432	0.41068
2La + 3O = /La ₂ O ₃ /	2600	1398.078	0.40489
Ce + 2O = /CeO ₂ /	2873	841.004	0.26058
Ca + O = /CaO/	2860	648.682	0.14596
2Al + 3O = /Al ₂ O ₃ /	2303	1207.036	0.39125
Mn + O = /MnO/	2058	293.729	0.12012

The Table 4 shows that the stability of the oxides in molten steel follows the sequence: Ce₂O₃ > La₂O₃ > Al₂O₃ > CeO₂ > CeO > MnO. On addition of RE to a melt containing dissolved oxygen the following reaction is mainly obtained:



The equilibrium constants obtained for the deoxidation with cerium and lanthanum (Table 5) by this experimental method appear to be extremely low:

Apart from the experimental determination, several authors [21,41,79,83,86-90] have tried to evaluate the equilibrium constant for the deoxidation reaction (24) using the Gibbs free energies as follows:



The values of the equilibrium constants obtained for the solubility product according to equation (24) is generally lower than those determined by experimental methods (Table 5) but the variations among the individual results are still important because of the uncertainty of the thermochemical data. For ΔG° of reaction (37) the Gibbs free energy of formation of Ce_2O_3 or La_2O_3 the data proposed by K.A. Gschneidner et al [91] seem to be reliable and for ΔG° of reaction (39) the established [91] and the determined [50] data are in satisfactory agreement at least at 1600°C. But there are no experimentally determined data for ΔG° of reaction (38) the Gibbs free energy of liquid iron and so there is no accurate evaluation of ΔG° of reaction (38) [92,93].

Table 5: Equilibrium of the reaction (36) in pure liquid iron

$\log\%Ce^2/a_{O^3}$	$l\%Ce^2.a^3_{O}$ at 1600°C	wt% of Ce	procedure	crucible & atmosph. [ref.]
-	10^{-4}	-	thermodynamic calculation	[15]
-	$2.5 \cdot 10^{-11*}$	0.009 to 0.048	chemical analysis of samples	Al_2O_3 vac uum[21]
-	$1.8 \cdot 10^{-9*}$	0.015 to 0.45	chemical analysis of samples	CaO/Ar [4]
-	1.0^{-14*}	>0.003	chemical analysis of samples	CaO/Ar [68]

Tab.5(cont.) -81100/T+20.20	$7.96 \cdot 10^{-24}$	-	thermodynamic calculation	[79]
-76000/T+24.00	$2.65 \cdot 10^{-20}$	-	Ce + Al ₂ O ₃ reaction	[80]
-68500/T+1.60	$1.07 \cdot 10^{-17}$	<0.25	EMF/thoria electrolyte/	Al ₂ O ₃ /Ar [81]
-	$4.05 \cdot 10^{-15}$ at 1650°C	<0.001	H ₂ O.H ₂ equilibrium	CaO [82]
-74712/T+18.80	$8.11 \cdot 10^{-22}$	-	thermodynamic calculation	[41]
-	$0.4-4.0 \cdot 10^{-}$	<0.20	chemical analysis of samples	MgO/vac uum[21]
$\log/La^2 \cdot a^3_o$	$/La^2 \cdot a^3_o$ at 1600°C	wt% of La	procedure	crucible material & atmosphere /ref]
-	$4 \cdot 10^{-2}$	-	thermodynamic calculation	[83]
-	$6 \cdot 10^{-9*}$	0.004 to 0.09	chemical analysis of samples	Al ₂ O ₃ va cuum[84]
-	$6 \cdot 10^{-10*}$	0.06 to 1.0	chemical analysis of samples	CaO/Ar [4]
-	$2.5 \cdot 10^{-13*}$	<0.7	chemical analysis of samples	ZrO ₂ ,He ThO ₂ [85]
-77300/T+20.79	$3.30 \cdot 10^{-21}$	-	thermodynamic calculation	[79]

Tab.5(cont.) -62050/T+14.10	$9.35 \cdot 10^{-20}$	-	La-Al ₂ O ₃ reaction	[80]
-	10^{-18}	-	thermodynamic calculation	[84]
-	10^{-19}	<0.04	combination	[86]
-75380/T+17.60	$2.24 \cdot 10^{-23}$		thermodynamic calculation	[41]
-	$0.4-4.0 \cdot 10^{-}$	<0.02	chemical analysis of samples	MgO, vacuum,[21]

1.4. Thermodynamics of system Fe-RE-S

The reaction between RE and sulphur is the following :



The equilibrium constant of reaction (41) can be expressed as follows [94-96]

$$K = \alpha_{\text{RE}}^x \cdot \alpha_{\text{S}}^y \text{ and } K^+ = \% \text{RE}^x \cdot \% \text{S}^y \quad (42)$$

The values obtained for the solubility product according to equation (41) are shown in Tables 6 and 7. These Tables have shown that the value of the free energy of formation of sulphides are in the following increasing

order CaS, CeS, LaS, La₂S₃, and Ca₂S₃. The sulphides Al₂O₃ and MnS not form.

Table 6. Standard free energies of formation of RE sulphides

reaction	- ΔH (kJ/mol)	- ΔS (kJ/°K.mol)	temperature range to (°K)
Ce + S = /CeS/	383.150	0.11145	2723
2Ce - 3S = /Ce ₂ S ₃ /	774.558	0.36194	2723
La - S = /LaS/	343.577	0.12049	2473
2La - 3S = /La ₂ S ₃ /	794.603	0.36110	2473
2Al - 3S = /Al ₂ S ₃ /	386.777	0.29616	2600

The equilibrium constant for the reaction (41) is given by:

$$\log K = \log \alpha_{RE}^x \cdot \alpha_S^y \quad (43)$$

and $\log K = \log K^+ + x \log f_{RE} + y \log f_S \quad (44)$

Using equation (14) in equation (44):

$$\log K = \log K^+ + x \left\{ e^{RE}_S \cdot \frac{M_{RE}}{M_S} \cdot \%S \right\} + y \left\{ e^{RE}_S \cdot \%RE \right\} \quad (45)$$

For the reaction /CeS/ = /Ce/ + /S/:

$$\log K = \log K^+ + e^{Ce}_S \cdot \%Ce + 4.37 \%S \quad (46)$$

and for the reaction /LaS/ = /La/ + /S/ :

$$\log K = \log K^+ + e^{La}_S \cdot \%La + 4.34 \%S \quad (47)$$

S interaction parameters for formations of CeS and LaS are obtained from the following:

$$e^{Ce}_S = \frac{\log K - \log K^+}{\%Ce / +4.37.\%S} \quad (48)$$

and

$$e^{La}_S = \frac{\log K - \log K^+}{\%La / +4.34.\%S} \quad (49)$$

So important reactions which are formed in the system Fe-RE-S are the following:



and

$$e^{RE}_S = \frac{\log K - \log K^+}{3 / \%RE / + 2 \frac{M_{RE}}{M_S} . \%S /} \quad (51)$$

where $\log K = \frac{-\Delta G^\circ}{2.203RT}$

The formation of sulphide inclusions depends mostly on temperature and the RE/S ratio [21,54,86,103,104,109-115]. At temperature range 1600 - 1650°C the occurrence of the reaction between sulphur and RE is very difficult. When RE/S ratio is less than 3, the sulphide (REMn)S will be formed. If RE/S ratio is greater than 3, it can't be formed.

1.5. Thermodynamics of system Fe-RE-O-S

The products of the reaction between RE, oxygen and sulphur were usually the complex oxysulphides. On addition of RE into a melt, containing dissolved oxygen and sulphur, the following reaction may occur:



The equilibrium constant of reaction (52) is given by:

$$K_{OS} = \alpha_{RE}^2 \cdot \alpha_O^2 \cdot a_S \quad (53)$$

and
$$K_{OS} = \%RE^2 \cdot \%O^2 \cdot \%S/ \quad (54)$$

The values of free energy of formation of oxysulphides RE_2O_2S are shown in Table 8 [21,115].

Table 7. Equilibrium of the reactions forming RE sulphides

equilibrium constants K^+ (1)	equilibrium constants K (2)	interaction parameter e_s^{RE} (3)	procedure (4)	author, year (5)
/CeS/=/Ce/+/S/				
$1.5 \cdot 10^{-3}$	-	-	CeS, MgO, Ar	Langenberg, 1957, [97]
$8.9 \cdot 10^{-4}$	-	-	MgO, vacuum	Langenberg, 1957, [97]
$1.0 \cdot 10^{-3}$	-	-	MgO, vacuum	Singleton 1959, [98]
$2.0 \cdot 10^{-3}$	-	-	thermodynamic calculation	Narita 1964, [99]
$4.0 \cdot 10^{-4}$	-	-	MgO, air	Du 1962, [100]
$2.5 \cdot 10^{-4}$	-	-	MgO, vacuum	Kusakwa 1965, [101]
$1.0 \cdot 10^{-3}$	-	-	MgO, Ar	Buzek 1965, [86]
$1.9 \cdot 10^{-4}$	-	1.9	CaO, vacuum	Fischer 1973, [4]



Tab.7con. (1)	(2)	(3)	(4)	(5)
$3.0 \cdot 10^{-4}$	-	-	MgO, vacuum	Din 1975, [100]
$1.7 \cdot 10^{-4}$	-	-	CaO, vacuum	Schurmann 1976, [13]
-	$3.2 \cdot 10^{-6}$	-	thermodynamic calculation	Vahed 1976, [41]
-	-	9.1	thermodynamic calculation	Sabongi 1979, [104]
-	$1.9 \cdot 10^{-5}$	-	Al ₂ O ₃ , Ar	Wang 1980, [105]
-	$2.8 \cdot 10^{-6}$	1.88	MgO, Ar	QiuyongHain 1985, [100]
-	$2.47 \cdot 10^{-5}$	-	thermodynamic calculation	Suzuki 1974, [14]
-	$1.23 \cdot 10^{-5}$	-	thermodynamic calculation	Suzuki 1974, [14]
-	$4.0 \cdot 10^{-4}$	-	thermodynamic calculation	Hitchon 1963, [100]
/LaS/= /La+/S/				
$3.0 \cdot 10^{-4}$	-	-	MgO, Ar	Du 1962, [100]
$159 \cdot 10^{-4}$	-	-	CaO, vacuum	Fischer, [4]
-	-	19	thermodynamic calculation	Sabongi 1979, [104]

Tab.7con. (1)	(2)	(3)	(4)	(5)
$1.0 \cdot 10^{-3}$	-	20	thermodynamic calculation	Buzek 1974, [86]
-	$4.0 \cdot 10^{-6}$	18	$\text{Al}_2\text{O}_3, \text{CeS}, \text{Ar}$	Ejima 1975, [103]
-	$7.4 \cdot 10^{-7}$	1.51	MgO, Ar	QiuyongHan 1985, [100]
-	$2.5 \cdot 10^{-4}$	-	thermodynamic calculation	Prosvirin 1986, [106]
$\text{/Ce}_2\text{S}_3/ =$ $2\text{/Ce/} + 3\text{/S/}$				
$1.41 \cdot 10^{-8}$	$4.91 \cdot 10^{-11}$	-	MgO, Ar	QiuyongHan 1988, [107]
$1.5 \cdot 10^{-9}$	-	-	Thermodynamic calculation	Prosvirin MgOAr [106]
$\text{/RE}_2\text{S}_3/ =$	$2\text{/RE/} +$	3/S/		
$6.3 \cdot 10^{-5}$	$1.0 \cdot 10^{-5}$	4.28-11	MgO, Ar	ToDuy Ca 1994, [108]

The Table 8 shows that there is greatest possibility of formation of $\text{Ce}_2\text{O}_2\text{S}$ then coming $\text{Y}_2\text{O}_2\text{S}$ and $\text{La}_2\text{O}_2\text{S}$. Under certain conditions of melts simultaneous equilibrium with both oxide and oxysulphide phases may exist. In this case the reaction of interest is obtained by combining reactions (37) and (52) i.e.:



The equilibrium constant for the above reaction can be expressed as:

$$K_{O}^{OS} = \frac{K_{os}}{K_o} = \frac{/S/}{/O/} \quad (56)$$

Table 8. Free energy of formation RE oxysulphides /21,115/

reaction	temperature range to (°K)	$\Delta G = \Delta H - \Delta S.T$ - ΔH (kJ/mol)	$\Delta S.T$ - ΔS (kJ/mol°K)
$2Ce + 2O + S = /Ce_2O_2S/$	2080	1339.114	0.37199
$2Y + 2O + S = /Y_2O_2S/$	2320	1250.928	0.35550
$2La + 2O + S = /La_2O_2S/$ *in pure state	logK= -10217/T-12.7	195.560	0.24480

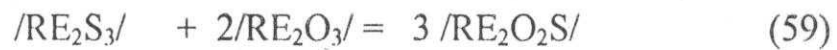
and by combining reactions (50) and (52):



The equilibrium constant for above reaction can be expressed as:

$$K_{OS}^S = \frac{K_s}{K_{os}} = \frac{/S|^2}{/O|^2} \quad (58)$$

It is known that RE oxysulphides can be formed by combination of reactions (55) and (57) as follows:



The equilibrium constant for reaction (59) can be expressed by equation:

$$K = \frac{K_{os}^2}{K^3} K_s \quad (60)$$

The addition of RE to molten steel containing oxygen and sulphur results in the formation of oxysulphides rather than oxides and sulphides [21, 116-120]. According to Wilson when oxygen activity is low, chances of formation of RE_2O_3 , are remote but RE_2O_2S is readily formed and in this case RE sulphide will be formed enveloping RE oxysulphides.

CHAPTER II

NUCLEATION STUDIES ON RARE EARTH METAL INCLUSIONS

2.1 Initial formation of inclusions

Plockinger and Wahlster [70], Samarin [121] and others [122,123] observed that aluminium inclusions separate more rapidly than silicates in apparent violation of Stokes law, and so the agitation or stirring of the steel generally favours the elimination of inclusions. The kinetics and fluid dynamics of deoxidation have been studied intensively [124] as highlighted by recent summary and review papers[125-128]

The sequence of events in inclusion formation and separation is generally described as follows [124,125,127,129,130]

1. Dissolution and mixing of the deoxidizer into the melt
2. Nucleation and precipitation of the inclusion phase
3. Growth of the nuclei on inclusions of an initial size distribution
4. Floation of the slag inclusions with concurrent growth by collision or other mechanisms
5. Assimilation of the inclusions at the metal surface or by slag or container walls

It is convenient to discuss the first three steps under the general heading "formation" and the last two as elimination of inclusion".

Inclusions originate from liquid steel by the well known processes of nucleation and growth [124-131]. It is difficult to apply classical nucleation theory [132,133] quantitatively to explain deoxidation phenomena for several reasons. Initial condition involves macroscopic fluctuations in composition and temperature that depend upon the manner in which the deoxidisers are mixed with the steel and are not amenable to exact description as duplication. The degree of supersaturation necessary for nucleation to occur at a finite rate is strongly sensitive to the interfacial free energy between the liquid steel and the inclusion phase such value are not known and can only be estimated. Because of the strong influence of interfacial tension, the phase that nucleates is not necessarily the stable equilibrium phase.

Substrates for heterogeneous nucleation may normally be abundant from oxide films or inclusions carried in by deoxidizing additions. However, homogeneous nucleation may occur in regions of high supersaturation formed during solution and mixing of the deoxidizer.

Nuclei thus homogeneously formed may subsequently be carried by convection into region of sufficient supersaturating for nucleation which is capable of contributing to growth.

In the first sequence of studies on homogeneous nucleation of oxide phases from liquid steel, Turpin and Elliott [134] calculated the necessary critical supersaturations and from estimated interfacial tensions and experimental observations deduced the conditions for nucleation of Al_2O_3 ,

hercynite, or iron aluminate in the Fe - Al - O system. Deoxidation by solid aluminium addition does not lower the dissolved oxygen content of liquid steel as rapidly as in the case of deoxidization by silicon. The size of the alumina inclusions as measured by quantimet, is closely distributed about a peak of 3-4 μm and the particles do not coarsen appreciably with time, as do silicate inclusions [135-137]. Gatellier and Olette [126] explained the slower reaction of solid aluminium by the entrapment of part of the deoxidant in a surface layer made viscous by small alumina particles and its slow release by diffusion into the bulk, or stabilizing films might form during mixing [137,138]. On the other hand, Schenck et.al [139] observed that the precipitation of Al_2O_3 was slower than calculated for control by diffusion and they attributed this to poisoning of the alumina surface. However, the initial rate of deoxidation depends on how the deoxidizer and instead of solid aluminium by RE is used [140]. Sigworth and Elliot suggested that the faster reaction is the result of the greatest density of nuclei obtained with the more rapid mixing with RE addition [132].

2.2. Kinetics of Nucleation of non-metallic inclusions in molten steels

There are several theories available for explaining nucleation phenomena. That developed by Cahn and Hilliard [141] is designed to treat the formation of nucleus of variable composition. However, the simpler classical theory [142-145] is more suitable for use here, primarily because there is no sufficient detailed information on the system to support

the newer treatment. In the classical theory, the work to form a spherical nucleus is:

$$w = 4\pi r^2 \sigma + \frac{3}{4} \pi r^3 \cdot \frac{\Delta G}{v} \quad (61)$$

where: σ ..is the interfacial tension between the matrix and new phase,

r .. is the particle radius.

ΔG .. is the difference in Gibbs free energy between the matrix and the new phase.

v ..is the molar volume of new phase.

In the process being analyzed the nucleus forms in a liquid matrix, solidification the problem of free energy is avoided. The critical radius r^* is the radius of the smallest cluster of molecule of new phase which will grow spontaneously:

$$r^* = -\frac{2\sigma v}{\Delta G} \quad (62)$$

The related work w^* to form this nucleus is:

$$w^* = -\frac{16\pi\sigma^3 v^2}{3\Delta G^2} \quad (63)$$

It is to be noted that:

$$\Delta G^* = -\frac{16\pi\sigma^3}{3\Delta G^2} \quad (64)$$

Thus ΔG^*_{hom} is minimum work of activation energy required to form the critical nucleus homogeneously from the melt. Gibbs [134] showed

originally that this is actually the Helmholtz free energy; however, with the process of interest here, the difference between the Gibbs and Helmholtz free energies is negligible, and also it is convenient to calculate the change in the Gibbs free energy directly from the available thermodynamic data. The rate of formation of nuclei in homogeneous nucleation process I_{hom} expressed as number of nuclei per cm^3 per second is given by,

$$I_{hom} = A \cdot \exp. \frac{-\Delta G^*}{KT} \quad (65)$$

where A is the frequency factor (is constant $\sim 10^{27}/cm^3 \cdot s$) which Turnbull and Fischer [145, 146] expressed as:

$$A = A' \cdot \exp. \frac{-\Delta G^a}{KT} \quad (66)$$

where A' is again a frequency factor,

ΔG^a is the free energy of activation for diffusion of atoms or molecules at the metal-nucleus interface

K is the Boltzmann's constant

T is the temperature $^{\circ}K$

Using Turnbull and Fischer [145] treatment and the pertinent data [146] the values of A of equation (65) were estimated from equation (66) for the pertinent oxides. The rate of formation of nuclei I_{hom} varies extremely rapidly with supersaturation, solidification and that for present consideration may be considered to be discontinuous with temperature. Also, the influence of the value of ΔG^* in equation (65) is solidification

dominant and it overwhelms the frequency factor. Accordingly I_{hom} equals to one nuclei per cm^3 of matrix a selection of 1 to 10,000 makes no significant difference in the analysis. The value of supersaturation necessary for homogeneous nucleation when I equals one is designated as $\Delta G_{\text{hom}}^{\text{crit}}$.

In the case of homogeneous nucleation very high energy barrier must be surmounted for nucleation heterogeneous nucleation is more likely to occur because of the high probability of the presence of particles in the melt that can serve as substrate for the formation of new phase. In the case of the formation of a spherical cap on a planar substrate the supersaturation must overcome the critical free energy barrier, ΔG_{het}^* , which Volmer [142] gives as:

$$\Delta G_{\text{het}}^* = \Delta G_{\text{hom}}^* \cdot f(\theta) \quad (67)$$

The contact angle of the nucleus on the substrate is θ , and:

$$\Delta G_{\text{het}}^* = \frac{1}{4} (2 + \cos\theta) \cdot (1 - \cos\theta)^2 \quad (68)$$

and

$$\cos\theta = \frac{\sigma_{\text{LS}} - \sigma_{\text{SC}}}{\sigma_{\text{SL}}} \quad (69)$$

where σ_{LS} is the interfacial tension between molten iron and catalyzer

σ_{SC} is the interfacial tension between solid iron crystal and substrate

σ_{SL} is the interfacial tension between solid iron and liquid iron

The rate of heterogeneous nucleation in a condensed system as given by Turnbull [147] is:

$$I_{het} = B \cdot f(\theta)^{1/6} \cdot \exp. \frac{-\Delta G_{het}^*}{KT} \quad (70)$$

where I_{het} is the number of nuclei per unit of surface

B is a frequency factor

The primary influence of the contact angle is in the exponential term which becomes vanishingly small.

To avoid the complication arising from the effect of a substrate on the nucleation it was attempted in the experimental work to avoid the possibility of heterogeneous nucleation arising from "dirt" in the melt. From equation (65), the critical supersaturation in terms of the free energy for homogeneous nucleation is

$$\Delta G_{hom}^{crit} = -2.7 \cdot v \cdot \left(\frac{\sigma^3}{KT} \cdot \log A \right)^{1/2} \quad (71)$$

A ternary melt, Fe-O-Me at constant temperature and pressure is defined thermodynamically by the concentrations of O and Me. For any given concentration of Me there will be an equilibrium concentration of O for the formation of the most stable oxide, usually Me_xO_y . Another concentration of O results in just sufficient supersaturation (i.e. by equation (71)) to cause nucleation of Me_xO_y and again another one nucleates for $Fe_u Me_v O_w$ and so on. These oxygen concentrations for supersaturation are determined by the thermodynamic properties of the Fe-O-Me solution and the interfacial tension between the melt and the oxide that form. Thus

in a plot of Me and O for this melt, it is possible to draw a curve representing the supersaturation of the melt necessary for nucleation of Me_xO_y relative to that of the equilibrium of the melt with bulk Me_xO_y .

Supersaturation by cooling

The liquid melt being considered above can be brought to a condition of supersaturation by first equilibrating it with pure Me_xO_y at a high temperature T_{eq} and then rapidly cooling it to a lower temperature T . The required temperature difference $T_{\text{eq}} - T$ necessary to achieve supersaturation is generally determined as follows:

$$\Delta G = \Delta G^{\circ} + RT \ln Q \quad (72)$$

The composition required for nucleation of the phase Me_xO_y is given by :

$$\Delta G_{\text{hom}(T)}^{\text{crit}} = \Delta G_T^{\circ} + RT \ln Q_{\text{Me}_x\text{O}_y(T)} \quad (73)$$

Using the appropriate activity coefficients, the temperature at which the equilibrated melt will have compositions dictated by equation (73) is given by:

$$\Delta G_{T_{\text{eq}}} = \Delta G_{T_{\text{eq}}}^{\circ} + RT \ln K_{\text{Me}_x\text{O}_y(T_{\text{eq}})} \quad (74)$$

In the present case it is necessary to assume that the activity coefficients are independent of temperature so equation (73) becomes:

$$\Delta G_{hom(T)}^{crit} = \Delta G_T^o + RT \ln K_{MexOy(T)} \quad (75)$$

It follows directly from $\Delta G_T^o = \Delta H^o - \Delta S^o T$ that

$$\Delta G_{hom(T)}^{crit} = \Delta H^o (T_{eq} - T) \cdot T_{eq} \quad (76)$$

Thus by equation (76) the temperature change necessary to obtain supersaturation sufficient for nucleation of Me_xO_y (without solidification) is determined.

Alternatively, the necessary temperature T_{eq} for equilibration of the melt containing a specified Me with the oxide Me_xO_y , which will achieve a sufficient concentration of oxygen to nucleate the phase $Fe_uMe_vO_w$ can be obtained by the following sequence of calculations: The critical supersaturation necessary to nucleate $Fe_uMe_vO_w$ at temperature T is:

$$\Delta G_{hom(Fe_uMe_vO_w)}^{crit} = \Delta G_{(Fe_uMe_vO_w)}^o - RT \{w \log \%O + w \cdot (e^O_O \cdot \%O + e^{Me}_O \cdot \%Me) + v \log Me + v \cdot (e^{Me}_{Me} \cdot \%Me + e^O_{Me} \cdot \%O)\} \quad (77)$$

The term on the left is obtained by equation (71). Thus for a given concentration of Me, the necessary concentration of O is obtained from equation (77). These two values can then be inserted into equation (72) to obtain ΔG_{MexOy} which in turn is inserted into equation (76) to obtain:

$$\Delta G_{MexOy(T)} = \Delta H^o_{MexOy} \cdot \frac{T_{eq} - T}{T_{eq}} \quad (78)$$

which is then solved for T_{eq} . The required temperature interval of supercooling to obtain supersaturation with regard to the several oxides

after equilibration of the melt with pure Al_2O_3 or with pure SiO_2 crucibles is shown in Fig. 1.

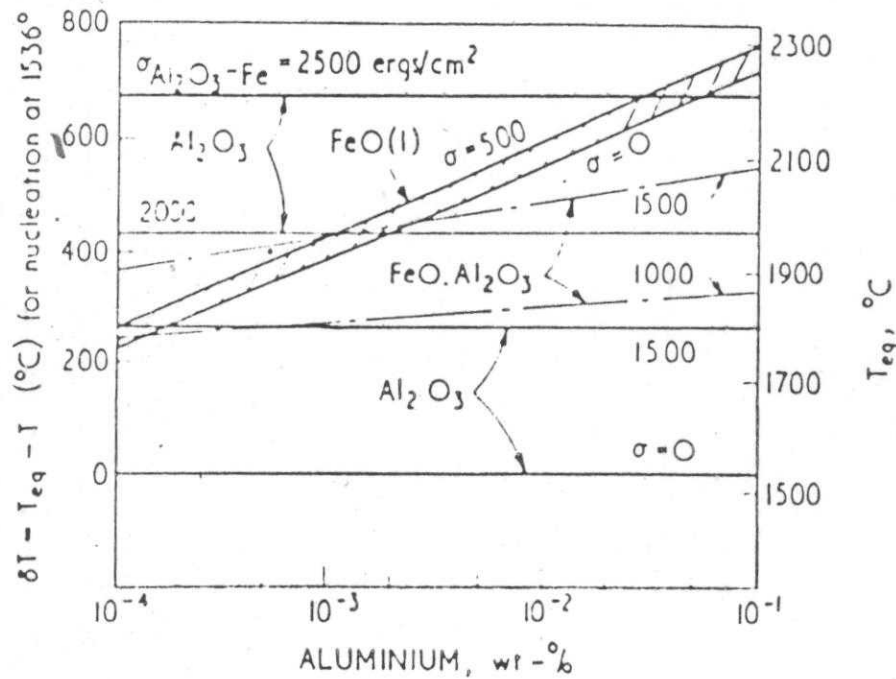


Fig. 1. Effects of supercooling and interfacial tension on possible types of nuclei in Fe-O-Al system; melt is equilibrated with Al_2O_3 at T_{eq} ; $T = 1536^\circ\text{C}$

The diagram predicts homogeneous nucleation of phase with a given interfacial tension if the line for that phase lies on or below the selected point of liquid composition (in equilibrium with Me_xO_y) and temperature.

The extent of supersaturation of the melt with reactants is readily obtained from the driving free energy:

$$\frac{K_s}{K} = e^{\frac{\Delta F}{RT}} \quad (79)$$

where ΔF is driving force

K is the thermodynamic solubility product

K_s is the corresponding product for the supersaturation solution

As the theory predicts, a slight change in supersaturation ratio K_s/K results a change in the frequency of nucleation by several orders of magnitude. Conversely, the value of K_s/K is very insensitive to the choice of a value of I_{hom} . In the following example I is taken to be 10^3 nuclei/cm³.s. The main source of error in the estimation of K_s/K for spontaneous nucleation is the uncertainty in the value of σ for the system under consideration.

Since the activity coefficient of reactants will not change much over this narrow composition range, the following approximation is permissible:

$$\frac{K_s}{K} \cong \frac{K'_s}{K'} \cong \frac{\{\%Me_1.\%Me_2.\%O\}^3_s}{\{\%Me_1.\%Me_2.\%O\}^3_l} \quad (80)$$

where subscripts s and l refer to the supersaturation (initial) and equilibrium states for the example; reaction $Mn+Si+3O = MnSiO_3$, given above $K'_s/K' = 34.2$. Where after deoxidation at 1600°C, O, Mn and Si percentages reduced from 0.05, 0.043 and 0.10 to 0.017, 0.40 and 0.08 respectively. Which is much below the supersaturation required for homogeneous nucleation of the deoxidation product. The dissolution of added deoxidizers in liquid steel takes a finite time during which certain regions of the melt are expected to be very rich in solute concentration in

these region the solution is sufficiently supersaturated locally for homogeneous nucleation of the deoxidation product.

Crystallographic considerations of nucleation potency

The nucleation potency of the oxide particles is defined as the reciprocal of the degree of supercooling. Then the relative magnitude of nucleation potency possessed by various oxides in molten iron should be related to the interfacial energy between these oxides and solid iron. Factors controlling this interfacial energy [148] include chemical properties of nucleating agents [149], topography of the surface from substrate nucleation [150], electrostatic potential between the catalyzer and crystal nucleus [151] and disregistry of crystal lattice between the two phases across the interface [144]. Of these various factors, the first three factors cannot be quantitatively estimated and their exact contribution to the heterogeneous nucleation has not been determined quantitatively. On the contrary, the disregistry of lattices between nucleation catalyzer and solid iron in heterogeneous nucleation was theoretically explained by Turnbull and Vonnegut [144]. Recently, Bramfitt [148] measured the degree of supercooling in liquid iron containing various types of inclusions in vacuum induction furnace and examined the disregistry aspect of six compounds which has effectively contributed to the heterogeneous nucleation of inclusions and developed the following equation which is applicable to substances having different crystal types:

$$\delta_{(hkl)_s, (hkl)_n}^{(hkl)_s} = \sum_{i=1}^3 \frac{\{(d(uvw)'_s \cos \theta_1) - d(uvw)'_i\}}{3 \cdot d(uvw)'_n} \cdot 100 \quad (81)$$

where $(hkl)_s, (hkl)_n$.. a low index plane of catalyzer and crystal

$(uvw)_s, (uvw)_n$... a low index direction of plane $(hkl)_s$, and $(hkl)_n$

$d(uvw)_s$, and $d(uvw)_n$...interatomic spacing along $(uvw)_s$, and $(uvw)_n$

θ_1 .. is angle between $(uvw)_s$, and $(uvw)_n$

Bramfitt calls this equation "planar disregistry" in contrast to the "linear disregistry" of Turnbull and vonnegut. Under consideration of the bonding between ionic oxide and Fe atom by electromagnetic force, cation or vacancy is needed for Fe atom to be absorbed on O atom. From this point of view the analyses for above mentioned bonding as per of planar disregistry theory are considered to be not strictly exact and rather more complicated.

The crystal structure of oxides of RE such as La^{3+} , Ce^{3+} , Pr^{3+} and Nd^{3+} is classified into types of oxides which are mostly spherical and opaque amorphous and spherical and have high reflection [152]. Crystal structure of nucleants of these oxides is shown in Table 9 [153]

Table 9. Crystal structure of nucleants [153]

nucleant	crystal system	lattice parameter (\AA)			linear thermal coefficient of expansion $10^6 \cdot \text{deg}^{-1}$
		a_0	c_0	a_0 (at 1583°C)	
La_2O_3	hexagonal	3.931	6.134	3.938	8.3
Ce_2O_3		3.888	6.062		
Pr_2O_3		3.856	6.008		
Nd_2O_3		3.836	6.000		
Al_2O_3		4.759	12.991	4.814	7.5
SiO_2	- cubic	7.120	-	7.153	3.0
MnO	-	4.445	-	4.520	11.0

Figure 2 shows the results of matching of the low index planes (111) of δ -iron with the plan (0001) of Ce_2O_3 . There is least misfit in the case of matching of the plane (0001) of Ce_2O_3 with the plan (111) of δ -Fe and the value is as small as 5%. The structure of Al_2O_3 to be considered here is of the α - Al_2O_3 type and has a hexagonal close-packed arrangement of oxygen atoms. Aluminum atom is placed in the center of an octahedron surrounded by six oxygen atoms. The lattice constant at ordinary temperature is a_0 equals 4.7589\AA at 15348°C when corrected in consideration of thermal expansion. The crystallographic relationship of Al_2O_3 and δ -Fe is shown in Fig. 3.

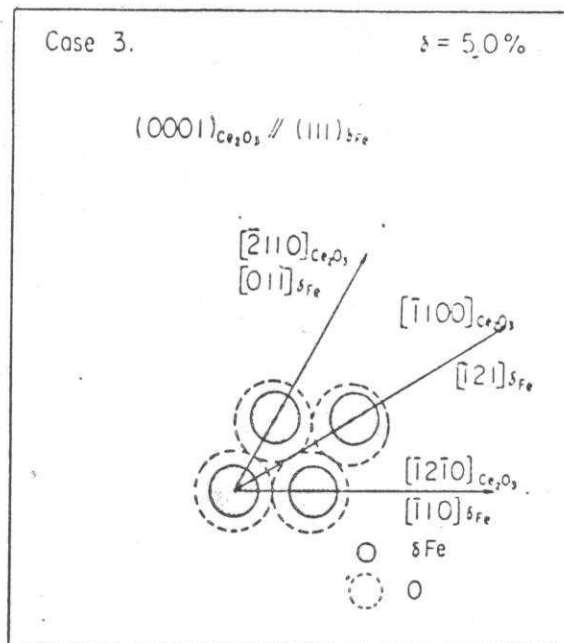


Fig. 2. The crystallographic relationship at the interface between the (0001) of Ce_2O_3 and the (111) of $\delta\text{-Fe}$.

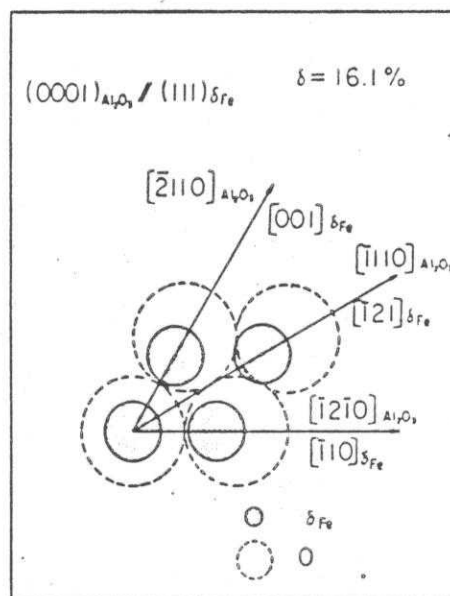


Fig. 3. The crystallographic relationship at the interface between the (0001) of Al_2O_3 and the (111) of $\delta\text{-Fe}$.

It has also been found that critical supercooling temperature can theoretically be explained in terms of "planar disregistry" δ at crystal line interfaces between the non-metallic inclusions and δ -Fe [148].

Fig.3 shows the condition under which the disregistry between CaS, CeS and δ -Fe becomes minimum.

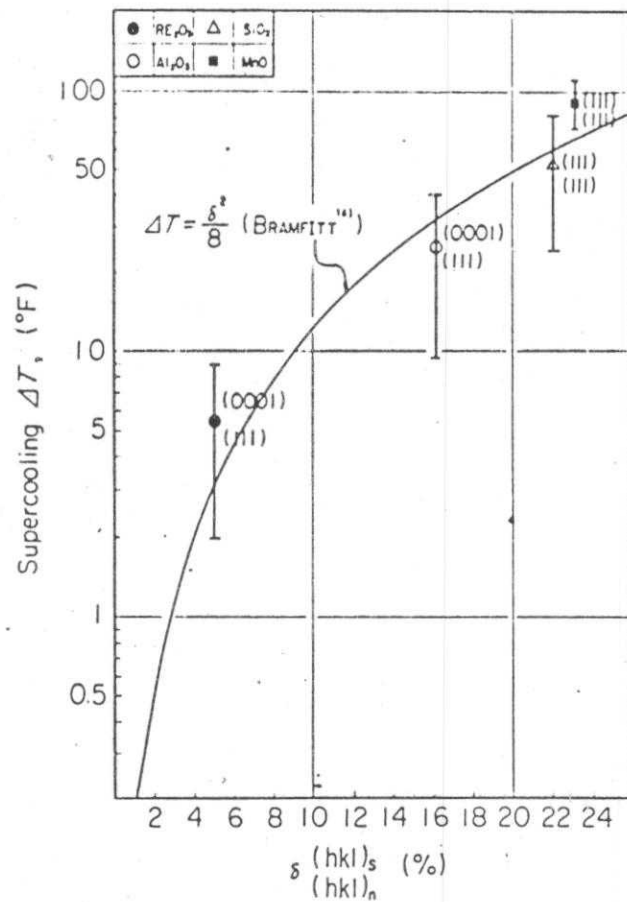


Fig.4. Relationship between the planar disregistry δ and supercooling ΔT of various nucleants

Fig. 4 shows the relationship between the calculated disregistry δ -Fe and critical supercooling temperature which decreases in the order of CaO, Ce_2O_3 , and CeS; this means that the potential of the heterogeneous nucleation increases in this order.

CHAPTER III

THEORETICAL CONDITION FOR INCLUSION PRECIPITATION

3.1. Precipitation studies

At thermodynamic equilibrium the following relation is valid:

$$\frac{a_{Me,E}}{a_{Me}^x \cdot a_E^y} = K = e^{\frac{-\Delta G^0}{RT}} \quad (82)$$

where T is the temperature in °K

R is the gas constant

The activity coefficients are dependent on compositions and thermodynamic interaction parameters for the elements present. In the case of RE, however no reliable thermodynamic interaction parameters are known, therefore it is customary to assume that all activity coefficients are equal to one [154]. Another commonly used simplification is that the activity of the formed constituent, a_{MexE} also equals one [42,49]. With these simplifications relation (82) can be written as:

$$\frac{-\Delta G^0}{RT} = -\log \%Me / ^x - \log \%E / ^y \quad (84)$$

Changing relation (83) to an unaquality, the condition for inclusion precipitation based chemical composition is obtained /49/

$$\frac{\%Me^l}{\%Me^s} = K^o \quad (84)$$

and

$$\frac{\frac{-\Delta G^o}{4.575.T}}{-\log \%Me^l/x - \log \%E^l/y} > 1 \quad (85)$$

where K^o is the temperature dependent equilibrium constant. Conditions of the same kind exist also for the other Me inclusions empirical relations of the type discussed above are only meaningful if the RE, O, and Al contents are fixed in the equation (85) i.e. no inclusions will be formed until the quotient of the left hand side of relation (85) is equal to one.

As was stated above most inclusions are assumed to be formed in the interdendritic regions, where the inclusion forming elements segregate during solidification. Therefore the composition in relation (84) must be interdendritic compositions. Some methods similar were used by Turkdogan [154] and Forward and Elliott [155].

Hence, it is simply assumed that the metal atoms (henceforth designated as Me) segregate according to Scheil's segregation equation [156-162]

Before considering segregation, normal freezing will be reviewed briefly. If a cylinder of molten binary alloy is made to freeze from one end as in Fig. 5. Usually there will be a segregation phenomenon where the solutes will concentrate from one end to the other end of ingot. If the constitutional diagram for the system is like that of Fig.6, the distribution coefficient K , (defined as the ratio of the concentration in the solid to that of the liquid at equilibrium), will be less than one and the solute will be concentrated in the

last zone to freeze. If the solute raises the freezing point, then $^{\circ}K$ will be greater than one and the solute will be concentrated in the first zone to freeze. Let us assume freezing of unit volume of solution. Assume that during the freezing process there is no diffusion

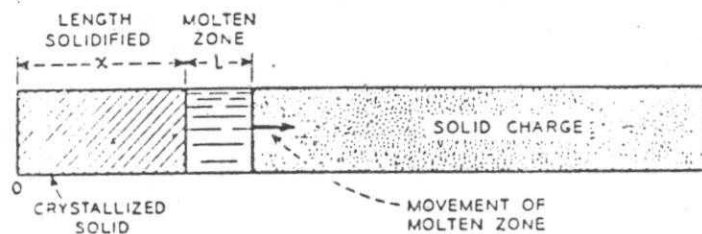


Fig. 5. Solidification by normal freezing (schematic)
 in the solid and complete diffusion in the liquid. Assume also that $^{\circ}K$, the distribution coefficient is constant:

Let: f_s is the fraction of the original volume which has frozen

s is the amount of solute remaining in the liquid

s_0 is the total amount of solute

Me is the solute concentration in the solid at the liquid - solid interface, in units of solute per unit volume of solution. Me^L is the solute concentration in the liquid by definition:

$$Me = K \cdot Me^L \quad (86)$$

since $Me^L = \frac{S}{1-f_s}$ (87)

then $Me = \frac{K \cdot S}{1-f_s}$ (88)

After a fraction f_s has frozen, freeze an additional amount, df_s , the the concentration Me in the frozen layer of volume df_s is:

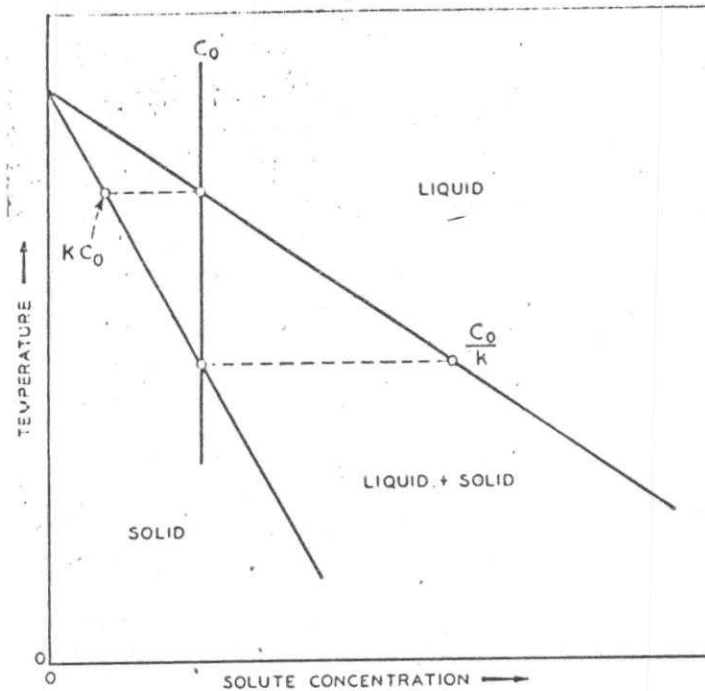


Fig. 6. Portion of constitutional diagram for a solute which lowers the freezing point of the solvent (schematic) [154]

$$Me = - \frac{dS}{df_s} \quad (89)$$

Eliminating Me and intergrating ,

$$\int_{S_0}^S \frac{dS}{S} = \int_0^{f_s} \frac{K}{1-f_s} \cdot df_s \quad (90)$$

from which $S = S_0 \cdot (1 - f_s)^K$

$$\text{and } Me = -\frac{dS}{df_s} = K \cdot S_0 \cdot (1 - f_s)^{K-1} \quad (91)$$

Since the original volume was unity, $S_0 = Me^0$ where Me^0 is the original solute concentration and hence Me^L :

$$Me^L = K \cdot Me^0 \cdot (1 - f_s)^{K-1} \quad (92)$$

This treatment neglects the change of density during freezing and it places no restrictions on the shape of the molten or solid portion during freezing. Here K is equilibrium partition coefficient between solid phase and liquid phase. Equation (92) is based on the following assumptions: i) important assumption in the derivation of Scheil's equation i.e diffusion in the solid phase is negligible. ii) diffusion in the liquid is complete (i.e, concentration in the liquid is uniform). Here $^{\circ}K$ is constant. For elements with high diffusion coefficients such as S and O (those elements, from now on designated E assuming K , the distribution coefficient, and L , the zone length to be constant, the concentration E of the freezing solid at any length Z , measured from the beginning of the ingot as shown in figure 7 and 8, may be found as follows:

Let E_o , the mean concentration of solute in charge be, assumed to be invariant with Z and expressed in units of solute per unit volume of solution.

S , the quantity of solute at any Z

S_o , the quantity of solute at $Z = 0$

Advance the zone by a distance dZ . An incremental volume dZ of solid will form, an equal volume dZ of charge will melt (see figure 7 and 8) the quantity of solute frozen out of it is $K.E_i \cdot dZ$, where E_i is the solute concentration in the molten zone. $E_i = S/L$, assuming unit cross sectional area. The quantity entering the zone is $E_o \cdot dZ$. The next change in S is therefore given by:

$$dS = \left(E_o - \frac{K.S}{L} \right) dZ \quad (93)$$

from which
$$\frac{dS}{dZ} + \frac{K}{L} S = E_o \quad (94)$$

The solution of equation (93) is :

$$S \cdot e^{\frac{K}{L}Z} - S_o = E_o \int_0^Z e^{\frac{K}{L}Z} \cdot dZ = E_o \cdot \frac{L}{K} \cdot (e^{\frac{K}{L}Z} - 1)$$

Since $S_o = E_o \cdot L$ then :

$$S = E_o \cdot L + E_o \cdot \frac{L}{K} (e^{\frac{K}{L}Z} - 1) \cdot e^{\frac{K}{L}Z} = E_o \cdot L \cdot \frac{K-1}{K} \cdot e^{\frac{K}{L}Z} + \frac{E_o}{K} \cdot L$$

while $E^L = \frac{K}{L} \cdot S$ then $E^L = E_o \cdot (K-1) e^{\frac{K}{L}Z} + E_o$

$$\text{or: } E^L = E_o / (1 - K) e^{\frac{K}{L} z} \quad (95)$$

Equation (95) and (92) can now be put into relation (85) giving a precipitation condition which accounts for microsegregation of the inclusion - forming elements:

$$\frac{-\Delta G^o_{Me_xE_y}}{4575.T} > 1 - \log\{M^o_L (1-f_s)^{k-1}\}^x - \log\{E^o (1 - /1 - K/.e^{\frac{k}{L} z})\}^y \quad (96)$$

This implies that the right hand side of the relation (96) must be increased with a factor; $p_{Me_xE_y}$ proportional to the supersaturation needed for nucleation of the Me_xE_y inclusions [163-169]. Therefore the final condition for precipitation of Me_xE_y inclusions based on average chemical composition is:

$$\frac{-\Delta G^o_{Me_xE_y}}{4575.T} > 1 + p_{Me_xE_y} - \log\{M^o_L (1-f_s)^{k-1}\}^x - \log\{E^o (1 - /1 - K/.e^{\frac{k}{L} z})\}^y \quad (97)$$

3.2. Precipitation condition of inclusions

The precipitation of Al_2O_3 can be calculated using the equation (97) as follows:

$$\Delta G^o_{Al_2O_3} = -296.900 + 94.4 T = 1138.696 \text{ cal} \quad (98)$$

$$\text{and } K^{AL} = 0.96 / 159/$$

$$K^0 = 0.05 / 157$$

and so: $p_{\text{Al}_2\text{O}_3} = 1.90$

Using the above values of the constants, relation (97) transforms to:

$$\frac{18.16}{-2 \log\{Al.(1-f_s)^{-0.04}\} - 3 \log\{O.(1 - e^{-\frac{0.05}{L} \cdot Z} + 0.05 \cdot e^{-\frac{0.05}{L} \cdot Z})\}} > 1.9 \quad (99)$$

For $Z/L=2$, equation (99) yields:

$$\frac{18.16}{-2 \log\{Al.(1-f_s)^{-0.04}\} - 3 \log\{O.(1 - e^{0.1} + 0.05 \cdot e^{0.1})\}} > 1.9$$

$$\frac{18.16}{-2 \log\{Al.(1-f_s)^{-0.04}\} - 3 \log\{O.(1 - 0.95 \cdot e^{0.1})\}} > 1.9 \quad (99)$$

i.e precipitation of Al_2O_3 can be expected to occur when the quotient called the "precipitation quotient" is equal to 1.90.

The precipitation of RE inclusions

The first step, is to calculate "precipitation quotients" for different inclusion types in all the steels the inclusion types considered are Al_2O_3 , Ce_2O_3 , Ce_2S_3 , and $\text{Ce}_2\text{O}_2\text{S}$.

The constants needed for the Ce inclusions are [11]

$$\Delta G^\circ_{\text{Ce}_2\text{O}_3, 1673^\circ\text{K}} = -341810 + 86 T = -197932 \text{ cal} \quad (100)$$

$$\text{and } \Delta G^\circ_{\text{Ce}_2\text{S}_3, 1673^\circ\text{K}} = -256660 + 78 T = -126166 \text{ cal} \quad (101)$$

$$\Delta G^\circ_{\text{Ce}_2\text{O}_2\text{S}, 1673^\circ\text{K}} = -323300 + 79.2 T = -190.798 \text{ cal} \quad (102)$$

$$\text{and } K^{\text{Ce}} = 0.36 \text{ [159]}$$

$$K^{\text{S}} = 0.03 \text{ [157]}$$

Which give the following precipitation conditions:

$$\text{for } \text{Ce}_2\text{O}_3; \frac{25.86}{-2 \log\{\text{Ce} \cdot (1-f_{\text{O}})^{-0.64}\} - 3 \log\{\text{O} \cdot (1 - 0.95 \cdot e^{0.1})\}} \rangle p_{\text{Ce}_2\text{O}_3} \quad (103)$$

$$\text{for } \text{Ce}_2\text{S}_3 \frac{16.48}{-2 \log\{\text{Ce} \cdot (1-f_{\text{S}})^{-0.64}\} - 3 \log\{\text{S} \cdot (1 - 0.97 \cdot e^{0.06})\}} \rangle p_{\text{Ce}_2\text{S}_3} \quad (104)$$

and for Ce_2O_2S :

$$\frac{24.93}{-2 \log\{Ce(1-f_s)^{-0.64}\} - 2 \log\{O(1-0.95e^{0.1})\} - \log\{S(1-0.97e^{0.06})\}} \rangle p_{Ce_2O_2S} \quad (105)$$

Comparing the 'precipitation quotients' of previous works for different inclusion types in the steel with Al_2O_3 inclusions, it was found that the quotients for Ce_2O_3 , Ce_2S_3 , and Ce_2O_2S varied between 2.3 and 2.6 when the Al_2O_3 quotient was equal to 1.90. This means that $p_{Ce_2O_3}$ and $p_{Ce_2O_2S}$ should be larger than 2.3 - 2.6 otherwise the Al_2O_3 in steels should have RE inclusions.

The general calculated fractions solid phase at the time for precipitation of Al_2O_3 , Ce_2O_3 , Ce_2S_3 , and Ce_2O_2S are given in Fig. 9, which illustrates how the "precipitation quotients" change during solidification

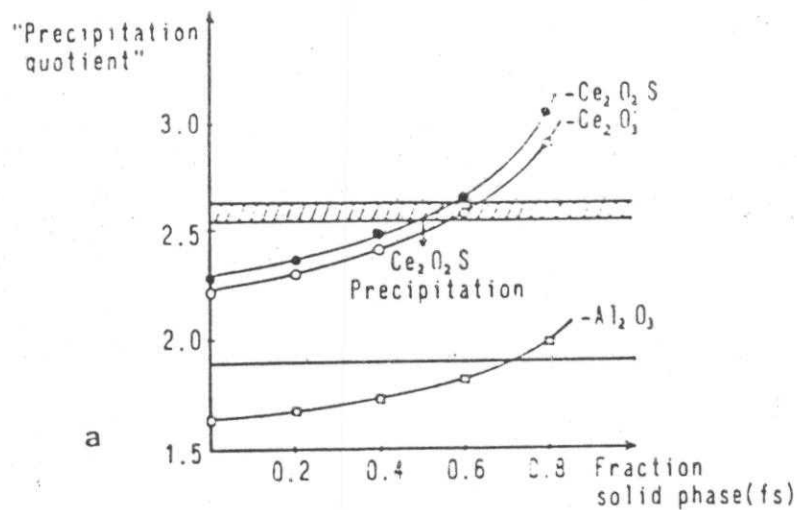


Fig. 9. "precipitation quotients" vs. fraction solid phase.

Since the calculation of the "precipitation quotients" is rather tedious it was considered quite urgent to construct some kind of RE inclusion diagrams, from which it should be possible to read the predicted inclusion types directly. Combining relation (92) and (95) and using the average f_s value ($\cong 0.49$); $p_{Al_2O_3} = 1.90$, $p_{Ce_2O_3}$, and $p_{Ce_2O_2S} =$ from 2.3 to 2.6, the following relationship was obtained:

$$(1.58 Ce)^2 = \frac{(1.03 Al)^{2.05} \cdot (1.87 O)^{1.07}}{(1.91 S)} \quad (106)$$

If the average O and S contents are known equation (106) can be used to construct RE inclusion diagram. Figure 10 shows such a diagram for O-content = 0.0045% and S-content = 0.0097%.

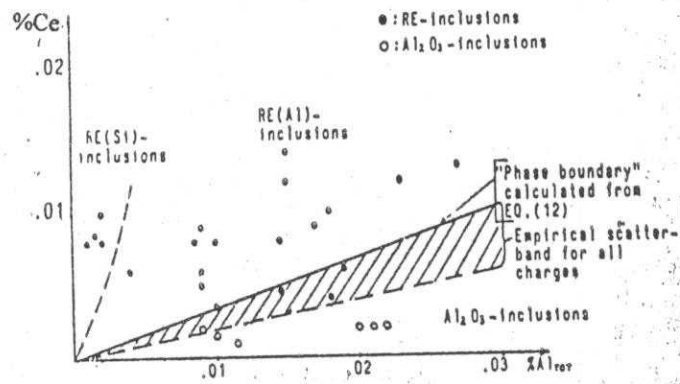


Fig. 10. Inclusion type vs. Ce and Al contents in the steels. "Phase boundary" calculated for mean values of f_s (0.49), O (0.0044%) and S (0.0097%) [49]

This figure shows that equation (106) can fairly indicate separation of RE - inclusion heats from Al_2O_3 inclusion heats in a Ce with Al diagram. It

should also be noted in Fig.10 that the critical Al content for avoiding Si in the RE inclusions (or vice versa) is 0.004%.

In this case relation (69) , (73) and (75) and the empirically established inclusion type criteria developed above were combined, giving two " phase boundary" equations .

considering the "equilibrium" between RE oxysulphide and RE oxide and oxysulphide heats,

$$(1.45 Ce)^{1.81} = \frac{(1.72.O)^{23.07}}{(1.74.S)^{25.86}} \quad (107)$$

and represents the boundary between RE oxide and RE oxide and oxysulphide heats:

$$(1.45 Ce)^{0.36} = \frac{(1.72.O)^{25.31}}{(1.74.S)^{25.86}} \quad (108)$$

Figure 11 shows the indentified RE inclusion types for different Ce and S contents of the steels. "Phase boundaries" calculated from equation (107) and (108) have also been drawn in Fig. 11. In a few cases not only the Ce/S ratios, but also the average S contents are given. This means that approximate CeS-solubility limits can be estimated by comparing the Ce-S products from steels with complete and incomplete sulphide shape control.

As can be seen, the lines, which represent approximate " phase boundaries" between RE oxides or RE oxysulphides and RE sulphides deviate substantially from each other. All are drawn in Fig. 11. As can be seen in Fig. 11 also shows that a few points from the literature

representing melts with incomplete sulphide shape control are grouped together with the points from earlier work [49]. However, it should be noted that the work of Luyckx et al [111] indicates that incomplete sulphide shape control can be found much higher Ce contents. Therefore the RE sulphide area in the Ce-S diagram in Fig. 11 must be considered highly inaccurate. More experiments are obviously needed in order to establish more accurate "phase boundaries" for the RE sulphide.

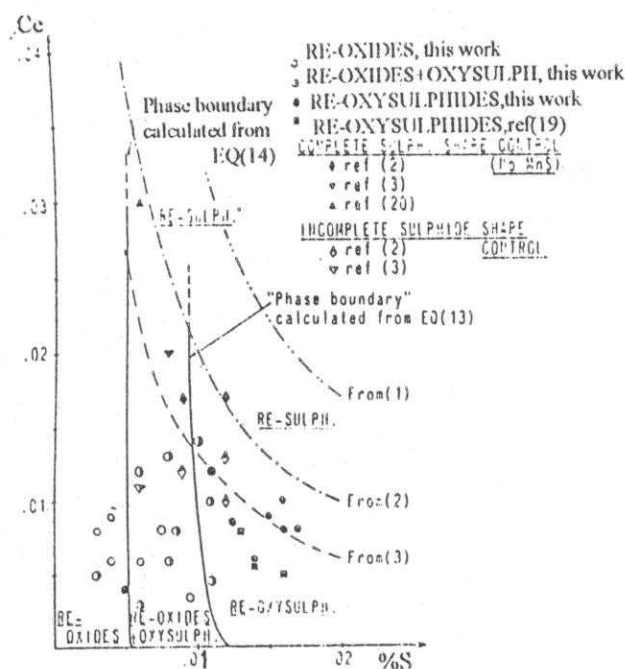


Fig. 11. Inclusion types vs. Ce and S contents in the steels. "Phase boundaries" calculated for mean values of f_s (0.44) and O (0.0044%) [49]

3.3. The inclusion precipitation diagram (IPD) of RE-O-S system in liquid iron

The standard free energies of formation of the RE oxides (RE_2O_3) at 1650°C are shown in Fig. 12 [36]. If RE oxides are formed, the RE should be the strongest deoxidizers available in steelmaking because they are the only materials which have boiling points high enough to allow retention of effective residual concentrations in solution.

The standard free energy of formation of the RE sulphides (RES) at 1650°C are shown in Fig. 13

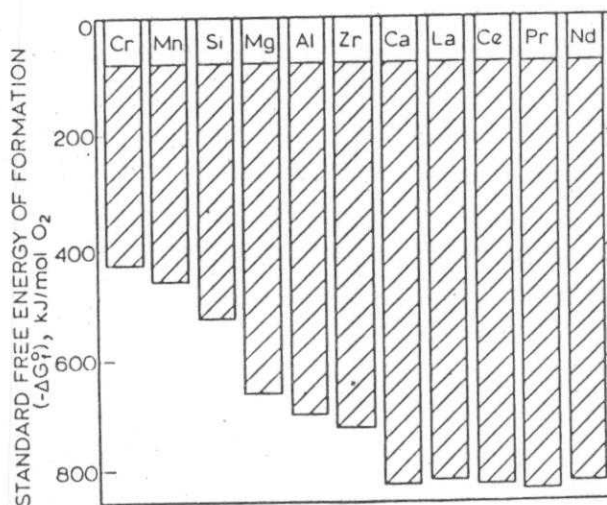


Fig. 12. Comparison of standard free energies of formation of RE and other oxides at 1650°C [36]

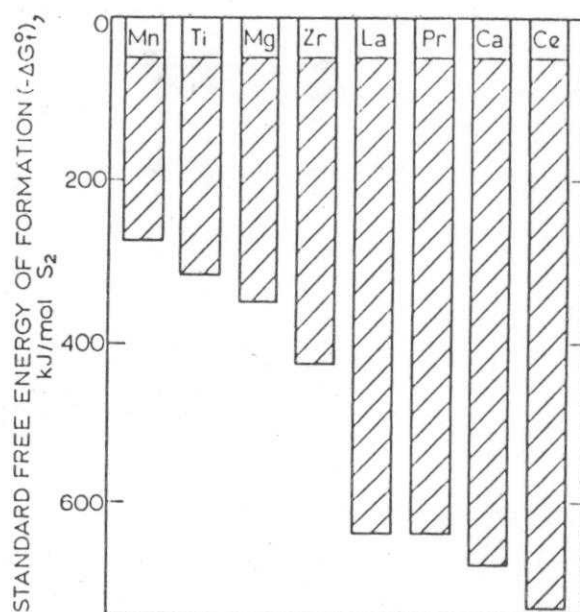


Fig. 13. Comparison of standard free energies of formation of RE and other sulphides at 1650°C [36]

Cerium sulphide CeS has a greater negative free energy of formation than any other sulphide. The other RE sulphides have slightly less negative free energy of formation (table 6) which overlap with calcium sulphide CaS, at lower temperature [11, 21, 47]. Since the standard free energies of formation of RE_xS_y sulphides are more negative than those of the other sulphides [1,21,47,163-165], it would be expected on purely thermodynamic grounds that these would be the first sulphides to form after the addition of RE and that RES sulphides should appear later when greater quantities of RE have been added. The standard free energies of formation of RE oxysulphides (RE_2O_2S) are shown in Fig. 14.

The standard negative free energies of formation of these oxysulphides are less by 40 kJ than those of the common RE oxides at

1650°C. Wilson and his colleagues [11, 41, 47] have constructed an inclusion precipitation diagram for the Fe-Ce-O-S system as shown Fig.15.

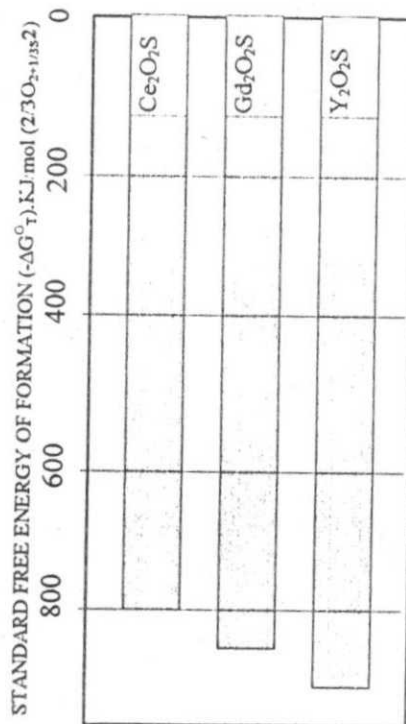


Fig. 14. Standard free energies of formation of RE oxysulphides at 1650°C [36]

The equilibrium constants of Ce-S , Ce-O and Ce-O-S inclusion systems in liquid iron determined by previous investigators [95,99,103,105,111,166-168] appear to be larger than would be expected. The thermodynamic data were different for each other. High values of equilibrium constant K, may have been obtained because of insufficient time in the experiments for the system to reach equilibrium [114] also it

seems to be a short coming that the reaction products were not indentified in some of the experiments. Contrary to the above experimental results, some of the equilibrium constants calculated thermodynamically by Vahed and Kay [41] appear to be lower.

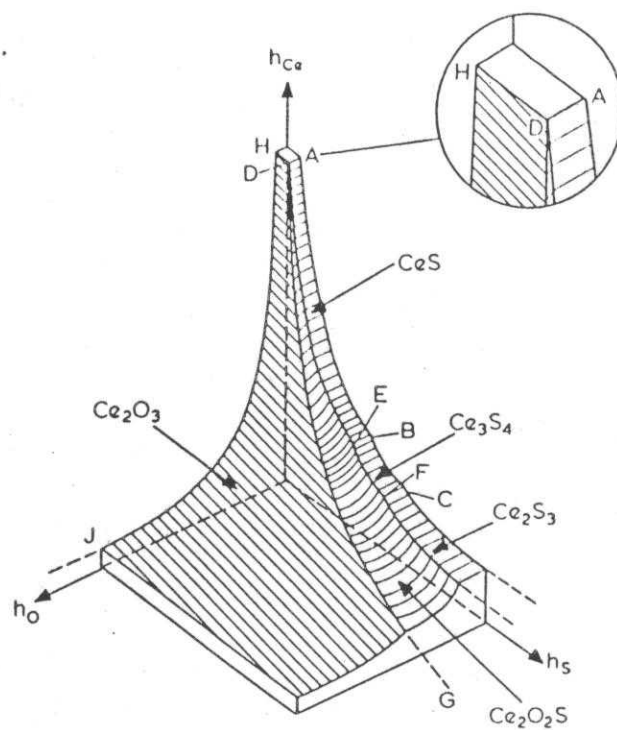


Fig. 15. Inclusion precipitation diagram [11]

The most recent investigation [169] has reported more convincing data than previous ones as shown in Table 10.

Table 10. Thermodynamic data of RE inclusions precipitating in in molten steel. at 1600°C

reaction No	equilibrium constant $\log K$ (2)	activity equation* (3)	correlation between $a_{/O/}$, $a_{/S/}$ value correlation** (4)	$a_{/S/}/a_{/O/}$ author (5)
(1). $\text{CeO}_{2(s)} =$ $/\text{Ce}/+2/\text{O}/$	$7.94 \cdot 10^{-10}$ -9.10	$\log a_{/Ce/} + 2 \log a_{/O/}$	2.90 $\log a_{/O/} = 2(1) - (2) = -0.89$	0.13 /170/
(2). $\text{Ce}_2\text{O}_{3(s)} =$ $2/\text{Ce}/+3/\text{O}/$	$4.9 \cdot 10^{-18}$ -17.31	$2 \log a_{/Ce/} + 3 \log a_{/O/}$	2.69	/90/
(3). $\text{CeS}_{(s)} =$ $/\text{Ce}/+/\text{S}/$	$2.7 \cdot 10^{-6}$ -5.54	$\log a_{/Ce/} + \log a_{/S/}$	2.46	/100/
(4). $\text{Ce}_2\text{S}_{3(s)} =$ $2/\text{Ce}/+3/\text{S}/$	$4.27 \cdot 10^{-12}$ -11.37	$2 \log a_{/Ce/} + 3 \log a_{/S/}$	8.63	/107/
(5). $\text{Ce}_2\text{O}_2\text{S}_{(s)} =$ $2/\text{Ce}/+2/\text{O}/$ $+/\text{S}/$	$6.2 \cdot 10^{-17}$ -16.21	$2 \log a_{/Ce/} + 2 \log a_{/O/}$ $+ \log a_{/S/}$	3.79	/107/
(6). $\text{Ce}_2\text{O}_{3(s)} + /S/ =$ $\text{Ce}_2\text{O}_2\text{S}_{(s)} + /O/$			$\log a_{/O/} - \log a_{/S/} = (2) - (5) = -1$	10 /170/
(7). $\text{CeO}_{2(s)} + /S/ =$ $\text{Ce}_2\text{O}_{3(s)} + 4/O/$			$2 \log a_{/O/} - \log a_{/S/} = 2(1) - (5) = -2$	100 /170/

Tab. 10 (cont.)

(1)	(2)	(3)	(4)	(5)	
(8). $\text{Ce}_2\text{O}_3(\text{s})$	$+/\text{S}/=$				
	$2\text{CeS}(\text{s})$	$+2/\text{O}/$	$2\log_{a_{\text{O}}}-\log_{a_{\text{S}}}$	$= (5)-2(3)=-5.13$	135000
				/170/	
(9). $\text{Ce}_2\text{O}_2\text{S}(\text{s})$	$+2/\text{S}/=$				
	$\text{Ce}_2\text{S}_3(\text{s})$	$+2/\text{O}/$	$\log_{a_{\text{O}}}-\log_{a_{\text{S}}}=\{(5)-(4)\} / 2$	$=-2.42$	263
				/170/	
(10). $\text{Ce}_2\text{S}_3(\text{s})$	$=$				
	$2/\text{CeS}/$	$+/\text{S}/$	$\log_{a_{\text{S}}}=(4)-2(3)$	$=-0.29$	0.51
				/170/	
(11). $/\text{Ce}/$			$\log_{a_{\text{Ce}}}=-3.32$	/170/	
			$\log_{a_{\text{Ce}}}=-1.25$	/170/	
(12). $/\text{O}/$			$\log_{a_{\text{O}}}+3.11$	/170/	
			$\log_{a_{\text{O}}}=1.29$	/170/	
(13). $/\text{S}/$			$\log_{a_{\text{S}}}=4.21$	/170/	
			$\log_{a_{\text{S}}}=3.71$	/170/	
(14). $\text{LaS}(\text{s})$	$=$				
	$/\text{La}/$	$+/\text{S}/$	$1.0 \cdot 10^{-5}$	***	
(15). $\text{La}_2\text{O}_3(\text{s})$	$=$				
	$2/\text{La}/$	$+3/\text{O}/$	$1.0 \cdot 10^{-23}$		
(16). $\text{La}_2\text{O}_2\text{S}(\text{s})$	$=$				
	$2/\text{La}/$	$+2/\text{O}/$			
	$+/\text{S}/$		$7.3 \cdot 10^{-22}$		

* redetermined value different from that in reference /107/

** redetermine value different from that in reference /170/

*** Henrian activity

Based on Table 10 and equations Fig.16 has been constructed.

The correlation among a_{Ce} , a_{O} , and a_{S} represented by the points, lines and phases in the figure are interpreted in Table 10.

If the activities of oxygen and sulphur are known, the types of RE inclusions can be determined from table 10 and Fig. 17 as follows:

Figure 17 is a projection drawing of the space precipitation diagram of Fig.16 at $\log a_{\text{O}} - \log a_{\text{S}}$ plane. Lu and Mclean [42,43] have also determined the thermodynamic relationship for the simultaneous RE inclusion precipitation paths as shown in Fig. 18.

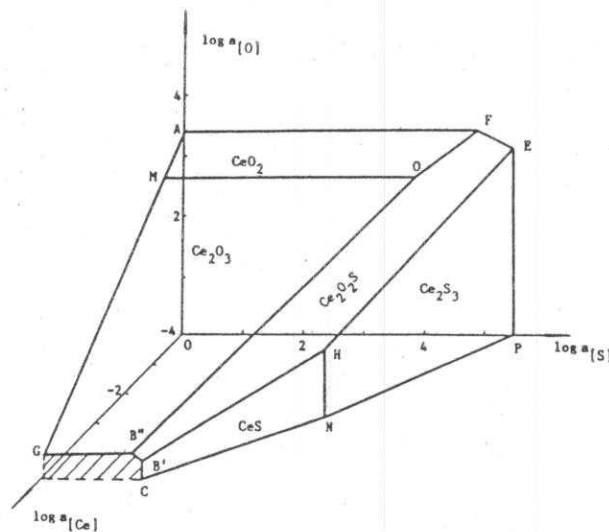


Fig.16. Heterogeneous /Ce/-/O/-/S/ precipitation at 1600°C,
($\log a_{\text{Ce}}$ vs. $\log a_{\text{O}}$ vs. $\log a_{\text{S}}$ plot)

Figure 18 shows several possible reaction paths for inclusions precipitation of oxide oxysulphides and sulphides at 1600°C. The actual path followed after the RE addition depends on the initial oxygen [%O] and sulphur [%S] contents. If [%S] < 10[%O] the reaction starts in the oxide field. Thus when [%O] = 50 ppm and [%S] = 250 ppm (point A in Fig. 18) the first phase to separate is RE₂O₃. As RE₂O₃ precipitates, the oxygen content decreases with no change in the sulphur content until coupled deoxidation-desulphurization reactions of RE inclusion precipitation take place at 1600°C, point B is reached, corresponding to 25 ppm oxygen. At this point, oxysulphide will

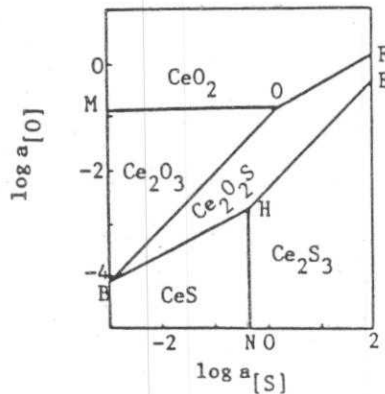


Fig. 17. Projection drawing at $\log a_{[S]} - \log a_{[O]}$ plane, $T = 1600^\circ\text{C}$

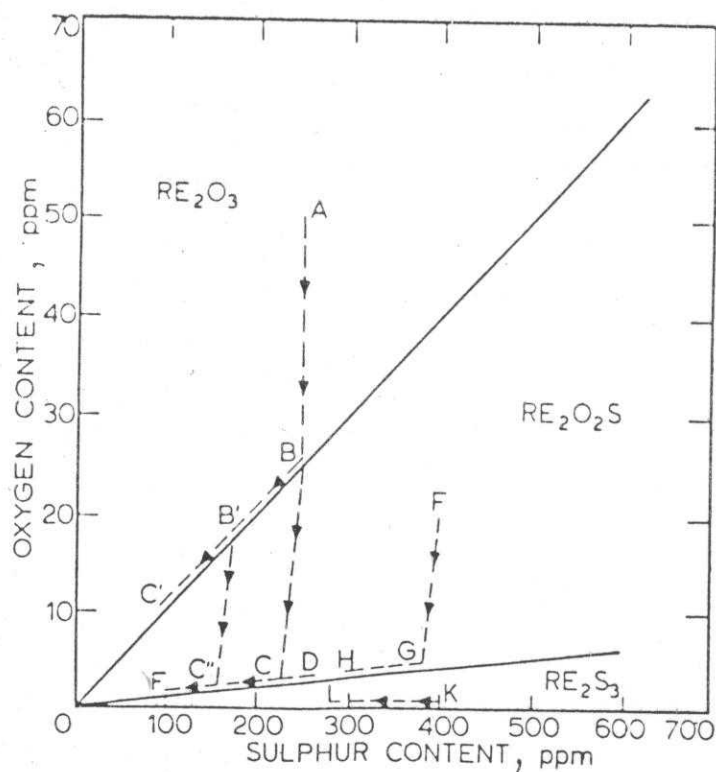


Fig. 18. Reaction paths for sequential and coupled deoxidation-desulphurization reactions /42, 42/

begin to precipitate and provided that all the oxides have been separated from the melt, the melt composition will move across the oxysulphide field in the direction BC. The slope of BC is determined by the oxygen to sulphur stoichiometric ratio for the precipitation of oxysulphide. At point C, the oxygen and sulphur contents are 2.27 and 227 ppm, respectively. The melt composition then moves along the equilibrium line CE with the precipitation of both oxysulphide and sulphide. The final sulphur level attained is determined by the initial condition of the melt and the size of the RE addition. Under these circumstances one would expect to observe inclusions consisting of an oxysulphide core surrounded by RE sulphide in figure 19:

When the melt composition reaches point B, all of the precipitated oxides have not yet been separated from the melt and the oxide to form oxysulphide and the melt composition will move along the transient state line towards C' until all the oxide has been coated with a layer of

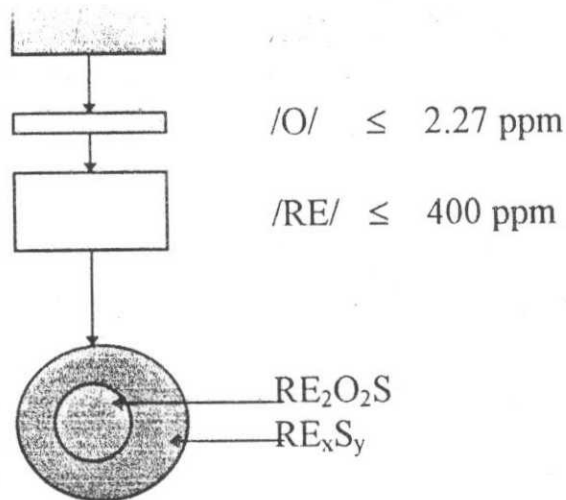


Fig.19. RE inclusion precipitation consisting of an oxysulphide core surrounded by RE_xS_y

oxysulphide, which will isolate the oxide from further reaction with the melt. At this stage, when oxide is no longer in contact with the melt, the melt composition will move away from the transient-state line BC' towards the final equilibrium line CE on a path parallel to BC i.e. B'C'' in Fig.18.

If $\%S$ is greater than $10.\%O$ but less than $100.\%O$ the initial melt composition located within the oxysulphide will precipitate and the melt composition will move from F towards G. When the oxygen content has

been reduced to G, both sulphide and oxysulphide will be separate until the final required sulphur level is reached.

3.4. Prediction of the precipitated inclusion size

1. Morphology of inclusions

The addition of RE to such steels produces a marked change in the nature of inclusions [11,41,47, 171-182]. However, before discussing the effect of RE on oxide and sulphide inclusion modification, it is pertinent to discuss briefly the factors which affect the precipitation of sulphide inclusions

In general, Manganese sulphide may be precipitated from molten steel in any of the three different morphologies. These are conventionally classified according to Sims [76] as:

- (i) type I: Randomly dispersed globular
- (ii) type II: Interdendritic eutectic (grain boundary eutectic)
- (iii) type III: Randomly dispersed angular

Hilty and Crafts [183,184] have examined the relationship between sulphur and oxygen in solution in liquid steel, deoxidation practice and the mechanism of precipitation of sulphide inclusions during solidification. The globular type I MnS are only formed if dissolved oxygen is present in the melt and they are therefore usually precipitated from rimming or semi-killed steels. Type II and type III MnS are both formed in the absence of oxygen, i.e. in fully killed steels and they have quite different as cast

morphologies, which are dependent upon steel composition. Even in the as-cast state, the type II MnS have a marked effect on steel ductility since they are formed as extensive eutectic colonies in which the sulphide is present as fine branched rods. Buzek Z. et al [19] have researched and constructed efficient schematic inclusion diagram as shown in Fig. 20.

Figure 20 shows that, when aluminum content is over 0.02%, and if it dissolve RE convenient, then usually precipitates from liquid steel type Ib. The RE inclusions are converted to manganese aluminates which form the cores of the resulting modification, surrounding them RE oxysulphides layer as shown in Fig. 21.

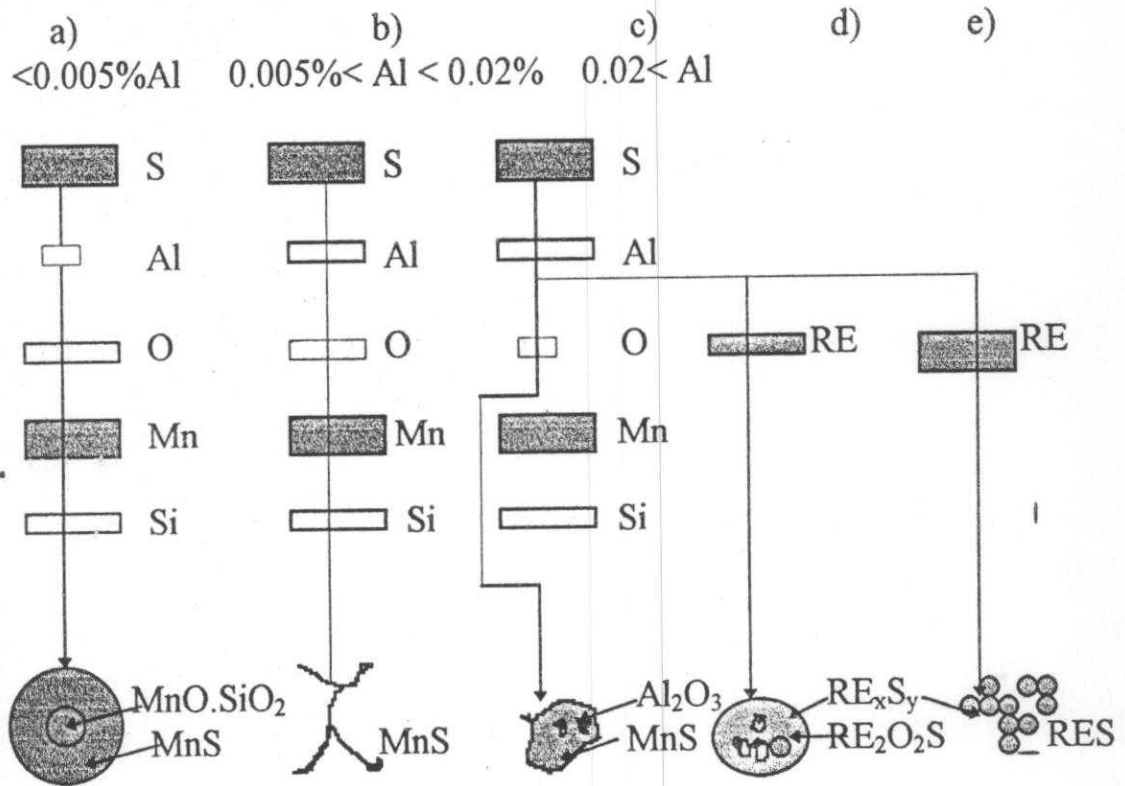


Fig. 20. Schematic of the effect of chemical compositions and deoxidizing methods on the formation of inclusion types in steels[19]

In the case of inconvenient RE contents in liquid steel will be formed unfavourable inclusions of type IV, it shows in the Fig. 22.

The RE addition is normally better deoxidation and improved cleanness of steel and RE treatment can easily get rid of and prevent the formation of solid aluminum clusters, castability is normally improved.

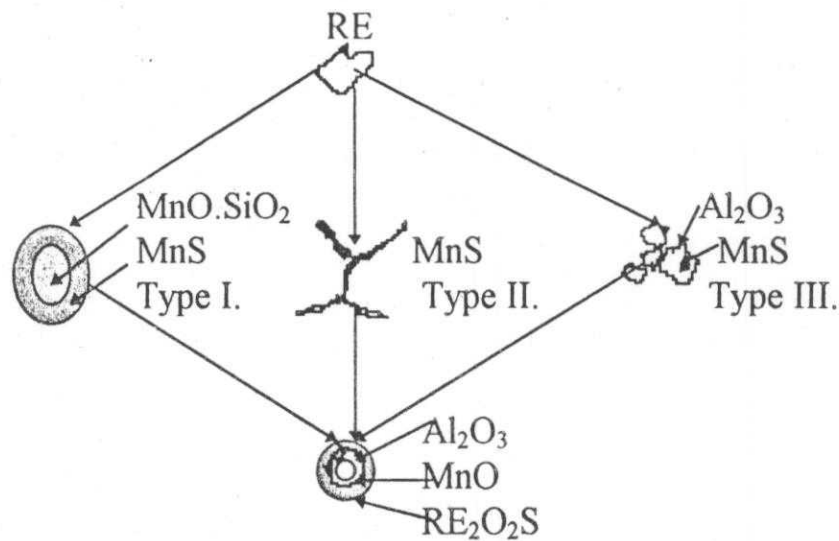


Fig. 21. Modification of inclusions with convenient RE

As can be seen, the points in Fig.23 are quite scattered, but there is a weak tendency of decreasing oxide size this is useful not only for predictions of inclusion type, but also for quantitative predictions of average inclusion sizes. More oxysulphides obviously means layer inclusions, and so does an earlier inclusion precipitation (for smaller value of f_s).

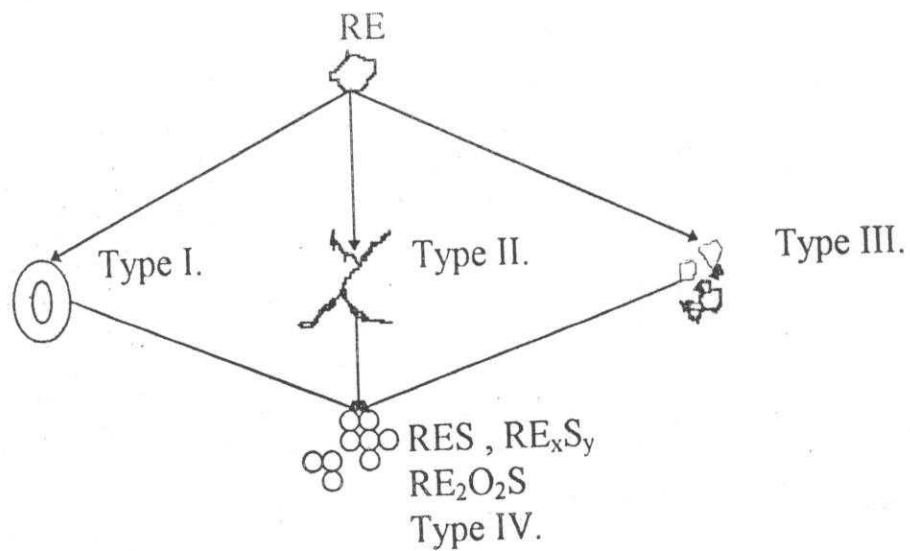


Fig.22. Modification of unfavourable inclusions with RE addition.

2. Inclusion sizes

As the nucleation is followed by a growth, which presumably is ended approximately at the solidus temperature ($f_s = 1$), it can be expected that a calculated smaller value of f_s should correspond to a larger inclusion size as in Fig 23

Figure 24 shows total sulphide projections as a function of sulphur contents and RE inclusion types. It has also been reported in the literature that the amount of elongated sulphide inclusions is decreased in steels with medium Ce additions, in spite of the fact that complete sulphide

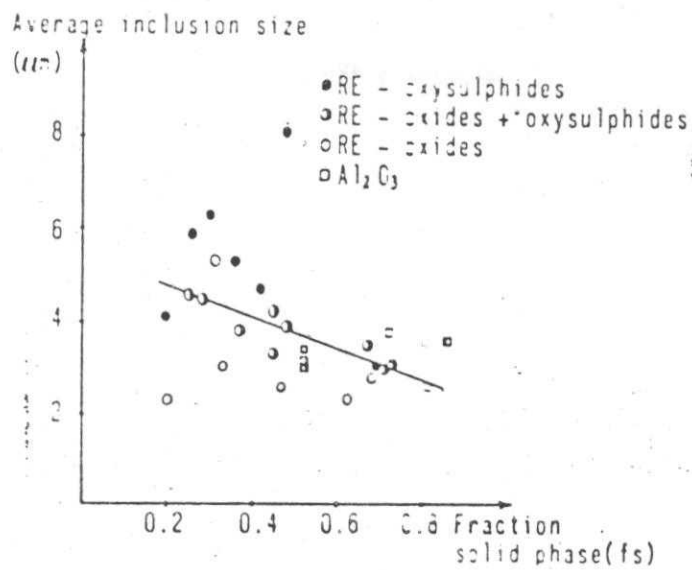


Fig. 23. Average inclusion size vs, fraction solid face at the inclusion precipitation

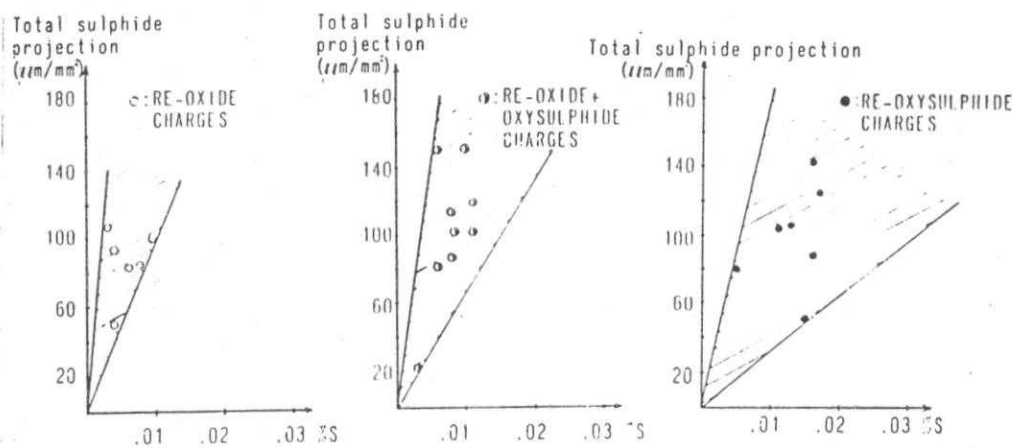


Fig. 24. Total sulphide projection vs. sulphur contents in steels with different RE inclusions.

transformation has not taken place [49, 110]. One reasonable explanation, suggested by Wilson [119] among others [185-191], is that RE are dissolved in the manganese sulphides, thereby making them less deformable. However in these experiments no RE have been detected in the MnS particles.

Another possible explanation is that the manganese sulphides precipitate earlier in RE-alloyed steels, due to the fact that RE lower the solubility of sulphur in liquid iron. This could very well give a change from type II to type I MnS inclusions as indicated by some authors [19, 21, 29]. As MnS particles of type I are known to be less deformable than those of type II [192-198], it is reasonable to expect a smaller total projection in RE-alloyed steels [199-209].

The case of RE sulphides (and sulphide shape control) obviously calls for some detailed experiments in order to establish better general criteria for transformation sulphide type. The mechanism of sulphide shape control in steels with in-complete sulphide transformation suggested in this work should also be verified by further experiments.

CHAPTER IV

STUDIES ON ELIMINATION OF INCLUSION OF MOLTEN STEEL

Efforts to explain the coarsening or coalescence, floatation and eventual elimination of inclusions and to clarify suspected deviations from Stoke's law have occupied the attention of several groups of investigators. Inclusions separate more rapidly from an agitated bath and the rate of elimination depends upon the material of the crucible, in accordance with many other observations Torssell's studies [124] were on melts stirred by induction and Torssell and Lindborg [129] developed a collision model based on the growth and separation of inclusions. Collisions brought about by velocity gradients in turbulent flow play an important role in the growth of particles. Using unstirred melts authors [210] Iyengar and Philbrook [211] and some other found that natural convection currents caused recirculation and retention of some inclusions longer than predicted by Stokes law. As noted above the ultimate removal of inclusions depends upon their floatation tendency to the free surface of the metal or their assimilation by slag or crucible wall. The latter step in turn depends upon the interfacial free energy [137, 212, 213] and the time required for rupture and drainage of metal film between the particle and the interface [210, 214]. A recent analysis of hydrodynamics and collisions of small particles in turbulent melts has been made by Linder [215].

The very small primary inclusions formed during deoxidation by aluminum, as cited above, would take a long time to float out according to Stokes law, even with correction for slippage. If however, such particles touch by gradient collision in a stirred melt, they may agglomerate or sinter to form three-dimensional clusters [116, 137,140,210]. Alternatively dendrites of alumina [216] might account for the effects observed. A cluster or dendrite of the steel is occluded within its arms which behaves as a sphere of large effective radius. Calculations of the rate of rise of such clusters [140,210] seem to account for the observed rapid rate of removal of alumina inclusion and dispel suspicions of mysterious surface effects as suggested years ago by Grussard [217].

Six possible steps of inclusion flotation during different models of solidification of steel are shown in Fig.25.

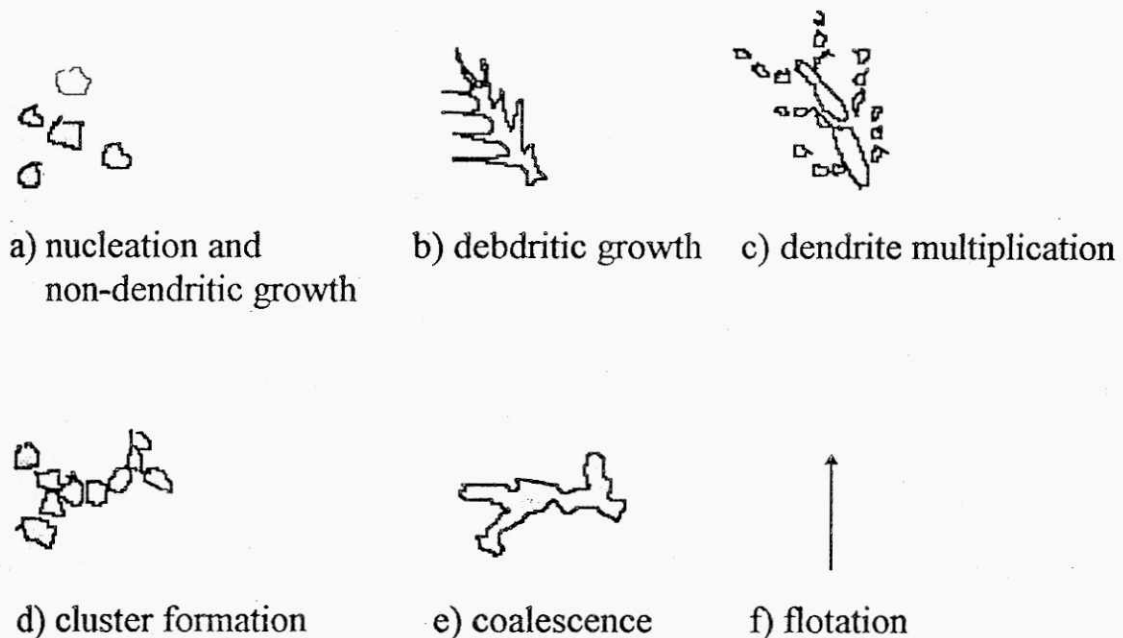


Fig. 25. Six possible steps in evolution of inclusions

4.1. The growth of inclusions

In order to understand the growth phenomenon of inclusions many studies have been done recently [218-234]. At the start of growth i.e. when $t=0$, oxygen and added deoxidizers are assumed to be in solution homogeneously in liquid steel. All the oxide nuclei present in liquid steel are taken to be of equal size and evenly distributed in the melt. It is considered reasonable to assume that a short time after the nucleation of oxides, which is assumed to occur during dissolution of added deoxidizers a state of equilibrium is reached at the interface of inclusions and the liquid iron. This interfacial equilibrium will be that which is ultimately reached between bulk liquid metal and the deoxidation product. If these assumptions are valid, the growth rate of spherical inclusions will be limited by the process of diffusion of reactants to the surface of the inclusions.

Further suppositions are necessary for the derivation of an appropriate usable diffusion equation. Let us consider that there are a fixed number of growing inclusions (Z/cm^3) each inclusion having its own spherical diffusion zone of radius r_o . For a free arrangement of these tangential spherical diffusion zones of equal size, the radius r_o of each zone may be computed from Z , thus:

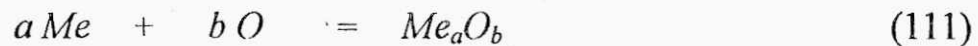
$$r_o = 3^{-1/2} \cdot Z^{1/3} \cong 0.58 \cdot Z^{1/3} \quad (109)$$

For about 75% of total liquid volume, the size of the diffusion zone is best represented by the following expression for the condition that the radius of

the growing inclusion r_i is much smaller than the radius r_o of the individual spherical diffusion cell:

$$r_o = (3 / 4\pi Z)^{1/3} \cong 0.62 \cdot Z^{1/3} \quad (110)$$

It is also assumed that the pseudo-steady-state conditions prevail in each diffusion zone, i.e. the flux of reacting element Me and oxygen O inclusion in iron to the surface of the inclusion are taken to be those corresponding to the stoichiometric requirements.



and flux:

$$a J_{Me} = b J_O \quad (112)$$

Therefore the rate of diffusion of only one of the reactants (oxygen) need to be considered.

The following initial and boundary conditions are assumed for the pseudosteady state diffusion process in a spherical shell having an impervious outer shell.

$$i) \quad c = c_o ; r_i < r_o \quad t = 0 \quad (113)$$

$$ii) \quad c = c_i ; r = r_i \quad t > 0 \quad (114)$$

$$iii) \quad dc/dr = 0 ; r = r_o \quad t > 0 \quad (115)$$

where c_o is the concentration of oxygen in liquid steel in g.atom O/cm³

c_o is the subscript for initial uniform composition

c_i is the subscript for initial uniform composition in equilibrium with the deoxidation product

r is the radial distance from the centre of growing inclusion

r_i is the instantaneous radius of growing inclusion

r_o is the radius of the spherical diffusion cell

t is the time

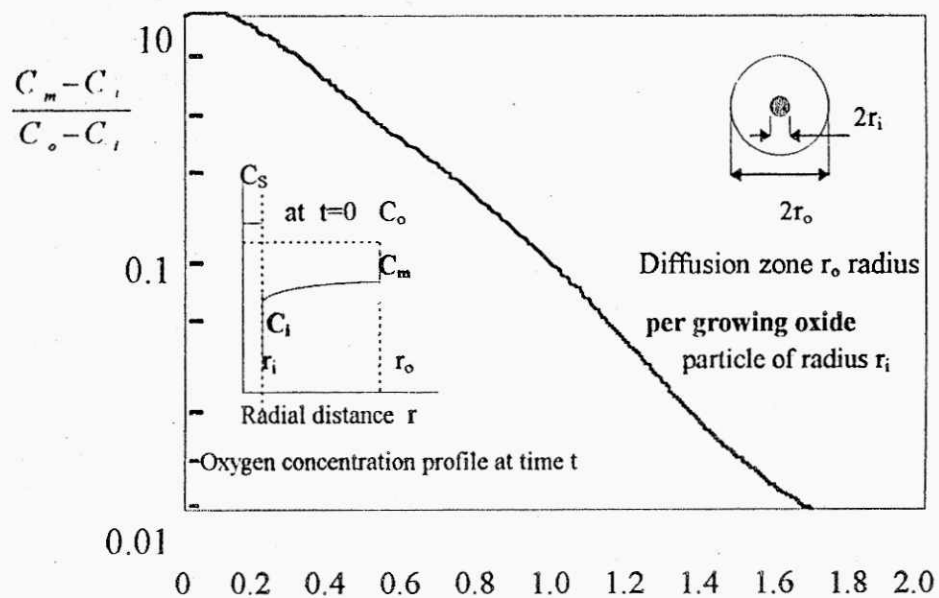
The nucleus of inclusion being small in size, the approximation $r_i \rightarrow 0$ at $t = 0$ is permissible, and moreover, since $r_i \ll r_o$, a simplified form of the diffusion equation derived by Ham [218] may be used:

$$\frac{D_t}{r_o^2} \cdot \left(\frac{c_o - c_i}{c_s}\right)^{\frac{1}{3}} = \frac{1}{6} \ln \frac{u^2 + u + 1}{(u - 1)^2} - \frac{1}{\sqrt{3}} \tan^{-1} \frac{2u + 1}{\sqrt{3}} + \frac{1}{\sqrt{3}} \tan^{-1} \frac{1}{\sqrt{3}} \quad (116)$$

where $u = \left(\frac{c_o - c_m}{c_o - c_i}\right)^{\frac{1}{3}} \quad (117)$

c_i is the oxygen concentration in inclusion g-atom O/cm³

Using this expression, fractional desaturation of the reactant in the melt is plotted in Fig. 26 against the dimensionless parameter $(D_t / r_o^2) \cdot \{(c_o - c_i) / c_s\}^{1/3}$ which may be used to calculate the concentration c_m at any reaction time for dimensionless



$$\frac{D_t}{r_o^2} \left(\frac{C_o - C_i}{C_s} \right)^{1/3}$$

Fig. 26. Fractional desaturation of the solute as a function of the parameter $(D_t / r_o^2) \cdot \{(C_o - C_i) / C_s\}^{1/3}$ for a diffusion process in a spherical shell having an impervious outer shell, the symbols are defined in the inset diagrams and the boundary conditions are

- i) $c = c_o; r_i < r_o; t = 0$, ii) $c = c_i; r = r_i; t > 0$,
- iii) $dc/dr = 0; r = r_o; t > 0$

known values of D , r_o , c_o , c_i , and c_s . Various concentration and distance terms are defined in the inset diagram in Fig. 26.

The instantaneous values of r_i at time t is then calculated from the equation based on the conservation of matter:

$$r_i = r_o \cdot \left\{ \frac{c_o - c_m}{c_s} \right\}^{1/3} \quad (118)$$

Taking an average value of $c_s = 0.08$ g-atomO/cm³ for the oxide inclusion and converting the oxygen concentration term c to more practical units, equation (118) takes the following form

$$r_i = 0.379 \cdot r_o \cdot (\%O/o - \%O/m)^{1/3} \quad (119)$$

where $\%O/o - \%O/m$ is the decrease in oxygen content at time t .

The term of difference $\Delta\%O/$ used subsequently in the text is for the difference between the initial and final equilibrium oxygen concentration i.e. $\Delta\%O/ = \%O/o - \%O/i$, if the diffusivity of oxygen is known similar values for carbon can be determined $D = 10^4$ cm²/s or $4.1 \cdot 10^{-5}$ cm²/s at 1450°C. Inserting these values in equation (117) one can calculate number of nuclei Z . According to the experimental work done on precipitation in aqueous solutions [235, 236], the number of nuclei formed apparently spontaneously in supersaturated solution is within the range $10^5 - 10^6$ /cm³. About the growth of nuclei there were many previous studies [237-245].

4.2. Flotation of inclusions

It is to be noted that as the growing inclusion float out of the melt before completion of the reaction, deoxidation in nuclei - free homogeneous melts will cease.

Processes involving solute diffusion through the melt deoxidation do not play a very important role, but instead, the particle coarsening takes place primarily from particles colliding and sintering (coalescing) as shown schematically in Fig.25d and 25e. The collisions which cause "inclusion clusters" to form result from two causes. First, according to Stokes law the larger particles rise faster than smaller ones and thus may catch up to and collide with smaller ones. Secondly, liquid shear resulting from convection also brings about particle collisions. Both these processes are analogous to the collisions between two rain drops which leads to coarsening of the rain drop. The simplest kind of collision to describe quantitatively is that resulting from inclusion flotation according to Stokes law; where the velocity v is given by:

$$v = \frac{2}{9} g \cdot r^2 \cdot \frac{\rho_L - \rho_i}{\eta} \quad (120)$$

where: g is the acceleration due to gravity

ρ_L and ρ_i are the densities of the liquid and inclusions respectively.

η is the liquid viscosity of metal ($\eta = 0.064$ g/cm.s for purified liquid iron at 1600°C).

Only inclusions that are within a horizontal distance of $r_1 + r_2$ from each other, can ultimately collide (Fig. 27).

The time required for this collision to occur depends on the relative velocities of the two particles and on their vertical centres of the two inclusion must therefore lie within a certain cylindrical volume w , which is:

$$w = k_s \cdot (r_1 - r_2) \cdot (r_1 + r_2)^3 \quad (121)$$

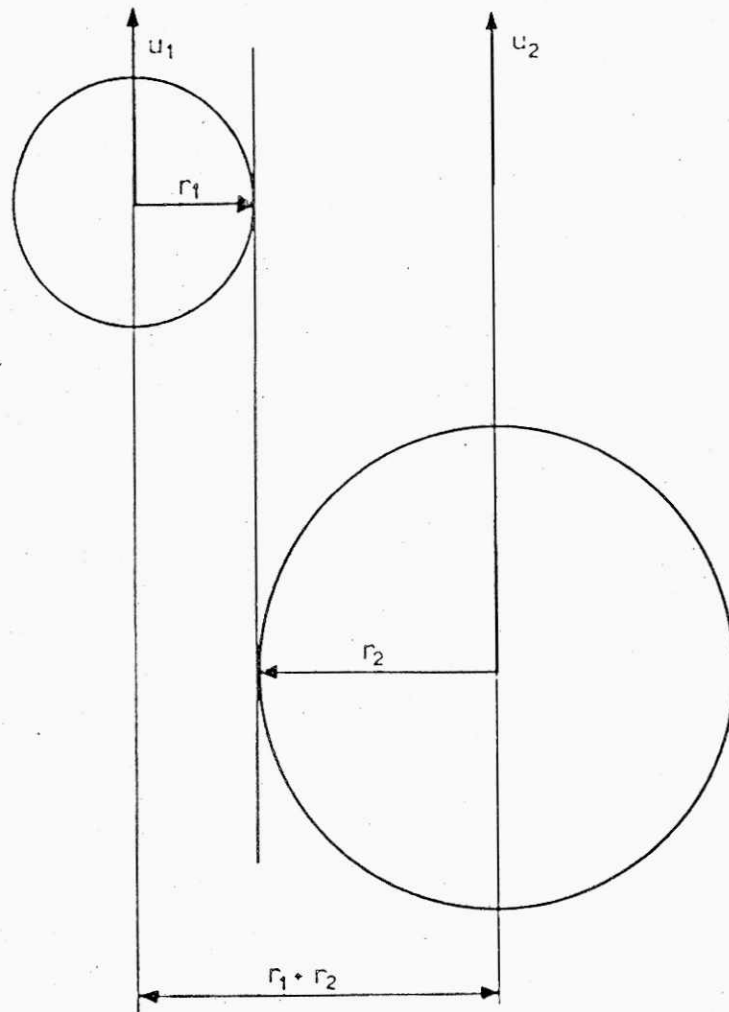


Fig. 27. Limiting case for collision between two inclusions /129/

Where the collision volume w has the units volume per unit time and k_s is the rate constant for Stokes flotation equation (120).

When any two inclusions strike, they sinter rapidly together to form a single spherical inclusion, the size distribution $f(r)$ of inclusions changes according to the relation:

$$\frac{df(r)}{dt} = -\int_0^{\infty} f(r_2) \cdot w(r_1, r_2) \cdot f(r) \cdot dr_2 \quad (122)$$

With the aid of equations (120)-(122) and knowing the size distribution of inclusions at any one instant, it is possible to calculate numerically the size distribution at any other instant, future or past. As a consequence of collisions, the size distribution is displaced towards larger particle sizes. Calculations show that simple Stokes's collisions can account for very rapid growth in particle size of inclusions in steel; this growth is further enhanced by liquid shear (e.g. stirring of the melt).

From Fig. 25 it is known that the question of homogeneous v , heterogeneous nucleation of alumina inclusion has been considered by a number of workers [236,126].

It is clear that in practice, supersaturations required for homogeneous nucleation could easily be reached locally where the aluminum is added to the oxygen containing melt. Growth of the nuclei that first form then appear to occur dendritically and it seems certain that dendrite multiplication then occurs rapidly, causing the dendrites to break up, as shown in Fig.25c. This break up and the subsequent collision of individual inclusions is favoured by vigorous stirring of the melt [246]. Collision of the particles to form inclusion clusters, as shown in Fig. 25d is governed by the same equations given earlier for silica, and extended to

inclusion clusters containing many hundreds or thousands of inclusions form in this way. The rate at which clusters build up is, as would be expected strongly dependent upon the degree of conversion [247-249].

The next step, that of coalescence sintering occurs at a much lower rate for alumina than it does for silica. This is the step where bonds begin to form between the alumina particles by a diffusional or viscous flow process as shown schematically in Fig. 25e. Kuczynski et al [249] Coble [250] and Kingery and Berg [251] have studied the sintering process for alumina particles and derived expressions governing the rate of formation of "necks" between adjoining particles, assuming four different mechanisms: viscous flow, volume diffusion, surface diffusion and evaporation condensation. For the case of alumina particles fully immersed in an iron melt, neither of the latter two processes would be expected to occur but a fifth is possible, that is transport by liquid diffusion. However the mathematics of the case for surface diffusion may be used for this case, simply by employing a liquid diffusion coefficient in place of a surface diffusion coefficient. Oei et al [246] have concluded that volume diffusion can explain the rate of sintering observed. Braun [210] agrees that volume diffusion is important but his calculation indicates that in some cases the liquid diffusion mechanism may also be important. A problem resulting from alumina inclusions is that sintering of these inclusions at usual steelmaking temperature occurs so slowly that, rather than coalescence into large spheres or compact crystals which would float out, they remain as elongated complex inclusions that contain many hundreds or thousands of inclusions. These float, but at a much lower rate than would more compact

shapes. Simple statistical study [252] shows that study of polished sections gives little or no information regarding the extent of these "multimembered" inclusions. For example, inclusions containing hundreds of partially sintered members typically appear on a polished section as having only a very few members. In the case of blowhole formation during solidification of liquid steel, it is important for thermodynamic driving force exists tending to reduce the dissolved gas content. The amount of gas in solution may decrease either by escaping at the free surface, or by the formation of a gas bubble in the liquid. The primary gases contributing to blowhole formation in steel are believed to be CO , H_2 , and N_2 although their relative contributions may vary somewhat.

Conditions of blowhole formation are well known. The critical gas pressure P_{total} under which a gas bubble becomes stable in liquid steel can be represented as [48]

$$P_{\text{total}} = P_A + P_F + \frac{2\sigma}{r} \quad (123)$$

where : P_A is the atmospheric pressure

P_F is the ferostatic pressure

σ is the surface tension of liquid iron

r is the bubble radius

When the sum of the pressures of H_2 , N_2 and CO at the maximum point (indicated by $P_{\text{H}_2}^{\text{max}}$ + $P_{\text{N}_2}^{\text{max}}$ + $P_{\text{CO}}^{\text{max}}$ as shown in Fig. 28) is greater than the gas bubble

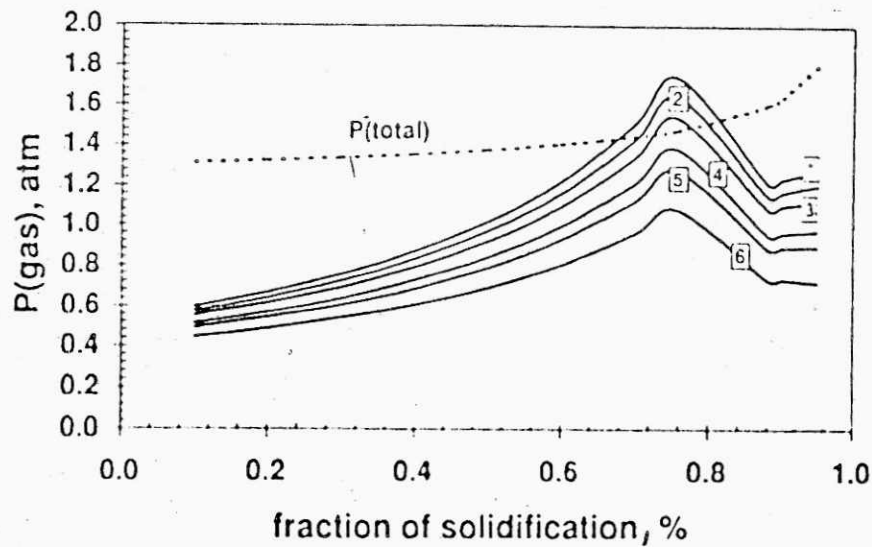


Fig. 28. Variation of total gas pressure formed in liquid steel, including H_2 , N_2 , CO on solidification. The critical pressure P_{total} for bubble formation is also indicated $\%C/O = 0.2$, $\%Si/O = 0.25$. [1]-9ppmH; 100ppmN, [4]-7ppmH; 80ppmN
 [2]-9ppmH; 80ppmN [5]-7ppmH; 50ppmN
 [3]-9ppmH; 50ppmN [6]-5ppmH; 50ppmN

would be formed i.e.:

$$P_{gas}^{max} = P_{H_2}^{max} + P_{N_2}^{max} + P_{Co}^{max} > P_{total} \quad (124)$$

Figure 28 presents the relationship between total gas pressure calculated from equation (126) and total formed gas pressure for $\%C/O = 0.20$, $\%Si/O = 0.25$ under various condition. It can be seen that for curve 3 at $g = 0.759$, $Co = 52.0\%$, $H_2 = 43.5\%$ and $N_2 = 4.5\%$. This implies that Co and H_2 are the main gas bubble sources. From equation (124) the critical equation for $\%C/O = 0.20$ is given by:

$$P_{H_2} + P_{N_2} + P_{CO} = 1.5 \quad (125)$$

By oxygen galvanic cell Hagen K. et al, has determined relationship between /Al/ and /O/ as follows [253]:

$$\log\%Al.10^3/ = 6.22 - \frac{7458}{T} - 0.595 \log a_o \text{ (ppm)} \quad (129)$$

for example, when $T = 1610^\circ\text{C}$, oxygen activity $a_o = 60$ ppm then the dissolved aluminum is 0.016% from the above equation.

Figure 29 [161] shows region of blowhole and no blowhole. When the oxygen content is kept lower than 60ppm, the corresponding dissolved aluminum is 0.016%.

4.3. Separation of RE inclusions by floatation

Most of RE inclusions are cluster-shaped RE_xS_y and RE_2O_2S with a relatively large density of about 5 to 7 g/cm^3 as compared with those of Al_2O_3

($\rho = 4.0 \text{ g/cm}^3$) and SiO_2 ($\rho = 2.5 \text{ g/cm}^3$). The property of floating separation of spherical inclusions has been extensively studied on the basis of the Stokes law and other similar principles, whereas in the current work the floating velocity which has been calculated by using the method previously employed by Perry [254] and Asans [255]. More specially since the cluster shaped inclusions form a number of aggregates having three dimensional bonding in molten steel, it is assumed from the method

adopted that these inclusions float up in the form of the aggregate having a large diameter as a unit. Density of cluster, ρ_{cl} is expressed as follows:

$$\rho_{cl} = \rho \cdot \varepsilon + \rho_{incl} (1 - \varepsilon) \quad (127)$$

where: ρ_{incl} is the density of inclusions

ρ is the density of molten steel (7.1 g/cm^3)

ε is the fraction of cluster in molten steel (0.97)

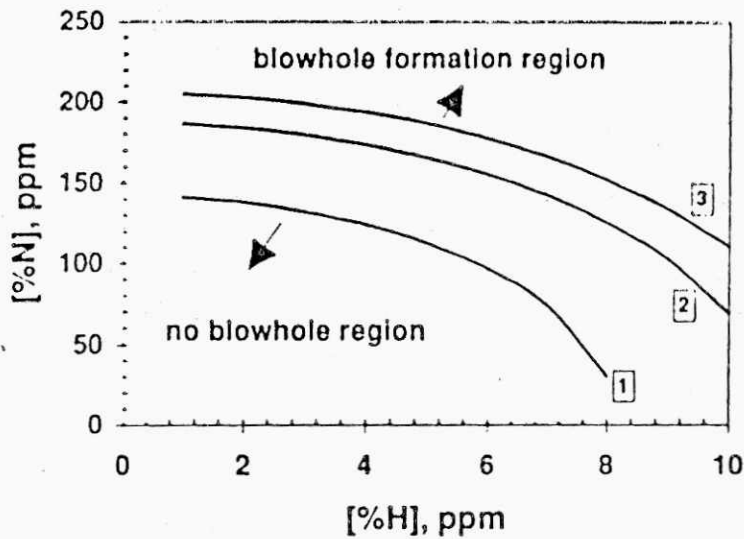


Fig. 29. Critical domain for blowhole formation in liquid steel [161]

The floating velocity in ferrostatic molten steel is given in Table 11. In the case of RE inclusions having an average diameter of $500 \mu\text{m}$, the floating velocity will be about $1/3$ of that of the Al_2O_3 cluster having the same average diameter. This means that it takes, for these inclusions about 40 min to float up through the entire height of 2.4 m of a 30t ingot. Floating separation is thus a phenomenon not easily taking place in this case.

Table 11. Floating velocity of cluster shaped inclusions

cluster size (μm)	50	100	300	500	1000	3000	5000
V_{REincl} (cm/sec)	$4 \cdot 10^{-4}$	$4 \cdot 10^{-3}$	$4 \cdot 10^{-2}$	10^{-1}	$3 \cdot 10^{-4}$	1.1	1.9
$V_{\text{Al}_2\text{O}_3}$ (cm/sec)	10^{-3}	10^{-2}	10^{-1}	$3 \cdot 10^{-1}$	$6 \cdot 10^{-1}$	2.3	4.0

During the solidification of killed steel, it is generally believed that a downward flow of the solidification front has taken place by the thermal convection, the flow velocity of which being 10 to 100 cm/min, according to Mori et al [256] and 165 cm/min according to Romanov [257]. Even RE inclusions with an average diameter of 1 mm have a floating velocity of 18 cm/min, which is smaller than the flow velocity of this downward flow.

The sedimentation of inclusions present in the solidification front can therefore be well estimated. Equiaxed crystals of steel are incessantly sedimented in the precipitation zone of ingot [88] trapping large RE inclusions during the process of floating up and thus the accumulation of RE inclusions occurs in the precipitation zone.

Previously there were many works finding way to remove inclusions in ladle treatment by injection of RE together with other reductants [258-268], but problem also were not included.

CHAPTER V

EXPERIMENTAL METHODS

5.1. Ingot casting experiments

Figure 30 shows a schematic diagram of the experimental set up for the casting of one kg ingots.

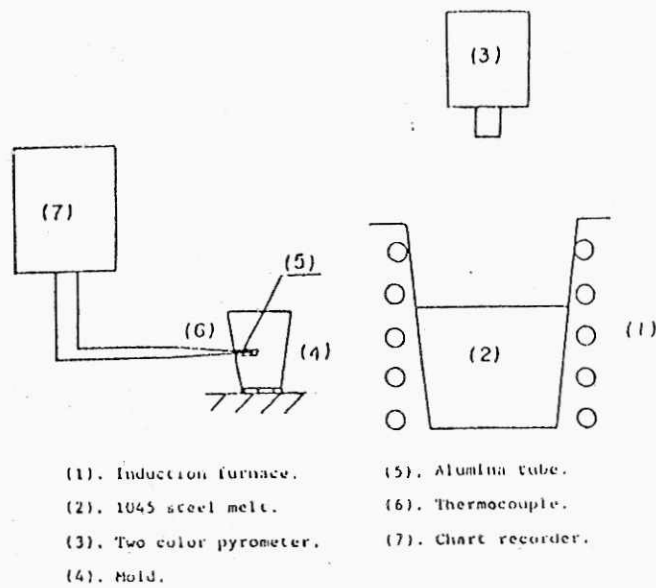


Fig. 30. Schematic diagram of the casting facility

Five kilogram of electrolytic iron of composition given in Table 12 is melted in a rammed magnesia induction furnace of 160 kW capacity and is then poured into a zircon sand mold to produce one-kg ingots. Temperature of the melt is measured with a 0.2 mm diameter PtRh-Pt 18 pct thermocouple protected by an alumina tube and recorded with a chart recorder.

The RE containing more than 96% RE given in Table 13 is used for additions.

Table 12. Analysis of electrolytic iron (w%)

C	Si	Mn	P	S	Al	Cu	Cr
0.004	0.001	0.001	0.002	0.0036	0.001	0.001	0.006
Ti	Mo	V	Co	O	N		
0.004	0.001	0.002	0.007	0.0474	0.0021		

Table 13. Chemical compositions of Mischmetal and metallic aluminum

RE _t	Ce	La +Sm	Nd	Pr	Fe	Mg	Al	Al
96.8	40.5	50.3	1.7	4.4	2.69	0.42	0.02	99.99

Before RE addition the steel was deoxidized with aluminum (see Table 13)The pouring temperature is held at $1600 \pm 10^\circ\text{C}$ for each test. The casting experiments were divided into five categories:

1. casting without RE addition

2. casting with RE addition in the furnace one minute before pouring
3. casting with low RE addition in the mold
4. casting with high RE addition in the mold
5. casting with the highest RE addition in the mold

5.2. Tammann melted examples

An alumina crucible was set in a 24 kVA Tammann furnace as shown in Fig.31

The crucible being filled with about 300g of electrolytic iron of composition given in Table 12 is changed into the crucible. The electrolytic iron is melted under slag of composition given in Table 14 and then allow to solidify to measure the degree of supercooling. A constant cooling rate was obtained, when the electric power

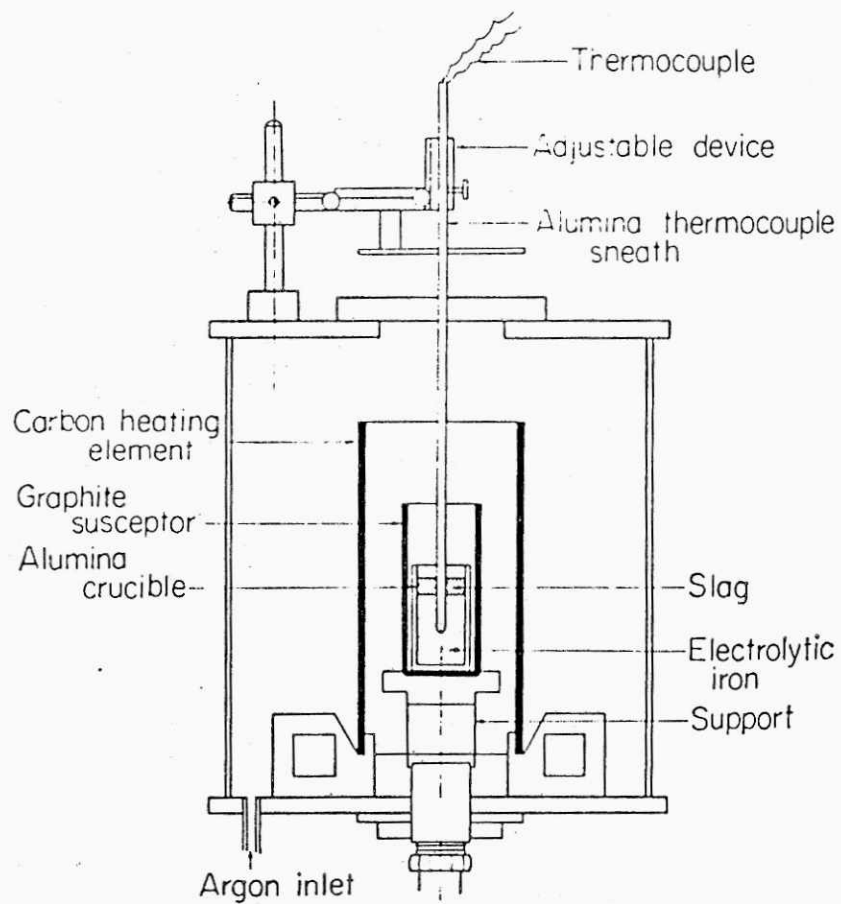


Fig. 31. A cross-sectional view of the Tammann furnace for supercooling experiments

Table 14. Slag composition used for supercooling experiments (w%)

SiO ₂	B ₂ O ₃	Al ₂ O ₃	Na ₂ O	BaO	CaO
76±3	85±1	4.3±0.5	6.7±0.8	4.0±0.3	0.5±0.5

was turned off. The specimen is then allowed to cool naturally after it is held for several minutes at temperatures in the range from 1600°C to 1620°C. As the processes of melting and solidification are repeated, the suspended particles in the molten metal move gradually toward the slag. Thus the degree of supercooling becomes larger. The slag was melted before iron melt with the composition given in Table 14.

Homogeneous supercooling condition were assumed to be satisfied, when the degree of supercooling approach a substantially constant value. The aluminum and RE having the compositions as shown in Table 13 were added to form oxides of these elements in the in molten metal. These oxides were used to investigate the behavior of the heterogeneous nucleation.

The measurement of electromotive forces was conducted by a Pt13pctRh thermocouple of 0.2 mm diameter covered with an aluminum protective tube of 4 mm OD and 2 mm ID. The thermal electromotive force was recorded with an X-Y recorder at an equilibrium speed of one second maximum .

5.3. Thermal analysis

i) cooling rate

It is considered necessary to increase the cooling rate as one of the factors which increase the degree of supercooling [276]. Under the conditions of this experiment, the maximum cooling rate was obtained by turning off the electric power when the predetermined melting temperature was reached.

Figure 33 shows a temperature - time curve in a typical supercooling experiment. Point N in this figure corresponds to starting point of nucleation cycles. Same cooling conditions are selected to have a comparison of cooling rates. The cooling rate as a matter of the bath varies within the range from 10° to 30° C/min. More precisely, however, there is a difference in the cooling rate especially in the supercooling zone below the solidification point, depending on the degree of supercooling attained. One example of such case is shown in Fig. 33.

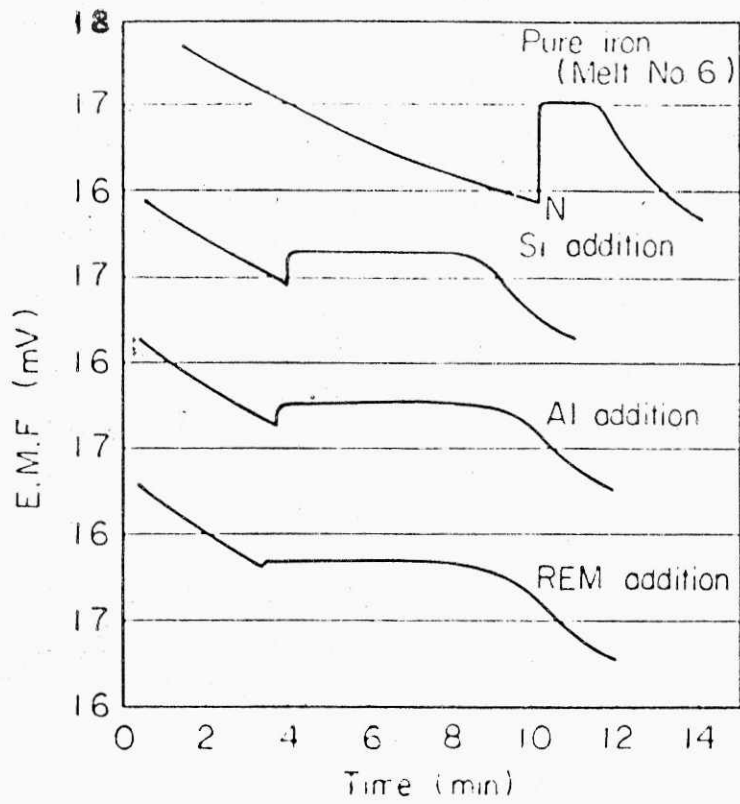


Fig. 32. Time-temperature curve of various supercooling experiments

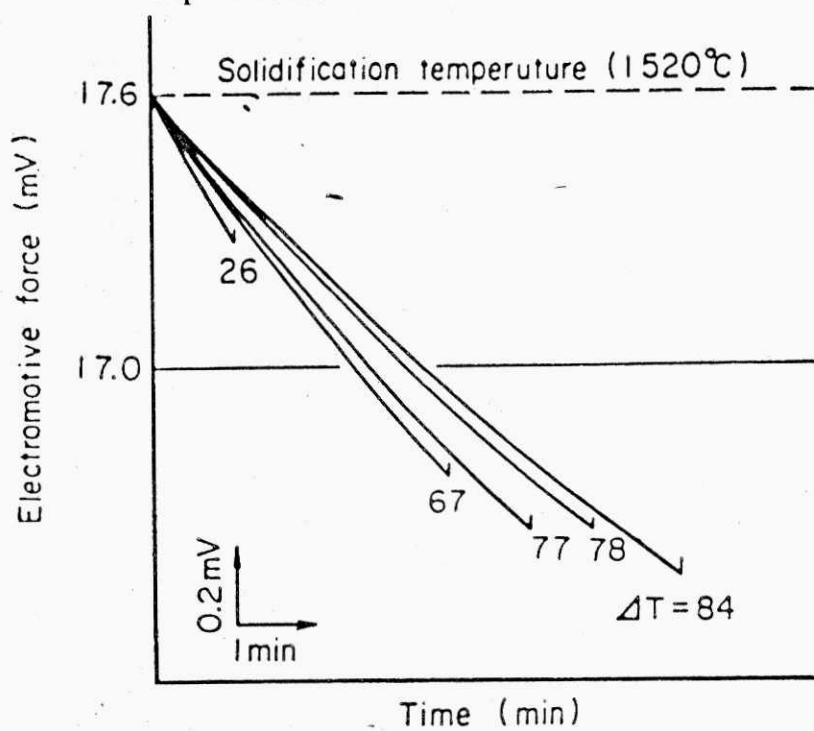


Fig. 33. Effect of supercooling on the E.M.F. change

In this case, however, it was observed that, as the degree of supercooling increases, the cooling rate decreases accordingly. Although the cause of such phenomenon is not exactly known, the behaviour of the formation of clusters and embryos prior to nucleation is supposed to be delicately affecting this phenomenon.

ii.) Homogeneous Supercooling

The degree of supercooling increases gradually, as the catalytic substrates contained in the molten metal move toward the slag the repeated melting and solidification under a given slag [276, 277]. When the slag composition is the same , the supercooling in general is influenced by superheating the solute concentration, the cooling rate etc. The influence of superheating on the degree of supercooling is particularly important [276]. The maximum supercooling for 300g molten metal is 140°C, a comparison with previous experiment on 80g of molten steel is 227°C and the cooling rate was 30°C to 50°C/min [278].

iii.) Heterogeneous Supercooling

After the homogeneously supercooling to 140°C attains by repetition melting, aluminum and RE are added in amounts of 0.05 to 0.10% to form Al_2O_3 and RE oxides in the bath .The change in the supercooling is then measured.

5.3. Determination of equilibrium between RE and oxygen in molten steel

The chemical composition of electrolytic iron used in the experiments is shown in Table 12 and the tube-shaped $ZrO_2(MgO)$ solid electrolyte oxygen probe is shown in Fig. 34.

The cell may be represented by:



The electromotive force (EMF) of the oxygen potential of the cell measured out in the experiments ranged from 9 to 40 ppm. According to Qujong Han [90], Janke and Fischer [279] the effect of electronic conductivity in the EMF range is so small that it needs no correction, provided Cr/Cr_2O_3 reference electrode is used with the $ZrO_2(MgO)$ or $ZrO_2(CaO)$ electrolyte.

The activity of the oxygen in the liquid iron is calculated using the equation

$$\log a_O = 3.64 - \frac{11.593 - 10.08 \cdot E}{T} \quad (129)$$

where: a_O is the oxygen activity in the liquid steel

E is the EMF to be determined (mV)

T is the absolute temperature

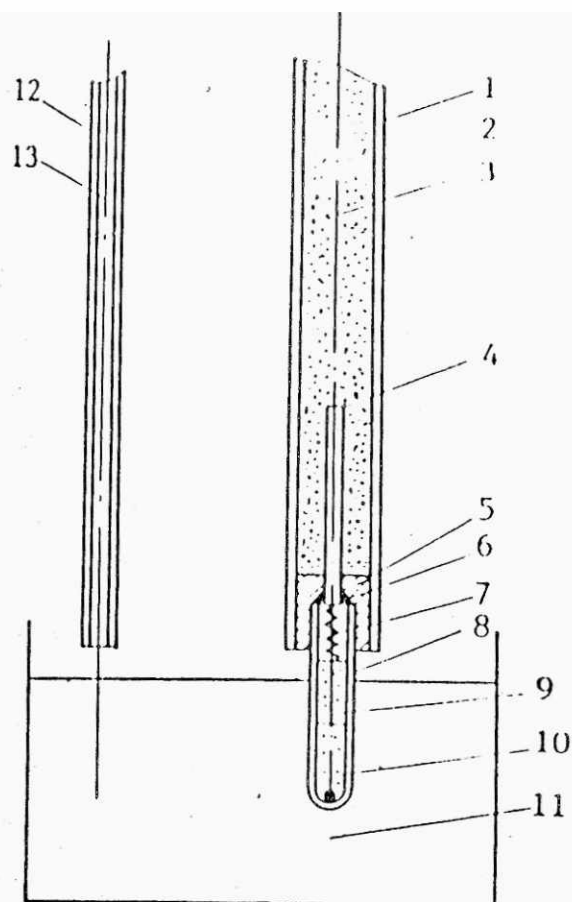


Fig. 34. Scheme of solid electrolyte probe: (1) quartz tube, 6 to 8 mm in diameter; (2) Al_2O_3 coarse powder; (3) Modification wire, 0.35 mm in diameter; (4) one-hole Al_2O_3 tube; (5) refractory cement ($\text{H}_3\text{PO}_4 + \text{Al}_2\text{O}_3$); (6) refractory cement (water glass, Al_2O_3 , No 600), (7) refractory fiber; (8) $\text{ZrO}_2(\text{MgO})$ probe; (9) Al_2O_3 powder, No 600; (10) $\text{Cr} + \text{Cr}_2\text{O}_3$ reference electrode; (11) metal bath; (12) quartz tube, 4 to 5 mm in diameter; and (13) Mo wire (counter electrode)

Several probes are compared to determine their precision: for example Chinese and French. After the probes are removed from the melt, samples for each heat are taken, and the oxygen contents are determined by the vacuum fusion coulometric method. All these results are listed in Table 15.

Table 15. Details of the experiment

Furnace	Carbon tube furnace
Atmosphere	High purity 99.99 pct Ar
Crucible height	MgO, CaO (self-prepared); diameter, 25mm; 40mm
Charge	Electrolytic iron 70 kg
Rare earth metals	¹⁴¹ Ce and ¹⁴⁷ Nd with purity 99.95 pct
Temperature control and measurement	Pt/Rh30-Pt/Rh6 thermocouple directly immersed in the iron melt in a crucible next to the crucible in which the experiment is being done. The emf is measured by using a digital voltmeter A w/Re5-w/Re20 thermocouple in contact with bottom of the graphide crucible is used to control the temperature. Temperature variations $\pm 3^{\circ}\text{C}$.
Time required to Reach equilibrium	For new crucible ≥ 8 h.
Solid electrolyteprobe	ZrO ₂ (MgO) probe; diameter 5mm, length 35mm
EMF measurement integrated- $\pm 5\text{mV}$); the duratuion of	The EMF is determined by using a DS-3 type digital voltmeter (error measuring is 15 to 20 sec

From Table 15, one can see that there is no great difference between Chinese-made and French-made probes. CaO crucibles are made from chemical agent of CaO powder by isostatic press. The crucibles are fired at 1800°C for 2 hours and cooled in the furnace. A survey of experiments is shown in Table 15.

Experiments are carried out in a carbon tube furnace under the protection of argon with a flow rate of 1.0 to 1.5 l/min. The flow rate is increased to 10 l/min to prevent air entering during the periods of temperature measurement, adding Ce or Nd and sampling. After the experimental temperature is reached, radioactive ^{141}Ce or ^{147}Nd is added several times to the bath, so that a reaction layer of Ce or Nd in CaO or MgO crucible and other particles of Ce or Nd oxide produce there after adhered to this layer. When equilibrium is reached, the oxygen activity of molten steel is measured using a $\text{Zr}_2(\text{MgO})$ oxygen probe. Then the samples are taken by using a quartz tube with an internal diameter of 4.5 to 5.0 mm. The quartz tube is evacuated after it is put into the furnace. Argon is put into prevent the liquid iron from absorbing air. The samples with a length of about 60 to 70 mm are used for electrolysis. Samples are electrolyzed in an organic electrolyte (5 pct triethanolamine, 1 pct tetramethylammonium chloride, 5 pct glycerin and 89 pct methylalcohol) at temperature of -15°C to -20°C; and current density of 50 mA/cm³. The electrolyte is filtered at low temperature immediately after electrolysis. The filtrate is placed on filter paper on the counting pan. After drying the filtrate under a mild heat, the radio activity of the filtrate is determined and the counts are converted into

the content of dissolved /Ce/ or /Nd/ in the samples. The advantages of this experiment are the exclusive of the RE inclusions during the electrolysis and direct determination of the ^{141}Ce or ^{147}Nd in the electrolyte (the amount of dissolved ^{141}Ce or ^{147}Nd in the specimens). Previous work shows that only 0.027 pct of Re oxide inclusions in the steel are broken during the electrolysis [280].

5.4. determination of equilibria between RE and sulphur in molten iron

Desulphurization equilibria for the reaction given by equation (129) have been determined by melting Fe-j-S alloys (j is Ce, La...) in an alumina crucible (96% Al_2O_3 , 3% SiO_2) lined by their sulphide, $j_x\text{S}_y(\text{s})$ of 3 mm thick.



For minimizing the effect of oxygen in the melt, 0.2 to 0.5% of aluminum is added in every heat. Then the melt kept at given temperatures from 1545°C to 1650°C for more than 60 min to reach the equilibrium, is quenched by He jet.

1. Experimental apparatus

A schematic of the reaction chamber is given in Fig. 35

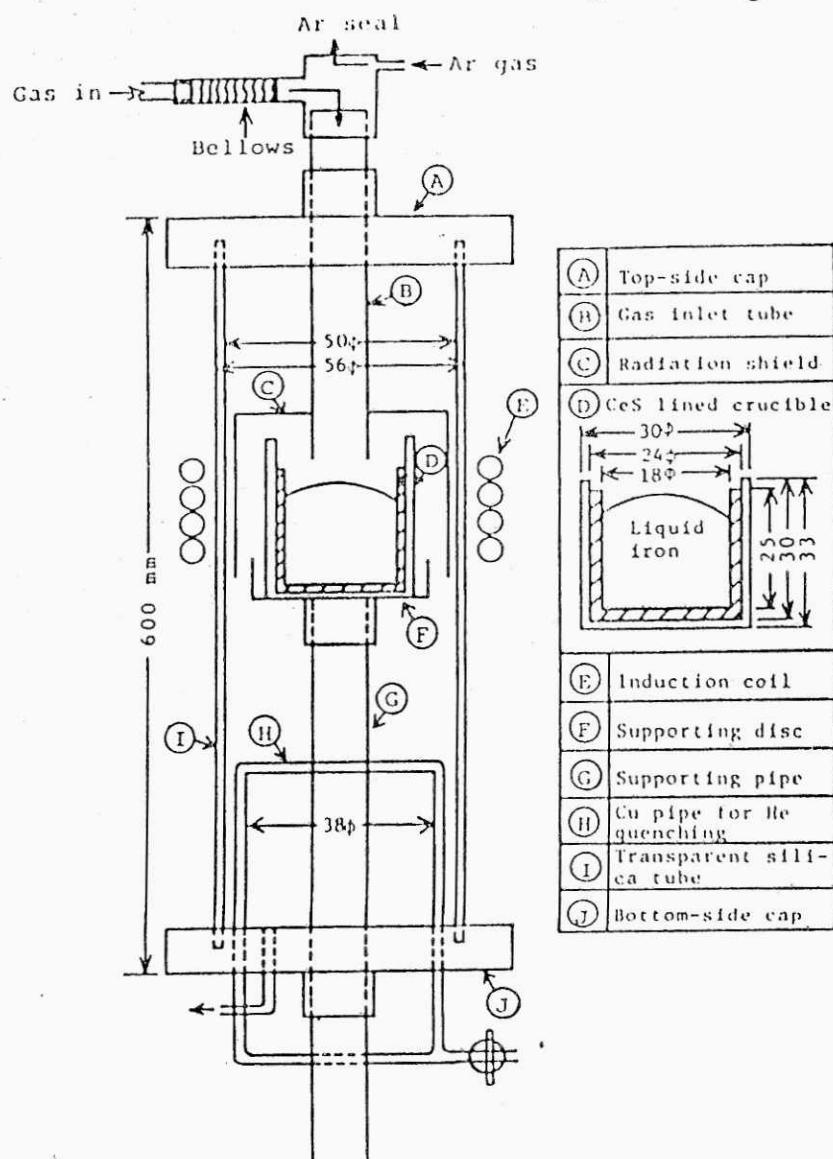


Fig. 35. Reaction chamber

Argon and hydrogen (99.999% supplied from cylinders) are introduced into the chamber after purification to an extent of P_{O_2} lower than 10^{-18} atm and of dew point lower than -60°C . Moisture content in the

mixed gas of Ar + H₂ (200 and 40ml/min respectively) become lower than 1.6.10⁻³ vol% at outlet (lower than -50°C by dew point) when the atmosphere in the chamber is completely replaced by purified Ar after evacuating the chamber to 10⁻³ mmHg. The chamber has an Ar sealing device to add the alloys into the melt without air leak.

2. Synthesis and sintering of sulphides

The sulphides like as LaS, CeS are prepared by heating stoichiometric mixtures of metal and its higher sulphide powders (LaS₂ and CeS₂ purchase from CERAC corp.) in an Ar atmosphere or in vacuum. One of such sulphides thus obtained and CeS block purchase from CERAC Corp., are stamped inner surface of aluminum crucible after pulverizing, and sintering at a temperature of 1200° to 1500°C for 30 to 60 min in high vacuum (10⁻⁴ torr). From the analysis of X-ray diffraction and EPMA of sulphide powder thus obtained the key points to ensure favourable condition.

The summary of sulphide lining is as follows:

1. The use of an Ar box, prevent powder mixtures from being affected by humidity in air.
2. Adding slightly surplus metal powder (about 0.10%) to the stoichiometric ratio.
3. To deoxidize purify Ar furthermore by metal powders is placed in a lower temperature zone of reaction chamber.
4. Temperature of sulphides is to attain raised reduced pressure less than

10^{-4} torr.

A gap about 0.2 mm is observed between sintered sulphide lining and inner surface of the aluminum crucible. The amount of oxysulphides phases in Ce_2O_2S and La_2O_2S lining, however attains to 10 to 20 vol%, which can not be diminished even by taking precise cautions on synthesis. The lining of these sulphides equilibrium study is carried out using the lining thus obtained. It is confirmed that the oxysulphides in the linings has no any detrimental effects on j - S equilibrium as described later. The linings proved to be able to hold the iron melts of about 50g. Any reaction between aluminum crucible and the linings is scarcely observed.

3. Experimental procedure

Iron specimens (about 50 g) are melted in an induction furnace (20kW, 330 kHz) at reduced atmosphere ($Ar+H_2$). The chemical compositions of iron prepared by vacuum melting and re-electrolyzed in a magnesia crucible are C from 0.01 to 0.016%, Si from 0.002 to 0.003%, Mn_{max} of 0.001, P_{max} of 0.002, S from 0.05 to 0.002, $Al_{sol,max}$ of 0.001 $Al_{insol,max}$ of 0.001, O_{max} from 0.0044 to 0.0054%.

Temperature of iron melt is measured by optical pyrometer which is calibrated by a Pt-6pctRh thermocouple immersed in the melt. The calibrated element; j (99.5% purity) is added into the melt in which $/S/$ and $/O/$ contents are controlled by adding FeS and Al, respectively. Subsequently, the iron melt is equilibrated with $j_xS_{y(S)}$ lined on inner surface of aluminum crucible (24 mm ID, 30 mmH) for about 60 min in Ar

atmosphere, and is subjected to quenching by He jet (about 30 NI/min) which ensured it to solidify completely within 10 sec. Cerium and lanthanum in the q quenched specimens are dissolved and are converted into fluoride which are subsequently determined by neo-thorin absorptiometric method [281].

The determination of S, Al and O in sample is determined by atomic absorptiometric method, Al senazo-III-absorptiometric method, combustion-alkali-metric method, atomic absorptiometric method, and by conductmetric method, respectively. Sulphide phases existing at the interface between the lining and the quenched iron ingot is identified by optical microscope, EPMA, and X-ray diffraction. It has been in equilibrium with the iron melt just before quenching.

5.5. Determination of Gibbs energies for formation of RE oxysulphides

The cell assembly is placed in a vertical furnace having an aluminum tube heats and resistance winding. The temperature in the even zone is controlled to ± 1 °K by a thyristor temperature controller. The reference electrode side of the (CaO)ZrO₂ crucible is flushed with purified argon gas for 2 hours before the furnace is switched on. The flow rate is then adjusted to about 100ml/ min. The emf of the cells:



where RE are Ce, La, Nd, Sm, Gd., they are measured in the temperature

range of 870 to 1300°K with a high impedance electrometer model 136 from Princeton Applied Research.

In preliminary experiments, it is found that the emf attain constant values in 2 hours near 1300°K, whereas periods in excess of 12 hours are required near 870°K, probably due to the low partial pressure of sulphur established by the Cu + Cu₂S buffer. It is found that the addition of approximately 0.02g of CaH₂ to the buffer results in quicker response of the cell.

Reversible emf are obtained in approximately 3 hours at 870°K and 0.5 hours at 1300°K. The CaH₂ is expected to react completely with Cu₂S to form CaS, releasing H₂ to the gas phase. The part of this H₂ will be converted to H₂S until the equilibrium ratio of P_{H₂S}/P_{H₂} corresponding to the Cu + Cu₂S buffer is established in the closed crucible. Since the partial pressure of H₂S in the crucible will be higher than that of S₂, H₂S will be the primary species responsible for the transfer of sulphur potential established by the Cu + Cu₂S buffer to the RE₂O₃ + RE₂O₂S electrode via the gas phase. The presence of a small amount of CaS will not alter the sulphur potential of the buffer. Even if compound formation occur in the pseudo-binary system CaS-Cu₂S, there will still be a large excess of Cu₂S at unit activity in the buffer. It shall be note that the buffer action of the Cu + Cu₂S electrode will be maintained only if the oxygen potential established does not alter the composition of the buffer electrode mixture. The equilibrium oxygen potentials in the present study are too low for the formation of Cu₂O. All experimental data report in this paper are obtained with the addition of 0.02 g of CaH₂ to the buffer which weighs approximately 4 g. The reproducibility of the cell emf is checked by

temperature cycling. To ensure cell reversibility, small currents are passed in either direction for short intervals of time and it is verified that the cell emfs return to their original values before the titration. The electrode pellets are examined before and after the experiment by X-ray diffraction. No changes are detected in the diffraction pattern suggesting the absence of significant solid solubility or chemical reaction during the experiments.

Materials for experiments: The RE oxysulphides are prepared by dissolving RE oxides of 99.9 pct purity in 60 pct sulphuric acid. The sulphate crystals so obtained are dehydrated by heating at 900°K. Further heating in air between 1073 and 1223°K produce the oxysulphate. The higher temperatures are used for the higher RE. The oxysulphate are subjected to hydrogen reduction at 1000°K to produce the corresponding oxysulphides. The formation of oxysulphides is confirmed by X-ray diffraction. The cooper sulphide is prepared from elements in evacuated quartz ampules.

Cell assembly for experiments is shown in Fig. 36. An equimolar mixture of the RE oxide and the corresponding oxysulphide is packed into a (CaO)ZrO₂ crucible. An aluminum crucible containing a Cu + Cu₂S mixture in the molar ratio 1:2 buffer is placed inside the (CaO)ZrO₂ crucible. The Cu + Cu₂S buffer is chosen because it establishes a reasonably high sulphur pressure

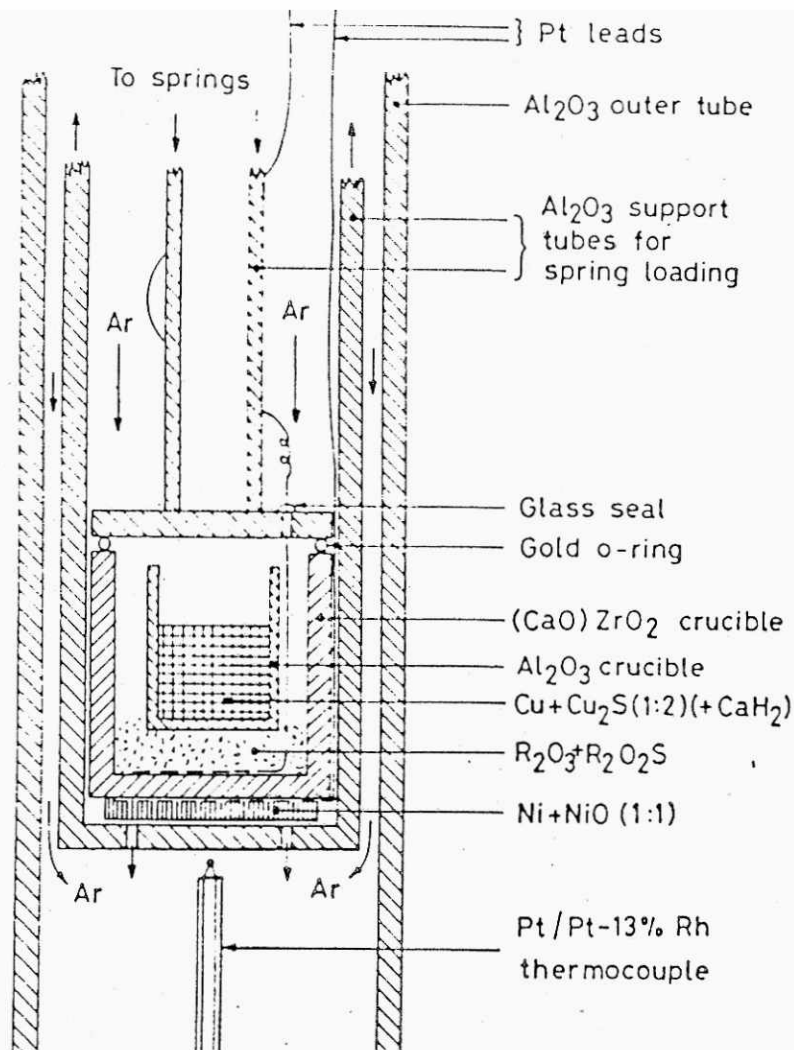


Fig. 36. A schematic diagram of the arrangement of the cell.

for gas transport. The $(\text{CaO})\text{ZrO}_2$ crucible is covered with an aluminum disk. The partial pressure of diatomic sulphur over the RE oxide/oxysulphide mixture is set by the dissociation of Cu_2S to Cu. A closed atmosphere for the dissociation reaction is provided by a gold O-ring placed between the $(\text{CaO})\text{ZrO}_2$ crucible and the aluminum lid. The aperture, which provide the cell design is the physical separation of the sulphur buffer from the RE compounds, so that effects due to solid solubility or chemical reaction between the buffer components and

electrode materials are avoided. The reference electrode is a mixture of Ni + NiO in the molar ratio 1:1 . A platinum wire served as the electrode is chosen as it results in a small cell emf, thus minimizing the electrochemical flux of oxygen through the electrolyte and the resulting polarization effects. The standard Gibbs energy for formation of NiO is well established. The cell assembly is spring loaded by a set of aluminum rods and slabs. The cell temperature is monitored by a Pt/Pt13pctRh thermocouple enclosed in an aluminum sheath.

5.6. Measurement on supersaturation activities of oxygen in Fe-Al-RE

A. Cell construction

A tube-type mullite probe (ϕ 5.0 x ϕ 2.4 x 40 mm) supplies by Nikkato Corporation is made from: $3\text{Al}_2\text{O}_3 \cdot \text{SiO}_2$ coprecipitates by the sol-gel method sinters at 1923 to 1973°K for 2 hours after rubber press. The chemical composition of the mullite probe is: 71.8pct Al_2O_3 , 28.1 pct SiO_2 , 0.06 pct TiO_2 , less than 0.04 pct Na_2O , 0.02 pct K_2O , and 0.04 pct ZrO_2 in mass content. A ZrO_2 -based plug-type (Zr-plug) probe is made as from 9 mol pct MgO and stabilized ZrO_2 rod (ϕ 4.0 x 10 mm) supplies by Nikkato Co. The rod is thick enough to eliminate electrochemical oxygen permeability, and is fixed into a high purity aluminum tube (ϕ 6 x ϕ 4 x 35 mm) with zirconia cement. A molybdenum rod (ϕ 3 mm) protects by a

high purity Al_2O_3 tube is dipped into liquid Fe-Al-RE alloy for measuring the EMF values. By doing so the residual Mo content dissolve in a liquid alloy is in the range of 0.005 to 0.15 mass pct.

B. Apparatus and procedure

A vertical resistance furnace with LaCrO_3 heating bars is used for high purity electrolytic Fe (120g, 99.99 mass pct) and for alloys (Fe 2 or 5 pct Al, Fe 4 or 6 pct RE in mass content) or metal (Mn). They are melted at 1873°K in an aluminum crucible (ϕ 44 x ϕ 39 x 50 mm) under a deoxidized Ar atmosphere (200 ml/min). Argon gas is passed through a purification train of H_2SO_4 , $\text{Mg}(\text{ClO}_4)$, and P_2O_5 , follows by deoxidation with Ti (973°K) and Mg (723°K). The melt is initially stirred for 2 minutes using an aluminum rod. Thereafter, the melt is left for at least 1 hour without stirring. Three or four probes place above the melt are preheated for 10 minutes and each probe is dipped alternately three to five times for each run. After the EMF measurements, the crucible is pulled out of the furnace and quenches rapidly in a He gas stream, follows by water quenching. The EMF is measured with the aid of a high resistance and acid-insoluble Al [282]. Total oxygen contents [283] have been given in previous articles.

The content of total Ce (RE) is determined by an inductively coupled plasma method after dissolving the sample with HCl and HNO_3 . The acid insoluble Ce can not be determined due to the dissolution of Ce containing inclusions by the acid.

5.7. Measurement on solidification microstructure of ingot treating RE

The test specimens are prepared from steels for welded structure melt in furnace(induction or tammann). The specified deoxidizing and alloying elements are added to the steels during tapping. The steels are then subjected to stabilizing for 7 to 10 min. In the early stage of stabilizing total oxygen is held below 20 ppm, then a bar of mischmetal 5.4 mm in diameter and 2 m in length is immersed through the slag layer in the molten steel. The steel bar, rapidly melt near the down comer. Then the molten steel is circulated several times, while making fine composition adjustment. The steel is then poured into molds to make ingots. To improve the properties of the rolled plate, a small quantity of RE is added in the mold immediately before completion of pouring. The concentration of RE in the product of and S (%) in the RE added molten steels is greater than their solubility product ($10 \cdot 10^{-5}$)[284].

This indicates that RES, RE₂O₂S or RE.Al₂O₃ or their composite inclusions have already precipitated in the molten steel. Ingots are longitudinally cut along the central axis. Then an approximately 200 mm thick piece is cut out from mid way between the top and the bottom. Dendritic structure is observed from the surface to the center of the width. Etching is performed with an etchant containing hydrochloric acid, ferric and cupric chlorides.

The spacing, length, deflection angle of dendrite arm, etc. are directly measured using a low power microscope. Photographs are taken and enlarged five times, as a supplementary measure to check the measurement.

Microsegregation of solute elements between the dendrite arm and the interdendritic zone is measured mainly by an electron probe-microanalyzer EPMA (phosphorus which is believed not to be detected accurately by EPMA is remeasured by iron microanalysis IMA)

The main measuring conditions are as follows: EPMA - A beam of electron is focused on a rectangular spot 3 μm wide by 100 μm long by considering the arm spacing of the dendritic structure after transformation. Acceleration voltage is 15 kV, specimen current is 0.05 μA , chart speed is 20 mm/min, and specimen speed is 100 $\mu\text{m}/\text{min}$.

IMA (Iron microanalysis) - O^+_2 is used as the primary ion with the beam diameter being from 200 to 250 $\mu\phi$, ion current is 200 mA, and vacuum in specimen chamber is from 6 to 8.10⁻⁷ torr. To increase the secondary ion yield of p^+ , the specimen is inclined (at approximately 50 deg) during the measurement.

5.8. Determination of equilibrium between the RE, oxygen and sulphur in molten steel

A. Charge material

Electrolyte iron containing about 170 ppm oxygen is used as the base material in the experiments. In the determination of RE -S equilibrium, the iron is deoxidized to about 10 ppm with high purity calcium. The oxygen activity is measured by a $\text{ZrO}_2(\text{MgO})$ solid electrolyte oxygen

probe. The iron is cooled down under argon and its layer removed before use. The FeS used is chemically pure. In equilibrium experiments involving high valency RE sulphides, the (S)/(O) ratio in molten steel shall be between 10 and 100 so as to ensure the formation of the equilibrium product RE_2O_2S [8]. In this experiment, the (S)/(O) ratio is around 15 before RE is added. A number of experiments have shown that in the molten steel (S)/(O) = 10-100.

B. Experimental procedure

Experiments are carried out in a carbon tube furnace under the protection of argon of 99.99 pct purity and iron melts in an MgO crucible. After the (S)/(O) ratio is adjusted to the value given above, the radioactive isotope ^{141}Ce , ^{140}La ,... is added to the bath in batches until sufficient RE_2O_2S can form and adhere to the MgO crucible and float to the surface of the molten steel. When equilibrium is reached, the oxygen activity of molten steel is measured using a $ZrO_2(MgO)$ oxygen probe and a DS 13 integrating digital voltmeter. Details of the experimental technique have already been given in the literature [286].

C. Determination of the radioactive isotopes

^{141}Ce , ^{140}La in the specimens

Samples are electrolyzed in an organic electrolyte (5pct triethanolamine + 1 pct tetramethylammoniumchloride + 5 pct glycerin

89 pct methylalcohol) in a deep freezer. After filtration, the electrolytes and the electrolytic residues after dissolution in acid are radio assayed.

Previous work has shown that, under such electrolytic extraction conditions, the amount of the RE sulphide decomposed during the electrolysis is less than 0.4 pct of the total amount of the RE inclusions, while the amount of the RE oxide decomposed is less than 0.027 pct of the total amount of the RE inclusions [287]. The experimental results of the present work showed that the RE oxysulphide decomposed is less than 0.03 pct of the total amount of the RE oxysulphide inclusions.

D. Determination of sulphur in the specimens

Experiments using a radioactive ^{35}S tracer has proved that almost all of the FeS entered the electrolytic residue during electrolysis. The evolution method for H_2S is therefore first used to determine the total amount of sulphur in the electrolytic residue prior to the determination of ^{141}Ce , ^{140}La by radio assay

The amount of sulphur combined with RES is calculated stoichiometrically according to the different equilibrium products $\text{RE}_2\text{O}_2\text{S}$ (or RE_2S_3). Hence, the sulphur in the form of FeS (which existed in the form of elemental sulphur in the molten steel) is equal to the difference between the total amount of sulphur, $/S/_{\text{total}}$, and the amount $/S/_{\text{inclusion}}$.

E. Determination of equilibrium products

Similar equilibrium experiments are carried out using nonradioactive RE elements. The reaction products which adhered to the crucible and on the surface of the molten steel are submitted to structural analysis using an APD-10 fully automatic X-ray diffractometer.

5.9. Phase analysis of sulphides of RE elements in steel.

1. Identification of RE precipitates

The electrolytically isolated residue is investigated by X-ray diffractometry for the identification of the precipitate. Some representative examples of the precipitate of RE observed by optical microscope are shown in Fig. 37 .

2. Determination of RE by photometric method with arsenazo I

Sample is dissolved in sulphuric acid (1+5) with heating, then REs are precipitated with hydrofluoric acids fluoride, and filtered. The precipitate is decomposed with sulphuric acid and nitric acid, and the color reaction with arsenazo I is used for determination of RE. The isolated residue is melted with potassium disulphate and the melt is dissolved with warm sulphuric acid (1+5). RE are separated as fluoride, and the

determination is completed by the arsenazo I method as described above.

Electron image

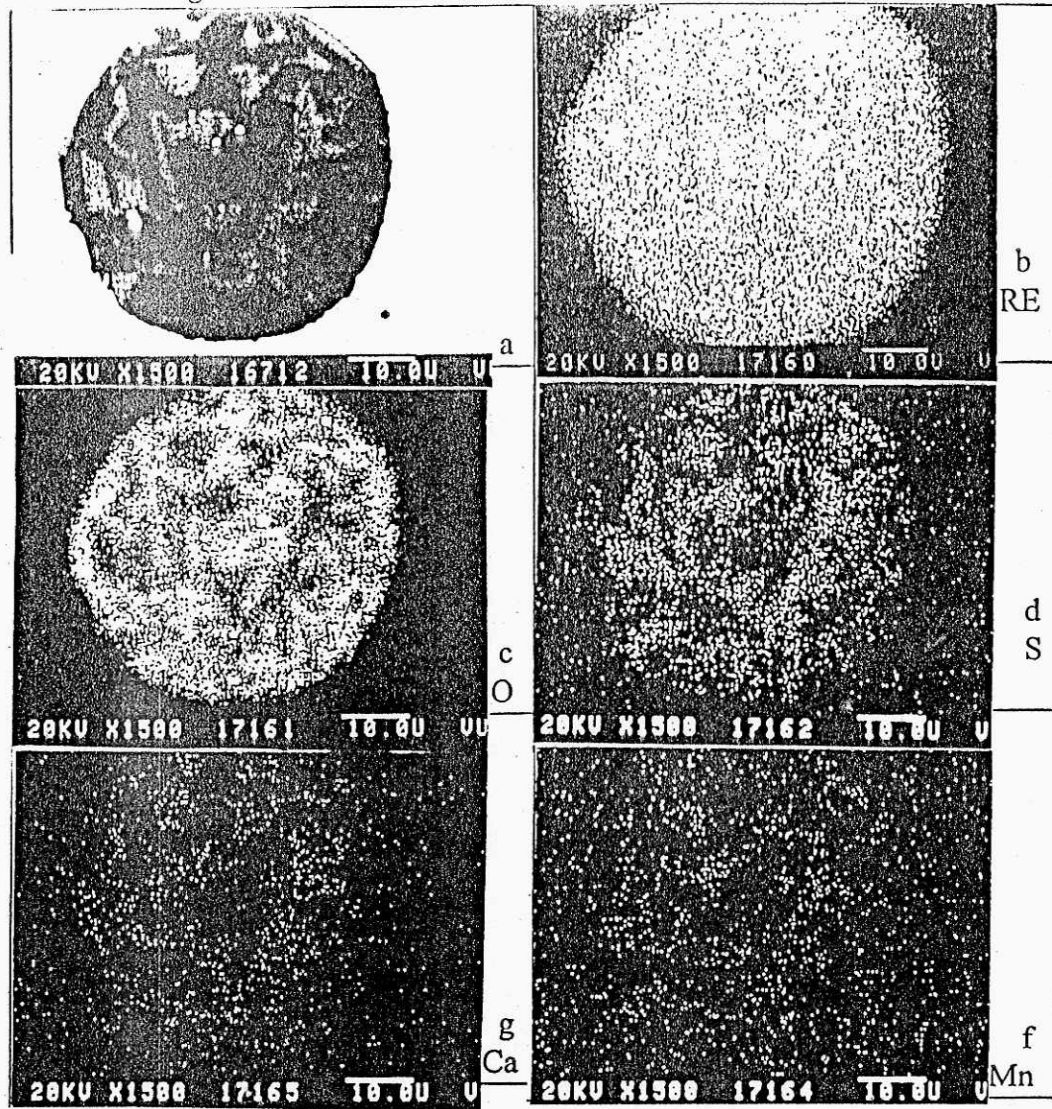


Fig. 37. An inclusion typical in steel after the RE addition

3. The method for isolation of RE precipitates

Methods are as follows: Acid dissolution methods with HCl (1+1), sulphuric acid H₂SO₄ (1+5) and cold HNO₃ [288], halogen-organic solvent method with 10% iodine solution in methanol; electrolytic solution method with electrolyte consisting of 15% sodium citrate, 30% citric acid and 1.2% potassium bromide at pH₃ [289], electrolytic solution method with electrolyte consisting of 5% sodium citrate, 2% potassium bromide and 1% potassium thiocyanate at pH₈ [290]; electrolytic solution method with nonaqueous electrolyte consisting of 5% triethanolamine and 1% tetramethylammonium chloride in methanol [199] which is hereinafter abbreviated as electrolytic solution method in nonaqueous solvent.

The chemical composition for isolation of RE precipitate are given in Table 16. The electrolytic solution method in nonaqueous solvent is studied on constant current densities in the range from 20 to 100m A/cm².

4. Separation and determination of RE sulphides.

The chemical behavior of various synthesized compounds of RE is studied as a preliminary experiment in order to establish a method for separation and determination of RE sulphides from the residue obtained by the electrolytic solution method in nonaqueous solvent.

Table 16. The composition of chemicals used for isolation of RE precipitates

Method	Chemical composition
1	HCl (1+1)
2	H ₂ SO ₄ (1+5)
3	Cold HNO ₃ (1+4); -5°C
4	I-CH ₃ OH 10%
5	Na citrate 5%-KBr 2%-KCNS 1%- electrolysis pH ₈ ; 300mV vs.SCE
6	Na citrate 15%-citrate 30%-Kbr1.2%- electrolysis pH ₃ -300mV vs.SCE
7	(CH ₃ CH ₂ OH) ₃ N5%-(CH ₃) ₄ NCl1%-CH ₃ OH-electrolysis-100mV vs.SCE
8	(CH ₃ CH ₂ OH) ₃ N5%-(CH ₃) ₄ NCl-CH ₃ OH 1%-electrolysis-100mV vs.SCE

The reagents used for decomposition of sulphide are from 50 to 100 mml of methanol containing 10% iodine, 10% bromine, 3% mercury (II) chloride, 3% mercury (II) iodide, 10% mercury (II) nitrate, 0.2% silver sulphate, or 1% silver nitrate, respectively. About 20 mg of synthesized sample is stirred for 40 minutes. The residue is filtered through a nuclepore filter (0.2 μ), and the content of REs are determined on the filtrate and the residue, respectively. The results are shown in Table 17.

Table 17. Chemical behavior of synthesized RE compounds

reagents / compounds	dissolved fraction (%)							
	CeS	La ₂ S ₃	Ce ₂ O ₂ S	CeO ₂	La ₂ O ₃	MnS	MnO	Fe ₃ C
		Ce ₂ S ₃	La ₂ O ₂ S			FeS		
I ₂ -CH ₃ OH/10%	87	100	0	0	0	90	0	0
I ₂ -CH ₃ OH/10%,60°C	95	100	0	0	1	100	21	31
I ₂ -CH ₃ OH/1%	71	90	0	0	0	80	0	0
Br ₂ -CH ₃ OH/10%	100	100	40	0	96	100	96	87
Br ₂ -CH ₃ OH/10%,60°C	100	100	88	0	100	100	100	100
HgCl ₂ .CH ₃ OH/3%	19	0	0	0	0	100	0	0
HgI ₂ .CH ₃ OH/3%	0	0	0	0	0	90	0	0
Hg ₂ (NO ₃) ₂ .CH ₃ OH/10%	19	0	0	0	0	100	0	0
Ag ₂ SO ₄ -CH ₃ OH/0.2%	33	8	0	0	0	28	0	0
AgNO ₃ -CH ₃ OH/3%	100	100	0	0	0	100	0	0
AgNO ₃ -CH ₃ OH/1%	100	100	0	0	0	100	0	0
AgNO ₃ -CH ₃ OH/0.5%	86	73	0	0	0	59	0	0

Sulphide is almost dissolved, while oxysulphides and oxide remain unaffected by treatment with 10% iodine solution in methanol and 1 or 3% silver nitrate solution in methanol often gives abnormal results in the succeeding separations as fluoride a determination of RE, the treatment is unsuitable for separation of sulphide. Thus, the residue obtained by electrolytic solution method in nonaqueous solvent is treated with 10% iodine solution in methanol to dissolve sulphide and leave oxysulphides and oxide as residues. The residues obtain by the electrolytic solution method

in nonaqueous solvent on samples are treated with 10% iodine solution in methanol. After filtration, insoluble residues are examined by X-ray diffractometry.

5.10. Measurement of surface tension

Surface tension measurements of the levitated droplets are carried out at the same time to investigate the possible effects of surface tension variations on the nucleation and crystallization behavior of the metals.

Figure 38 is schematic diagram illustrating the levitation apparatus used in this investigation. Details of the experimental technique used for the measurement of surface tension of levitated droplets and a description of the experimental apparatus have been published elsewhere [291, 192]. The two-color optical pyrometer and chart recorder shown in figure 38; allowed monitoring of the cooling behavior of the sample. In the course of this study, samples weighing 0.2g of electrolytic iron containing (< 0.05 pct O) are used as levitation droplets. Mischmetals of 96.8% RE are incorporated within small holes drilled in the original samples prior to levitation. Hydrogen and helium serve as protective atmospheres as well as effective coolants for controlling the temperature of the molten droplets. The surface tension of samples with and without mischmetal is determined as a function of levitation time in a hydrogen atmosphere at 1700°C.

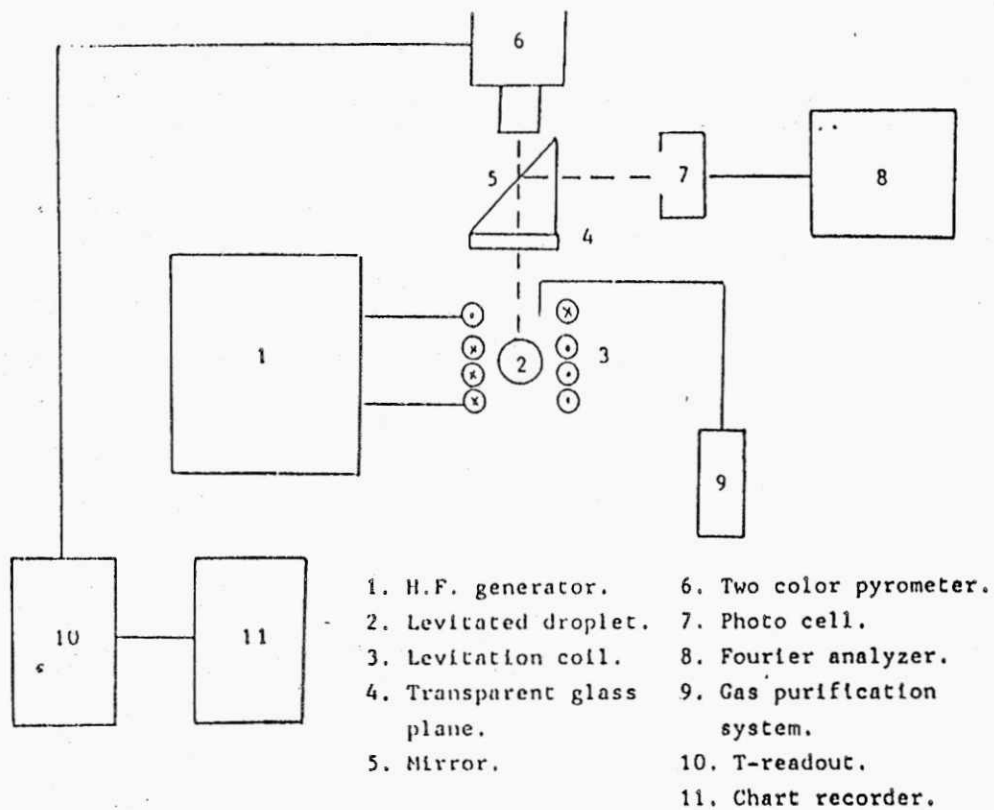


Fig. 38. Schematic diagram of the levitation apparatus

This method is based on Rayleigh's equation [293].

$$\tau = \frac{3}{8} \pi m \cdot w^2 \quad (130)$$

where: τ is the surface tension

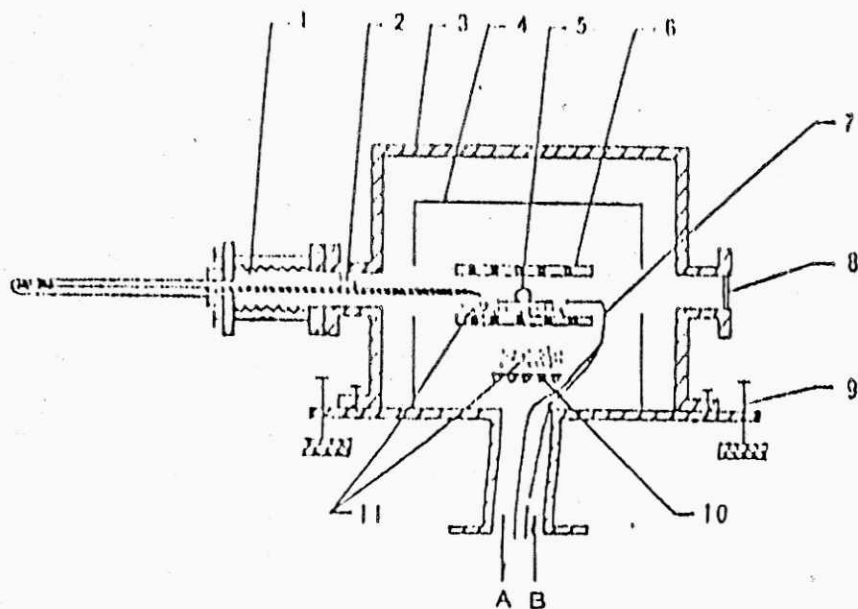
m is the mass of the droplet

w is the oscillation frequency of the droplet measured with the photocell and Fourier analyzer

Measurement of the surface tension by the sessiledrop method

The method has been applied successfully in some works [294-303]. The apparatus consists of: the furnace, the measurement television and microcomputer processing system. The measuring television system in principle is the same as that reported in previous article [296]. The furnace part uses for the liquid iron - RE substrate is shown in figure 39. The measurements are carried out in an argon atmosphere.

The ceramic substrate and the metal sample are cleaned by ultrasonic vibration in acetone for 20 minutes before starting the experiments. The ceramic substrate is then placed in the furnace, its upper surface is leveled carefully. In order to avoid sample oxidation, a vacuum sample conveyer is employed to prevent the gas absorbed in the system from contaminating the alloy melt in the experiment process.



(1) vacuum sample conveyer, (2) position of sample before experiment, (3) furnace and water jacket, (4) reflecting jacket, (5) metal drop and alumina plate, (6) tungsten heater, (7) thermocouple, (8) observation window, (9) leveler, (10) interpurging furnace, (11) purging agent, (A) gas-off, and (B) gas-in.

Fig. 39. Schematic apparatus for measurement of surface tension of liquid iron alloy.

The steel sample containing RE is placed at the tail of a molybdenum channel in the vacuum sample conveyer before heating. After the vacuum is reached 1.1 mPa, the temperature is held to out gas at 1500°C for 10 minutes, during which the highest temperature of the sample in the vacuum sample conveyer is lower than 300°C. The temperature in the furnace is

then lowered to about 1000°C and high purity argon (over 99,999 pct) is flowed into the furnace until 30 kPa. Thereafter, the interrupting system is turned on heating Zircon filling to purge the argon in the furnace for about 40 minutes. Finally the sample is conveyed onto the aluminum substrate, and the dimensions required for the calculation of the surface tension are taken by the measuring television system at the specific temperature. After the experiments, the as-solidified sample is used for the bulk impurity concentration and surface composition analysis.

CHAPTER VI

EXPERIMENTAL

INFLUENCE OF RARE EARTH METALS ON NUCLEATION AND PRECIPITATION OF INCLUSION IN MOLTEN STEEL

6.1. EXPERIMENTAL PROCEDURE

6.1.1. Ingot casting experiments in induction furnace

The experimental arrangement for the casting of five kilogram ingots is carried out in induction furnace of type TOCCO-MELTMASTER model-123 with 60kW, 400V and Ac 2500Hz in MTP Division of National Metallurgical Laboratory Jamshedpur as shown in Fig. 40



Fig. 40, Five kg induction furnace for experiments

Five kilogram electrolytic iron of compositions: 0.03%C, 0.06%Mn, 0.285%Si, 0.053%S, 0.00%Al, 290ppmO and 88ppmN was melted in a basis lined induction furnace and then poured into preheated permanent small iron mould.

Temperature of the melt was measured by two color pyrometer. The temperature of the molten bath varied from 1600°C to 1650°C. The melt was first deoxidized by CaSi (0.1kg/t) and aluminum wire according to Table 18.

The molten bath was stabilized for about 10 minutes and the temperature adjusted to 1660-1680°C. Then SiCe wrapped with aluminum sheet was directly plunged into the bath using a steel plunger. The slag and steel samples of bath were taken before and after addition of SiCe for comparison. After five minutes samples for chemical analysis and inclusion study were prepared by pouring steel melt into small cast iron moulds..

The latest steel sample was poured into ingot iron mould with flux for measuring supercooling by the thermocouple PtRh 13pct. Totality of experiments were 60 as shown in table 18.

Table 18. Experimental amount of cerium addition

sample cerium addition		sample cerium addition		sample cerium addition	
No	(kg/t)	No	(kg/t)	No	(kg/t)
seri A	/%S/=0.01	seri B	/%S/=0.02	seri C	/%S/=0.035
	/%Al/=0.005		/%Al/=0.025		/%Al/=0.070
1	0.15	21	1.10	41	2.10
2	0.20	22	1.20	42	2.20
3	0.25	23	1.30	43	2.30
4	0.30	24	1.40	44	2.40
5	0.35	25	1.50	45	2.50
6	0.40	26	1.60	46	2.60
7	0.45	27	1.65	47	2.75
8	0.50	28	1.70	48	2.90
9	0.55	29	1.75	49	3.05
10	0.60	30	1.80	50	3.20
11	0.70	31	1.85	51	3.35
12	0.80	32	1.90	52	3.50
13	0.90	33	1.95	53	3.65
14	1.00	34	2.00	54	3.80
15	1.10	35	2.05	55	3.95
16	1.20	36	2.10	56	4.10
17	1.30	37	2.20	57	4.25
18	1.40	38	2.30	58	4.40
19	1.50	39	2.40	59	4.55
20	1.60	40	2.50	60	4.70

6.1.2. A study of superheating and supercooling samples

An alumina crucible (99.8%Al₂O₃) was set in carbon tube furnace (Graphite Resistance Furnace; mode 1000-4560 FP-20) as shown in Fig. 41. The furnace was covered by argon gas. The crucible was filled with steel sample taken from induction furnace and flux of the composition given of 76%SiO₂, 8.5%B₂O₃, 4.3%Al₂O₃, 6.7%Na₂CO₃, 4.0%BaO, 0.5%CaO and the it was heated in stream of argon .

The steel was melted to measure the degree of superheating. The heating rate is calculated by furnace programme during 16° to 20°C/min. Total heating time spreaded from 84 to 87 min.

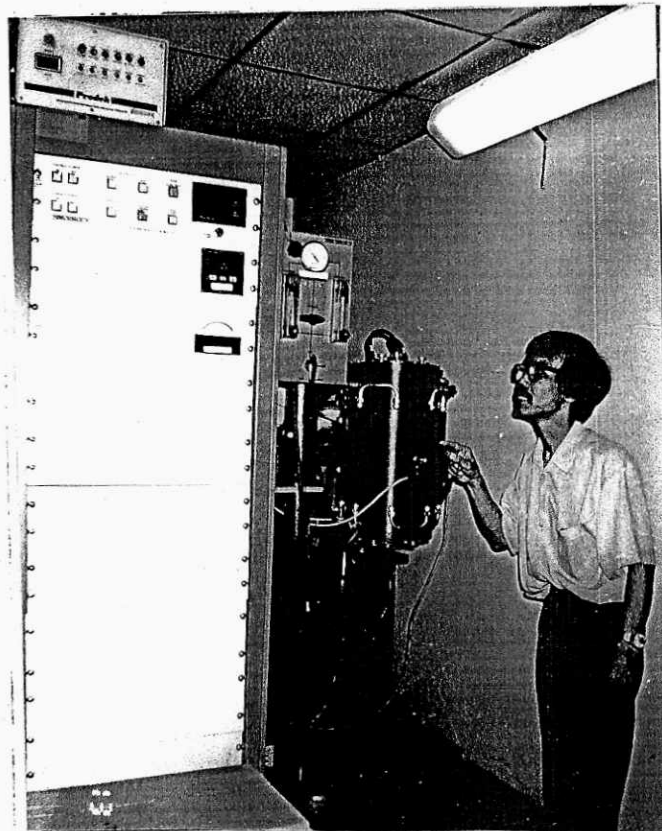


Fig. 41, Graphite resistance furnace mode 1000-4560 FP20

After heating temperature reached 1650°C (measured by thermocouple PtRh13pct), the melt was held for during 10 to 25 min. It was then solidified to measure the degree of supercooling. The constant cooling rate was obtained by inserting automatically in direction furnace box - Prodek with 1 kW (servomotor operated simple phase line voltage corrector).

Under the conditions of the experiment, the cooling rate were obtained according to programme as follows: Heating rate from start to 150°C is $15^{\circ}\text{C}/\text{min}$, from 150° to 1650°C is $15^{\circ}\text{C}/\text{min}$, the totality of heating time is 84-87min), holding at 1650°C from 10 to 25 min thereafter during cooling from 1650° to 1000°C is from 20 to 25 min, the totality of cooling time is 23-27min (it will be cited hereafter in Fig. 58).

The condition of experiments are shown in the Table 19

Table 20 Chemical compositions of steel sample

sample No	chemical content (wt%)									
	C	Mn	Si	P	S	Al _t	O _t	N	Ce	other
0	0.03	0.06	0.285	0.012	0.053	0.003	290	88	0.000	
3	0.005	0.05	0.29	0.018	0.050	0.0032	800	500	0.001	
4	0.03	0.02	0.082	0.021	0.047	0.003	425	320	0.001	
6	0.04	0.05	0.25	0.011	0.050	0.003	720	421	0.002	
11	0.04	0.03	0.25	0.012	0.057	0.0035	796	288	0.002	
13	0.03	0.07	0.35	0.014	0.061	0.003	580	102	0.002	
14	0.03	0.07	0.24	0.011	0.055	0.003	378	315	0.003	
15	0.03	0.06	0.22	0.012	0.055	0.0035	566	329	0.003	
16	0.03	0.06	0.30	0.013	0.056	0.003	400	326	0.003	
21	0.03	0.05	0.28	0.014	0.056	0.003	948	350	0.003	
22	0.03	0.06	0.31	0.009	0.065	0.016	600	320	0.003	
25	0.05	0.07	0.25	0.011	0.063	0.016	782	330	0.003	
26	0.03	0.30	0.27	0.011	0.040	0.050	820	340	0.004	
27	0.14	0.05	0.25	0.011	0.060	0.020	701	77	0.004	
28	0.11	0.05	0.27	0.010	0.060	0.020	780	123	0.004	
33	0.03	0.11	0.30	0.011	0.062	0.044	880	130	0.004	
36	0.03	0.11	0.30	0.011	0.062	0.040	790	128	0.004	
40	0.03	0.17	0.30	0.011	0.060	0.040	875	123	0.004	
42	0.03	0.26	0.995	0.014	0.050	0.050	862	430	0.004	
43	0.11	0.06	0.24	0.012	0.069	0.020	409	103	0.004	
46	0.03	0.30	0.29	0.012	0.040	0.050	800	380	0.004	
47	0.03	0.30	0.30	0.011	0.020	0.050	610	320	0.004	
49	0.05	0.08	0.30	0.013	0.005	0.05	320	307	0.005	
54	0.06	0.24	0.95	0.015	0.005	0.095	390	303	0.005	
57	0.09	0.28	1.14	0.015	0.022	0.125	340	300	0.005	

The chemical composition of slag samples are shown in Table 21

Table 21. Chemical composition of slags

sample	chemical content (wt%)							
	Fe _K	CaO	SiO ₂	P ₂ O ₅	MgO	MnO	Mn ₂ O ₃	TiO ₂
1	25.60	1.10	6.42	0.045	28.85	1.34	13.30	0.07
2	8.10	1.18	7.80	0.055	53.40	0.22	3.08	0.04
3	4.70	3.54	28.18	0.060	15.30	0.20	41.06	1.18
4	2.80	4.16	41.86	0.070	25.84	0.12	19.20	0.76

Before and after measuring superheating and supercooling , the samples were analyzed for macrostructure using microscope of MTC Division National Metallurgical Laboratory which there is type of Leitz MM 6 Macroscope. Macrostructural study was done to determine nucleation and growth of grains of steel and inclusion and segregation of inclusion in the surface of steel samples.

To determine precipitation and morphology of non-metallic inclusions of type I, II, III and IV affecting by RE there was investigation in optical microscope of type Nikkon Microscope system III image in MTC Division of National Metallurgical Laboratory.

Using analytical scanning microscope JEOL JSM 840A/WDS/EDS

of MTC Division of National Metallurgical Laboratory Jamshedpur
SEM and EDX about influence of RE on precipitation of inclusions
and their compositions before and after supercooling was studied. Together
with comparing thermodynamic analysis and calculation of precipitation
and growth of nucleus. This work found out thermodynamic and kinetic
relationship on the acceptance of dates of convinced works publishing
recently. On the basis of this work models was constructed.

6.3. RESULTS AND DISCUSSIONS

6.3.1. Chemical compositions of steel samples

1. Effect of RE on oxygen and nitrogen in steel

At the beginning, content of oxygen was very low (290 ppm). afterwards oxygen content increased in steel to 948ppm. It was completely. Here was perhaps reoxidation of steel took place by furnace atmosphere or air stream around melt bath [304, 305]. From quantity of 948ppmO, this work conducted to study the effect of cerium on oxygen content in steel.

The results of study were shown in Fig. 42.

Fig. 42 shows that the cerium addition into steel have reduced oxygen content from 984 ppm obviously. The experiments were done in opened furnace with continuously and strong stirring melt bath by frequency mixing. So oxygen was absorbed from furnace atmosphere into steel.

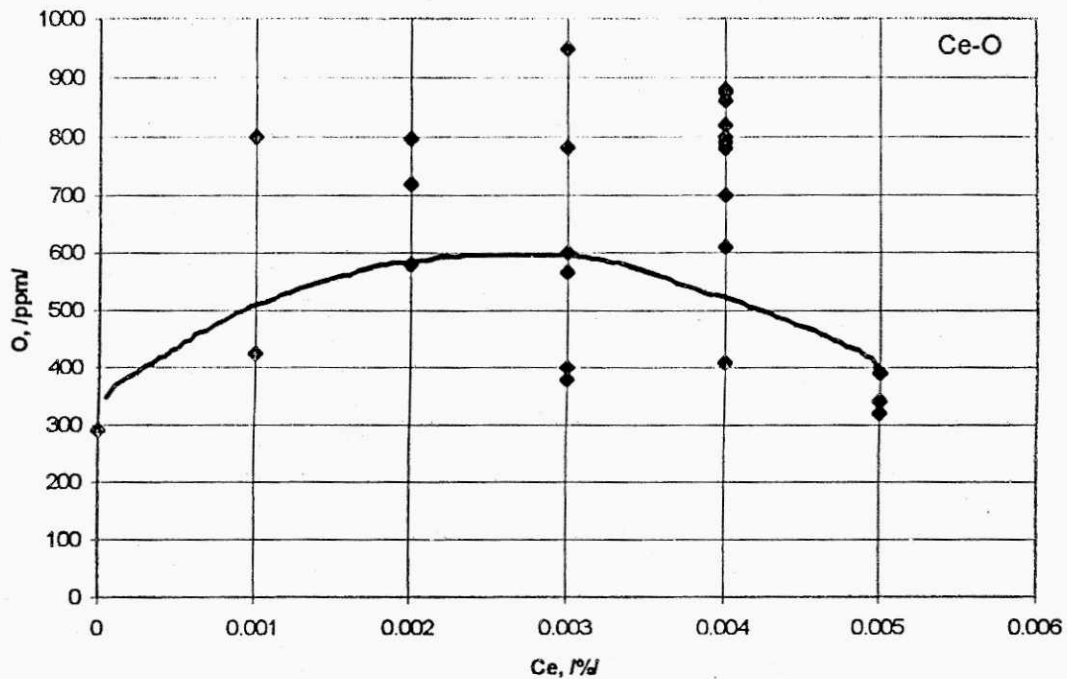


Fig. 42, Effect of cerium on residual content of oxygen in steel

The residual cerium content of 0.005% in steel has decreased residual oxygen content to minimum of 300ppm. The cerium addition affected on deoxidation of steel, because with induction stirring the part of deoxidation product removed into slag. The nitrogen content in steel was very low from the beginning, therefore the was no change during processing.

2. Effect of RE on residual sulphur content in steel

When cerium addition was lower than 0.9 kg/t and cerium content is less than 0.003% cerium did not effect on sulphur content in the steel as shown in Fig. 43.

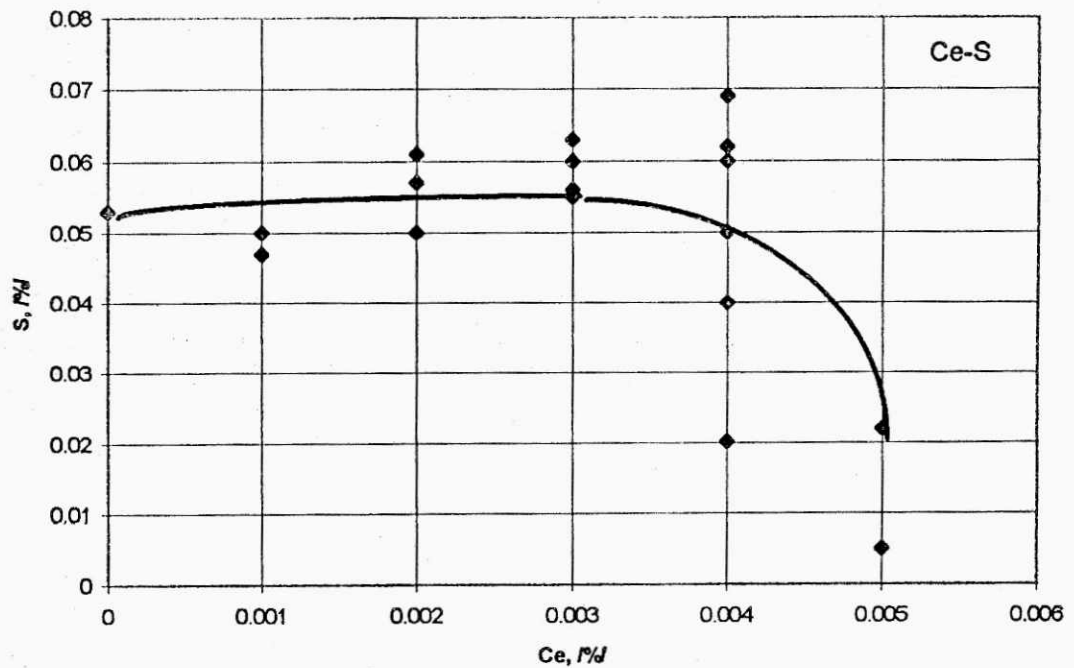


Fig. 43, Effect of cerium on residual sulphur content in steel.

The residual sulphur content decreased with residual cerium content higher than 0.003% and when it was higher than 0.004%, the sulphur content fast reduced. The residual cerium content in steel was 0.005%, the sulphur content in steel was minimum of 0.005%.

The results were also compared with our recent work [306, 308], but these results were specific, because the sulphur content was lower than 0.005%. Therefore it is very much necessary to study reasons for these results. A study of stirring reason was armed according to equation (127). Here induction stirring was strongly refined inclusions to smooth -smaller than 4 μm size and there is also smaller than 2 μm , which subjected to form more cluster, as decreased densities of cerium inclusion to nearly equal iron, then they could be floated into slag owing to induction stirring. The sulphur reduction was examined on the other side, it is the modification of inclusion in steel (will be cited hereafter).

The furnace slags, from Table 21, show that the main composition was MgO from 15.30% to 53.40%, SiO_2 from 6.42 to 41.86%. The slag sample 4 having high percentage of SiO_2 might be here errors of analysis or analyzed in defective place. The slag samples 3 and 4 were unsuitable.

6.3.2. The interaction relationship

1. Relationship between Ce/S ratio and residual oxygen content in steel

In the relationship of RE in steel, the interaction between RE/S ratio and oxygen in steel was very important. It was from basis of thermodynamics and also kinetics of reactions. As the chemical activity of cerium to oxygen and sulphur is high. If each from two elements was presented higher, this element will be occurred reaction with cerium firstly. Especially cerium also absorbed oxygen of atmosphere to take place reoxidation of steel.

Fig. 44 shows that when cerium content in steel was low, Ce/S ratio was low than oxygen content was high. When Ce/S ratio increases the oxygen content will decrease. The Ce/S ratio is equal to one, the oxygen content in steel is minimum (300ppm).

On the base of this interaction relationship, research work chose to direct optimal sulphur content in steel for effective deoxidation by cerium or not use cerium to deoxidate, but use aluminum to instead it

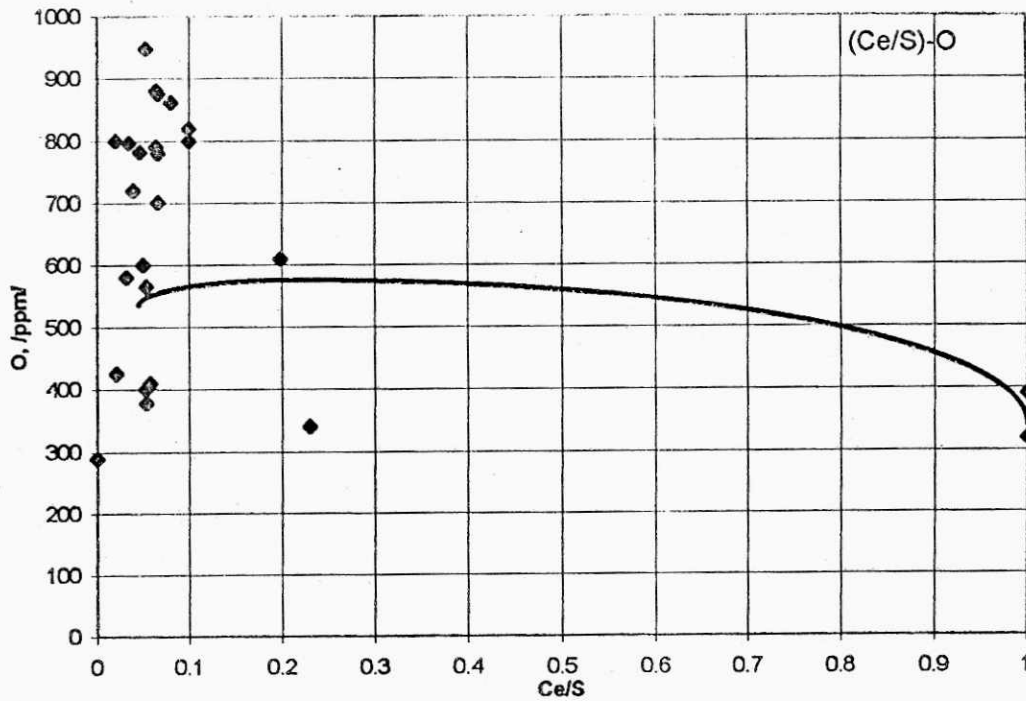


Fig. 44, Relationship between Ce/S ratio and residual oxygen content in steel

2. Relationship between summary of contents (Ce+Al) and sulphur content in steel

The most harmful inclusion in steel is sulphide. When its morphology and distribution are not inconvenient, will have more harmful for machineworkable and using. So metallurgists paid more and more attentions

these inclusions to get clean steel. Commonly from thermodynamic base aluminum is not inconvenient element for desulphurization, because it have more positive free enthalpy of reaction forming Al_2O_3 , therefore this work investigated to push aluminum to reaction together wit cerium in interaction relationship. Actually main idea of this question is that firstly aluminum reacts strongly with sulphur. Total result is obvious desulphurization occurred. Fig. 45 shows that sulphur content decreased obviously and very characteristic.

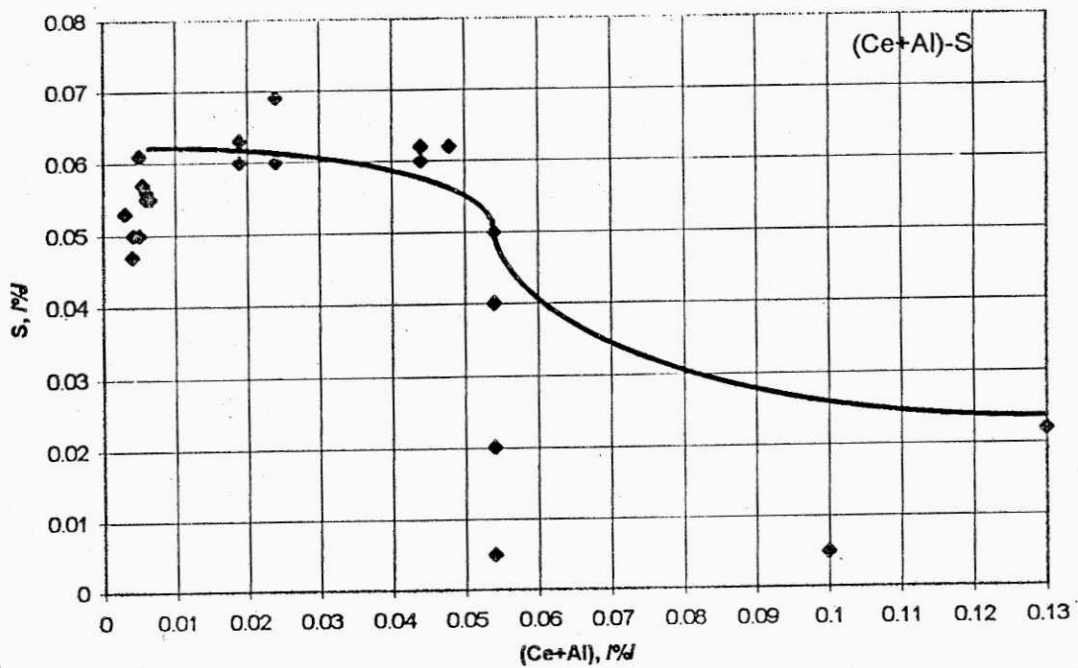


Fig. 45 Relationship between Ce+Al and sulphur content in steel

It means a study of combination of cerium and aluminum in desulphurization was beneficial.

3. Relationship between Ce+Al and oxygen content in steel

Similar relationship of desulphurization cerium is strong active to sulphur and the same absorbed oxygen element, so after deoxidation by aluminum, then residual oxygen continuously reacts with cerium and forms oxysulphide. When inconvenient reaction took place with induction stirring, the oxygen content in steel decreased very clearly (Fig.46).

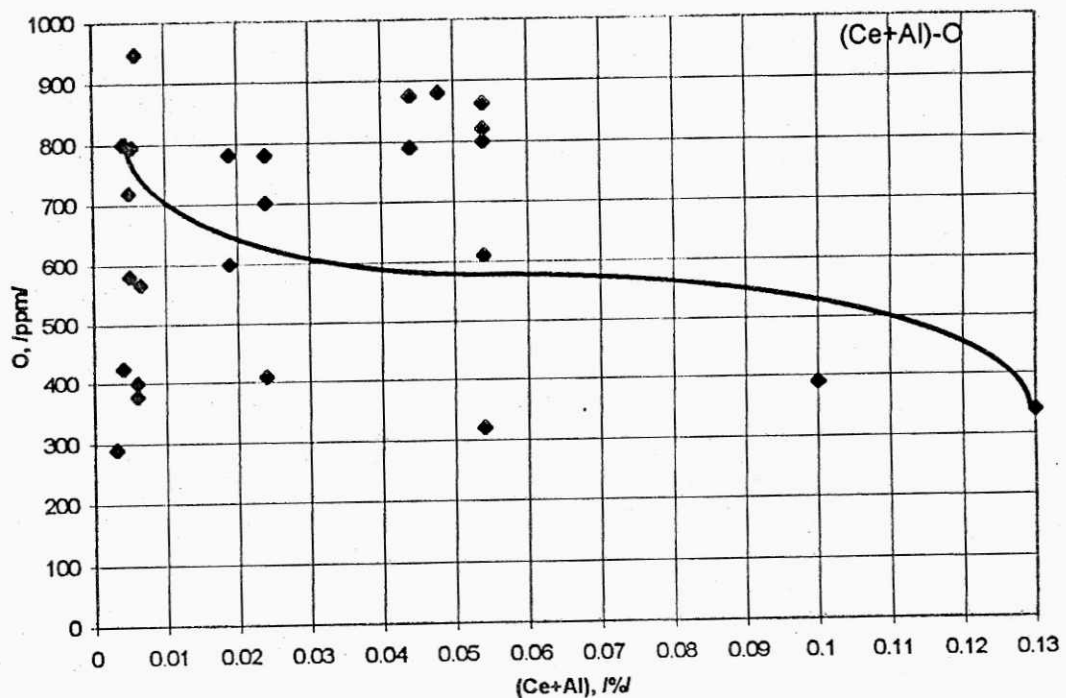


Fig. 46, relationship between Ce+Al and residual oxygen content in steel

4. Relationship between Al+Si/Ce ratio and oxygen content in steel

The heterogeneous inclusion of type IIIb containing cerium exists very specially. In these inclusion there are compositions of aluminum and silicon. Here there is interaction of aluminum, silicon and cerium combining. The result is shown in Fig. 47.

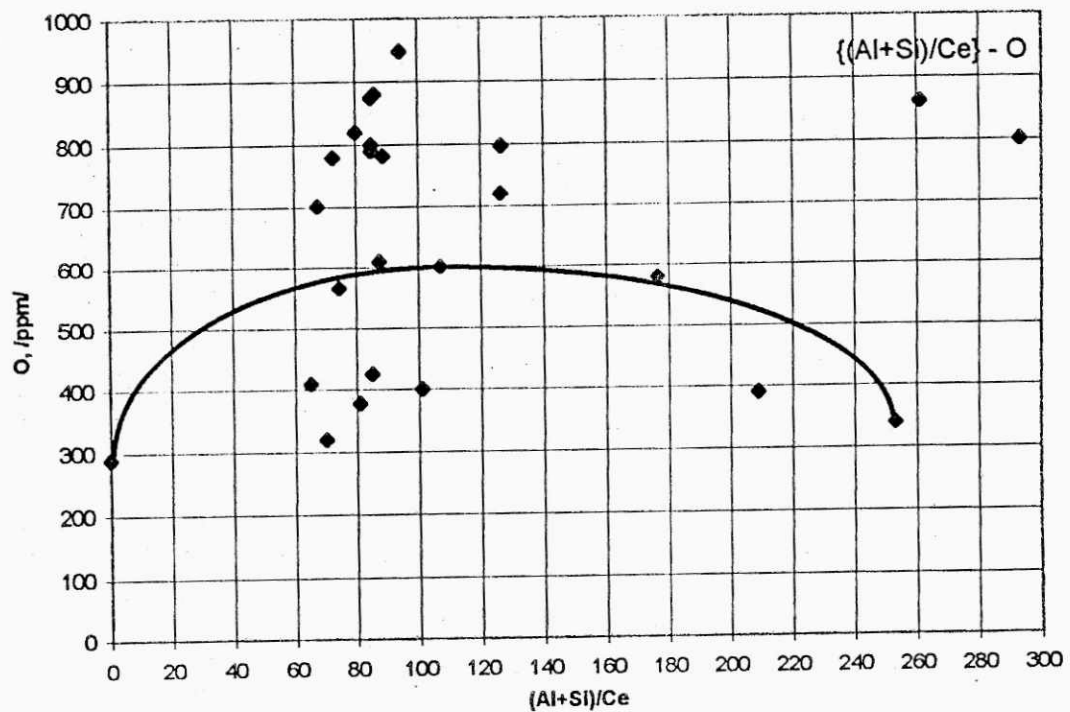


Fig. 47 Relationship between Al+Si/Ce ratio and oxygen content in steel

5. Relationship between Al+Si/Ce ratio and sulphur content in steel

Fig. 48 shows Al+Si/Ce affected negligibly on sulphur content in steel.

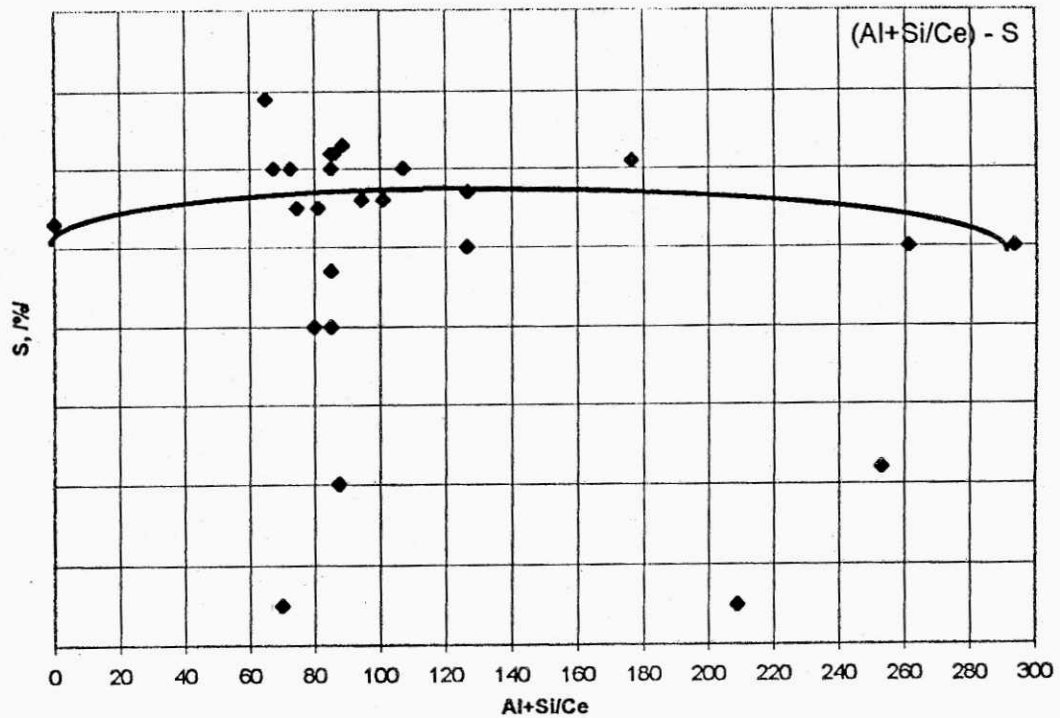


Fig. 48, Relationship between Al+Si/Ce and sulphur content in steel

Here this work discussed on inclusion side (will be cited hereafter).

This result was contrary to previous works [19,20,309]. This work will be continuously investigated.

Fig. 47 shows that when the ratio of Al+Si is higher than 120, the oxygen content in steel decrease obviously. Here silicon from SiCe and CaSi affected on deoxidation. This result was discussed in recent works [18-21]. This result is necessary for using FeSiCe and SiCe, because there were some contrary discussions and conclusions. Actually here silicon together with aluminum reacted interaction in heterogeneous inclusion and formed less harmful inclusion for machineworkability and the use.

6.3.3. The results of supercooling

1. Effect of cerium addition on cooling time

The result was shown in Fig. 49.

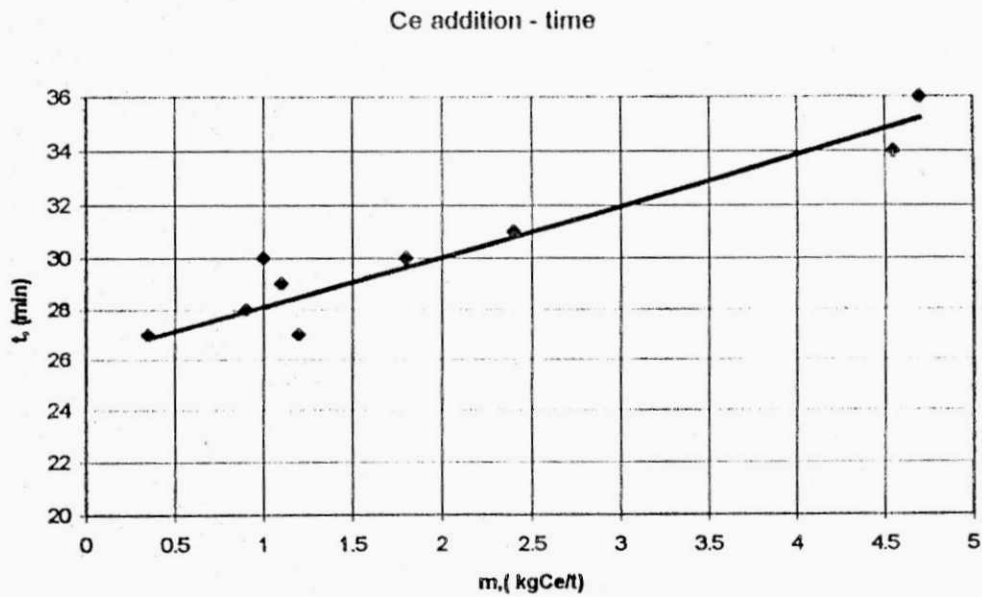


Fig. 49, Effect of cerium addition on cooling time

Fig. 49 shows that more is the cerium addition slowly is the cooling time. When cerium addition is 0.5 kg/t the cooling time was 27 min , with the increase of cerium addition to 4.25 kg/t, the cooling time increased to 36 min. This relation was needed to study more than these data to receive convinied results.

2. Effect of residual cerium content on supercooling

The result is shown in Fig. 50. Fig. 50 shows that cooling is very special.

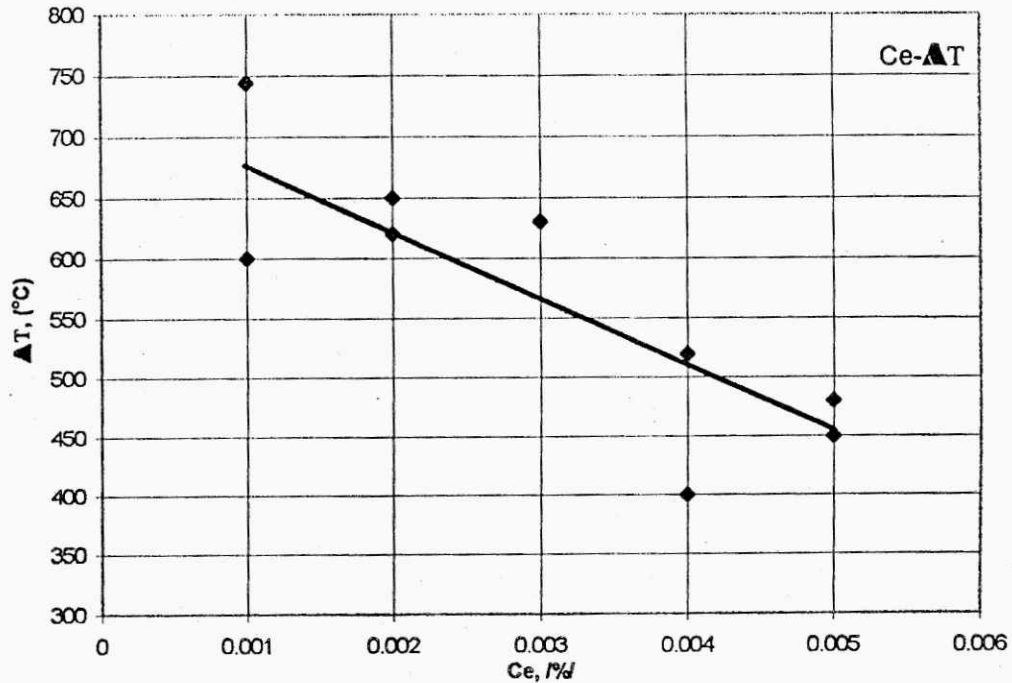


Fig. 50 Effect of cerium content on degree of supercooling

It is relation of straight line. It means the increase of cerium content more is the increase of degree of supercooling. With cerium content in steel of 0.004% the lowest degree of supercooling attained 400°C. A study of these influences is very important for investigation of nucleation of inclusion. Especially effect of cerium on growth of nucleus

and size of inclusion in steel. The refine and distribution of inclusions depended more on degree of supercooling of steel.

3. Relationship between EMF and cooling time

It is effect of degree of supercooling on variation of EMF (see Fig.51)

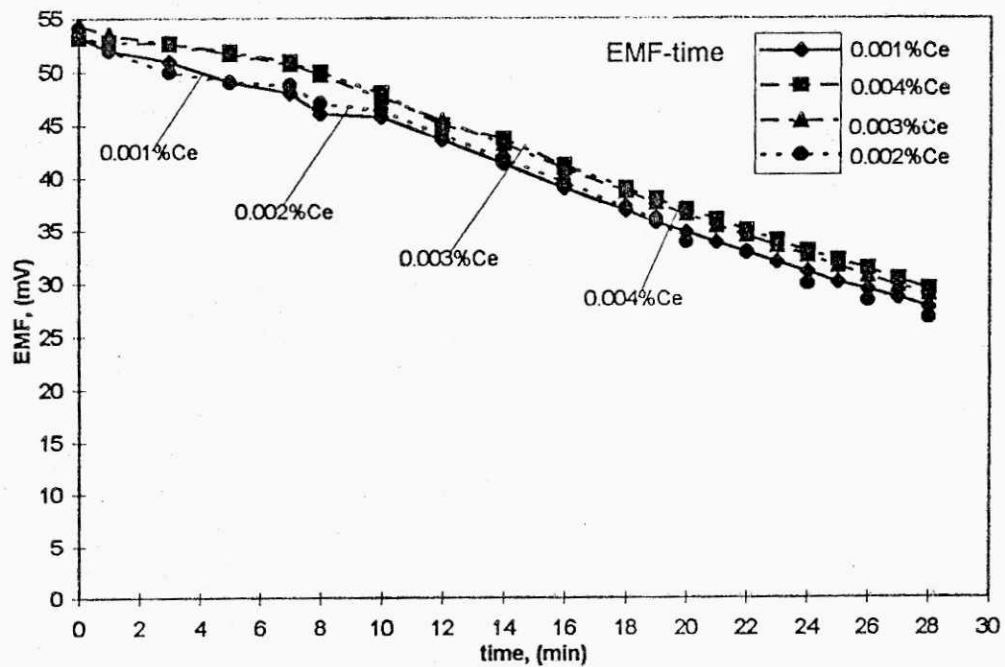


Fig. 51, Relationship between EMF and cooling time

Fig. 51 shows that the EMF decreased with cooling time. The decrease of EMF depends on cerium content in steel. It means when

residual cerium content is low, the EMF decrease is faster when cerium content is high the EMF decrease is lower. Really in Fig. 51 there is less difference. It might be obtained without central and concrete results. Here it needs to be considered important, that cerium affected to EMF decrease. It influenced strongly in side of nucleation and growth of inclusion nucleus.

Fig. 51 was plotted for samples, with same kind of weight (50g). Here the decrease of EMF was 26.5 mV with sample of 0.001% Cerium and 22 mV with sample of 0.004% Cerium after 27 min. The influence of covering flux was also important because the samples of 0.003% Cerium and 0.004% Cerium without covering flux resulted obviously on the decrease of EMF.

When sample weight increased to 60 g, the decrease of EMF was great of 28.9 mV after 30 min (see Fig. 52)

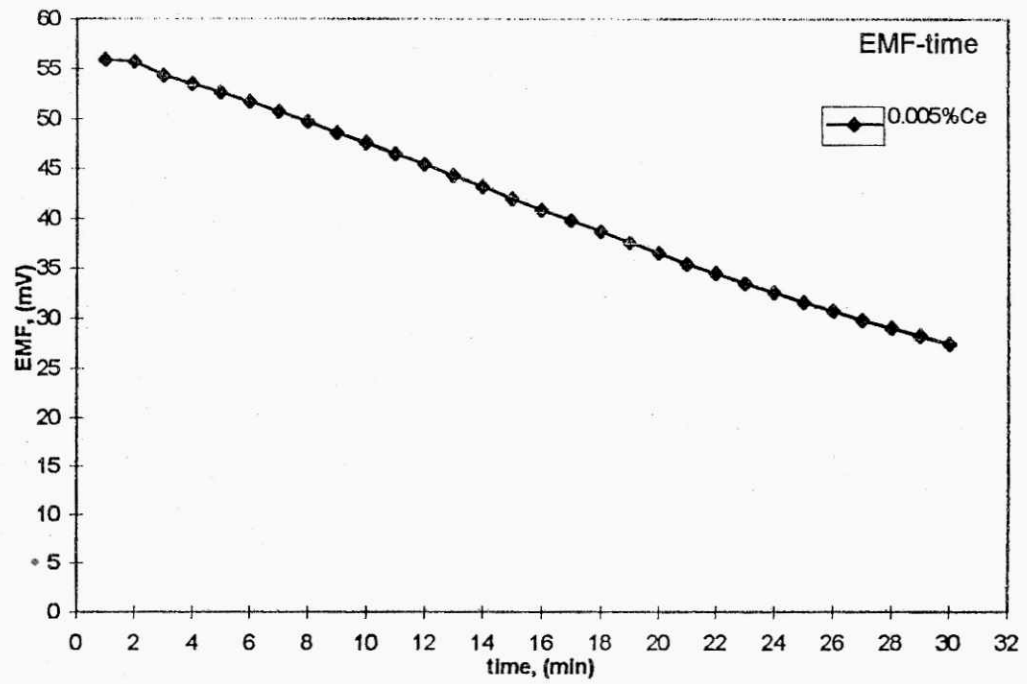


Fig. 52, Relationship between EMF and cooling time of 60g sample without flux cover.

The flux cover affected on 70g sample as shown in Fig. 53.

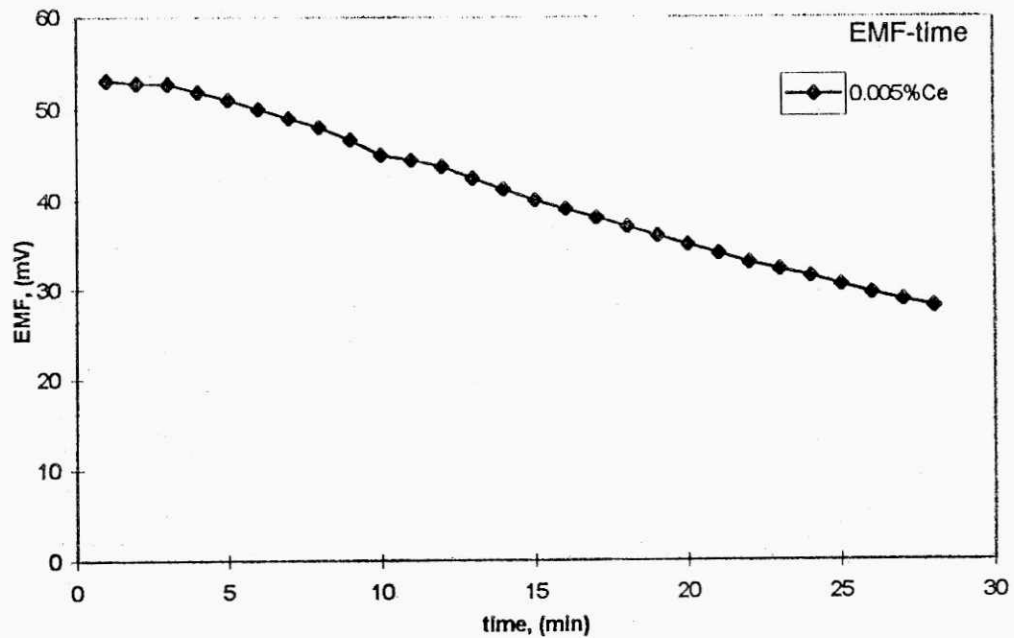


Fig. 53, Relationship between EMF and cooling time of 70g sample with flux cover.

Fig. 53 shows that the increase of samples weight with good flux cover resulted slow decrease EMF of supercooling, e.g. obtained 24.4 mV after 27 min. This result was found in Fig. 54.

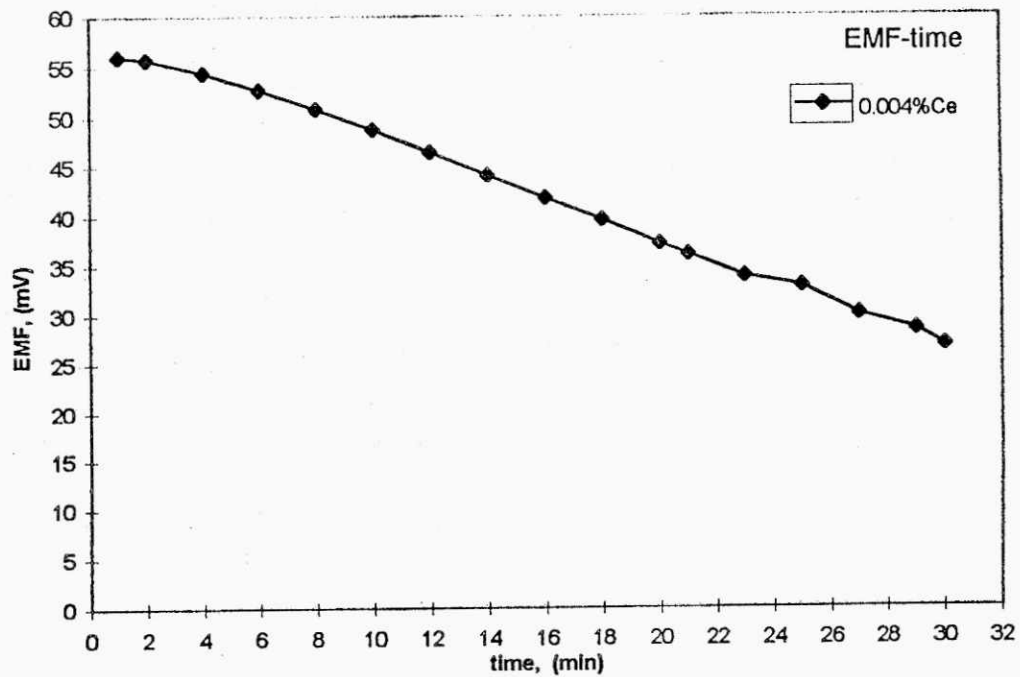


Fig. 54, Relationship between EMF and cooling time of 81g sample with flux cover.

4. Relationship between cooling temperature and time

It is a characteristic relation for influence of cerium on degree of supercooling of solidification of steel. Hence it can be known

clearer effect of cerium on characters of nucleation of non-metallic inclusion in steel. The result was shown in Fig. 55.

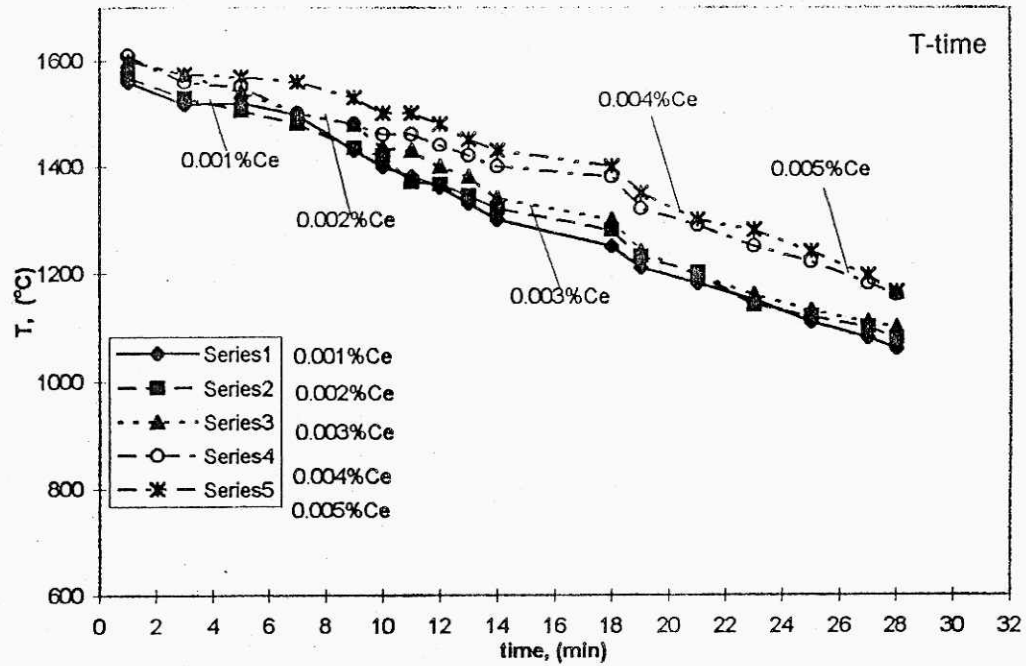


Fig. 55, Relationship between EMF and cooling temperature and time with 50g samples and difference of cerium content

Fig. 55 obviously shows when high cerium content in steel, the cooling temperature also was high. Generally after 12 min cooling the inclusion in steel begun nucleation [249].

The temperature of sample was 1385°C for 0.001%Ce, 1400°C for 0.002%Ce, 1410°C for 0.003%Ce, 1415°C for 0.004%Ce and 1430°C for 0.005%Ce.

These results might be had low exact degree causing from measurement in machines, but features were observed effect of cerium on nucleation of inclusion nucleus in steel. The samples weight did not affect on cooling temperature (see Fig.56).

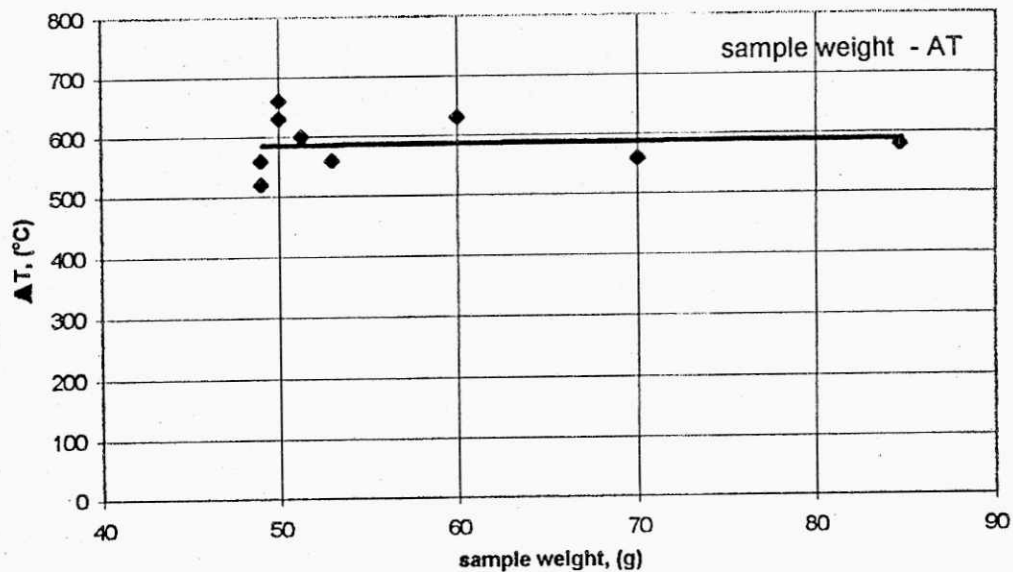


Fig. 56 Effect of sample weight on cooling temperature

Fig. 56 shows the relation was straight line. It means no change of relation. This result was different from previous work of Ohashi

[249]. The work will be fill in more than experiments to prove high belief. This work measured degree of supercooling of 50g samples with different cerium content in steel to clear influence of cerium on superheating. The results were shown in Fig. 57.

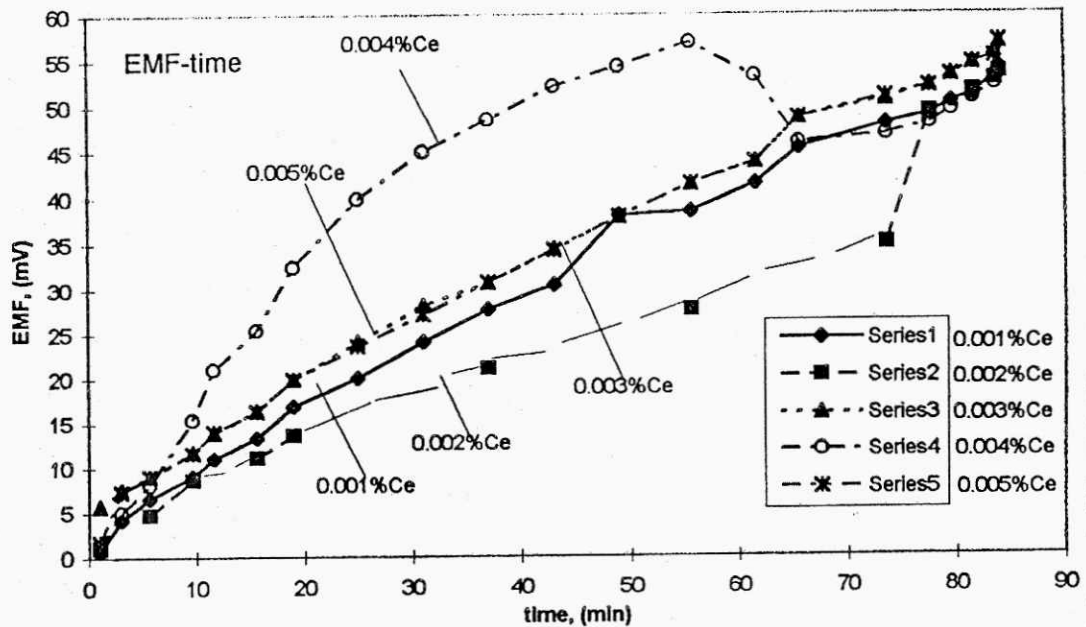


Fig. 57, Relationship between EMF and heating time of 50g samples with different cerium content.

Fig. 57 shows that the sample of 0.002%Ce had the lowest increase of EMF and sample of 0.004% Ce had the highest increase of EMF. The samples of 0.003%Ce and 0.005% Ce had same line to 70 min, after 70

minutes they had relation that more is the increase of cerium content, more is the increase of EMF.

Before 70 minutes there was difference of relation, which may be explained for effect of flux cover. The concrete samples with flux cover and difference of cerium contents were plotted affective curves in Fig. 58.

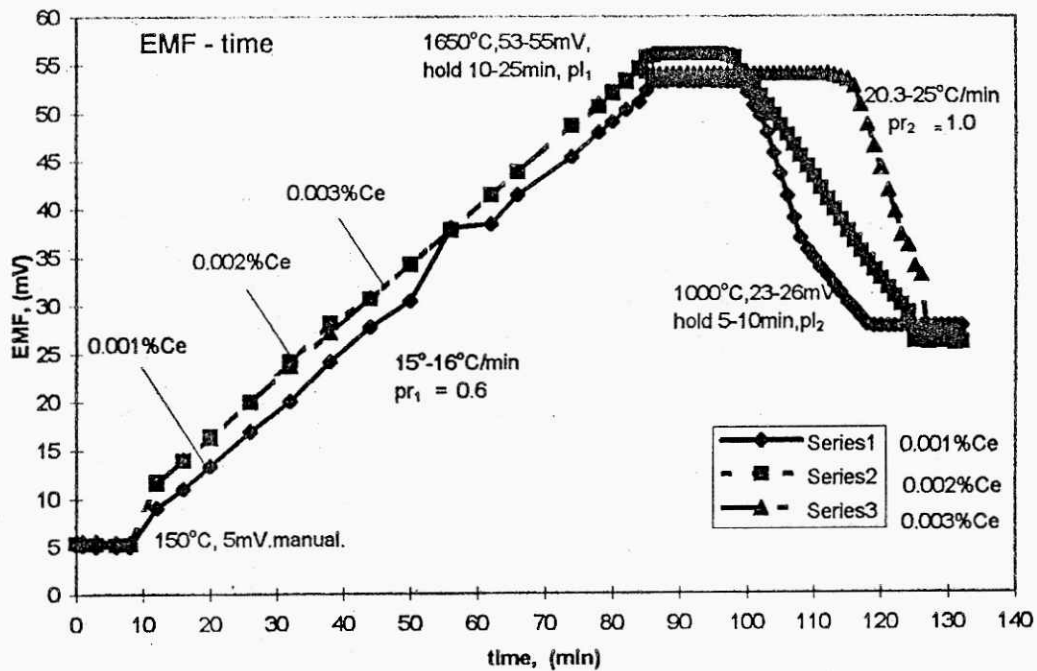


Fig. 58, Effect of cerium content on superheating and supercooling.

6.3.4. Effect of cerium on macrostructure of steel

The samples without cerium were shown in Fig. 59.

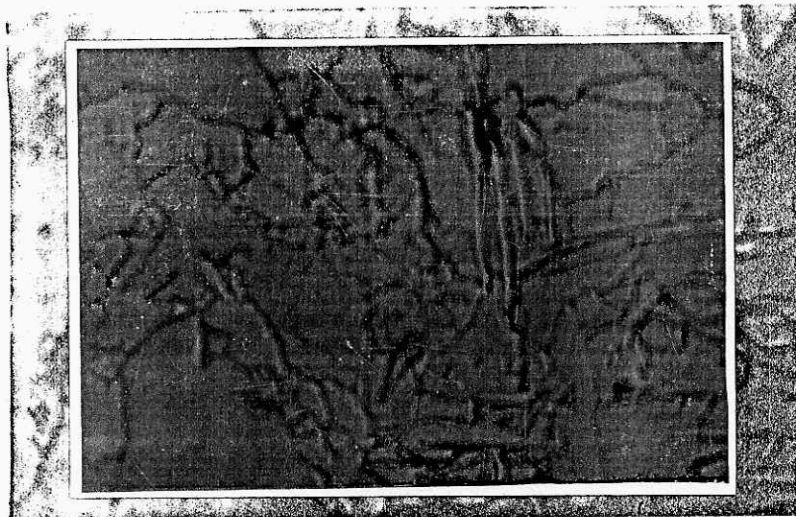


Fig. 59 Macrostructure of steel sample S₁, without cerium, 500x

Fig. 59 shows that the crystal grains were columnar with size according to ASTM from 4 to 5 μ macrostructure. In the grains existed inclusions. The cerium addition with residual content of 0.002%Ce took place change of crystal structure. The cerium refined grain, the columnar grains decreased. The inclusions were distributed interior of grain, which were morphologied small-smooth inclusions of type Ib. The grain boundaries changed from rough to thinner (see Fig. 60).

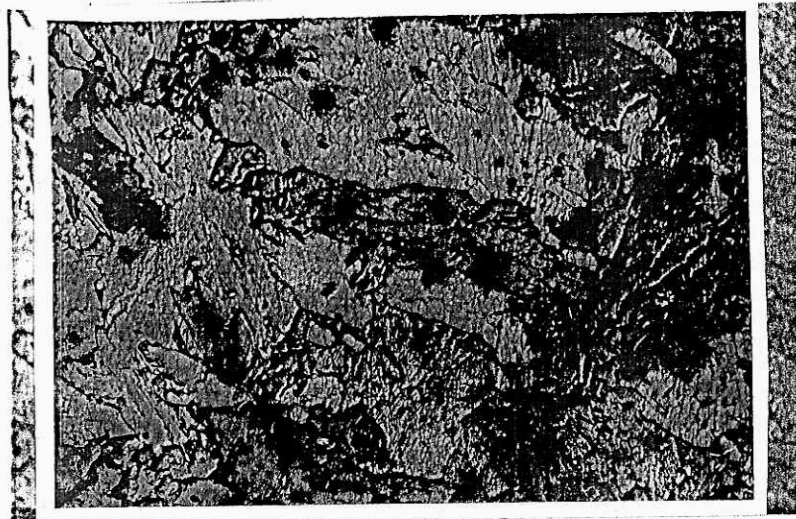


Fig. 60, Macrostructure of steel sample S₁₁, with 0.002%Ce,
500x

When the cerium content increased to 0.003%, the columnar grains near hardly disappeared (see Fig. 61). The inclusion lying near grain boundaries coalesced and heterogeneous inclusions observed clearer. The space of grain boundaries was larger.

The continuous increase of cerium content to 0.004% (see Fig.62) was done bolder grain boundaries, the inclusions appeared more than. Meantime, the inclusions treadle moved to this samples begun to change crystal structure from columnar to polygonal.

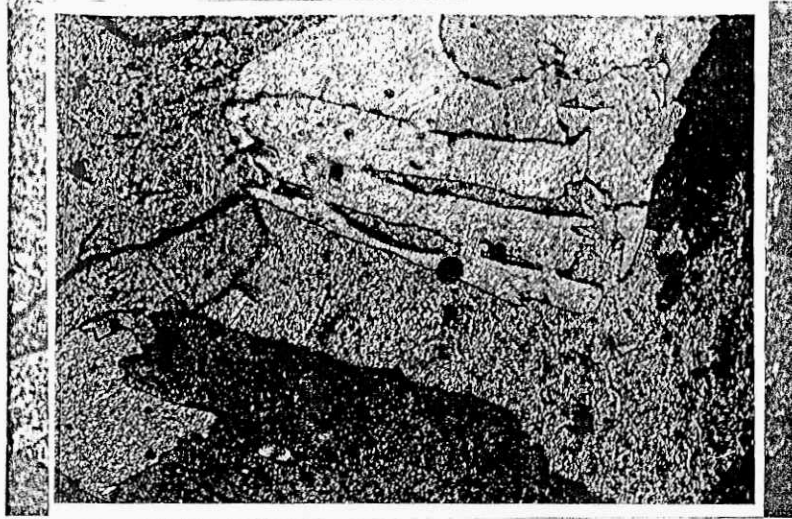


Fig. 61, Macrostructure of steel sample S₁₅, with 0.003%Ce, 500x

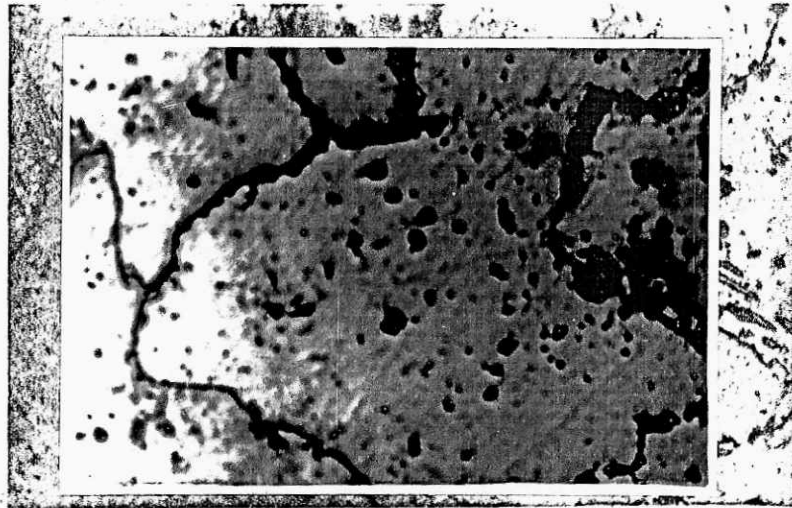


Fig. 62, Macrostructure of steel sample S₂₈, with 0.004%Ce, 500x

When the cerium content in steel is 0.005%, the samples showed polygonal grains. In grain there were more small-smooth globular inclusions. Here the matrix and grain boundaries was observed clearer (see Fig. 63).

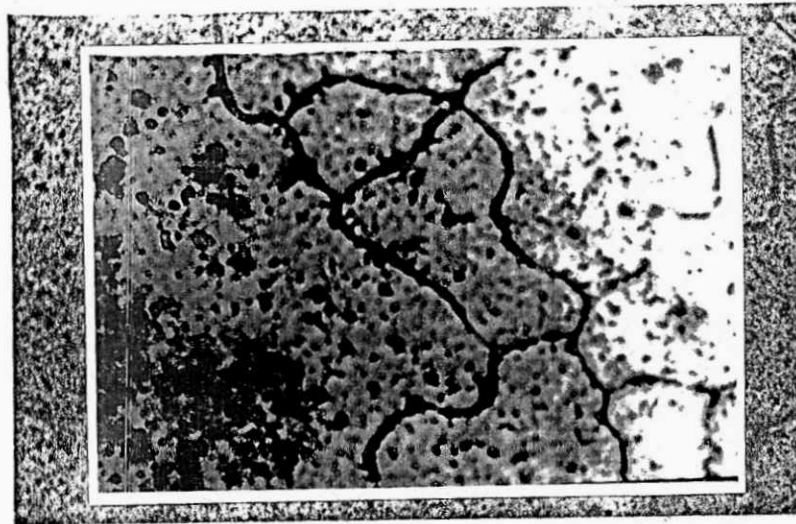


Fig. 63, Macrostructure of steel sample S_{54} , with 0.005%Ce, 500x
As with increase of cerium content in steel the structural transformation of crystals and inclusion will be done.

Although residual cerium contents in steel were only analyzed to 0.005%, but the cerium content according to predetermination of samples from 40 to 60 will be from 0.04% to 0.08%. Here might be caused from dissolution of cerium into this steel very low.

The macrostructures reverted that in these inclusions existed cerium compositions (will be cited hereafter) with high content, so they had t end to form clusters. This is obvious characteristics of the existence of high cerium in steel, that more recent works were proved [18-21, 306-309]. According to these works the cerium content was higher than 0.06%, the cluster inclusion formed.

6.3.5. Effect of rare earth metals on morphology of inclusion in steel

The steel sample containing 0.053%SAMPLES was observed inclusion morphologizing according to qualifying of type II. It was ribbon-stringer sulphides lying in grain boundaries (see Fig. 64)
The cerium content was presented in steel of 0.003%, which occurred formation of small-smooth globular inclusions of type Ib (see Fig.65)

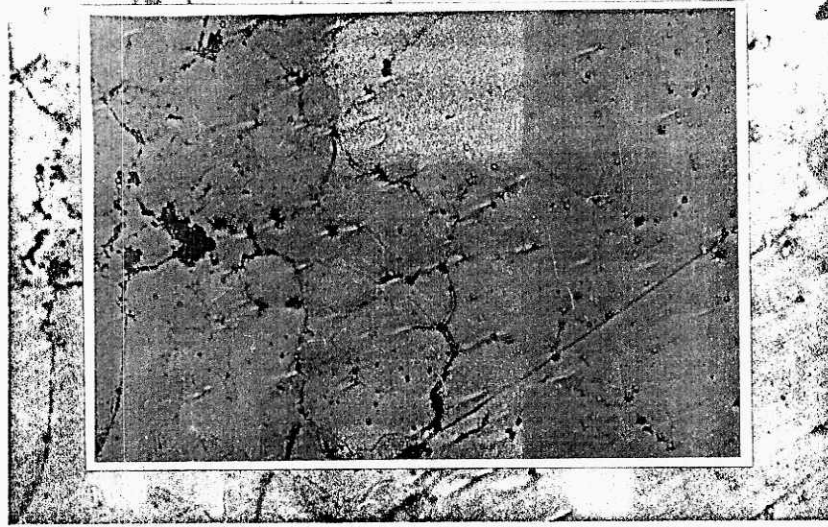


Fig. 64, Microstructure of steel sample S_A, containing 0.053%S and without cerium, 500x.

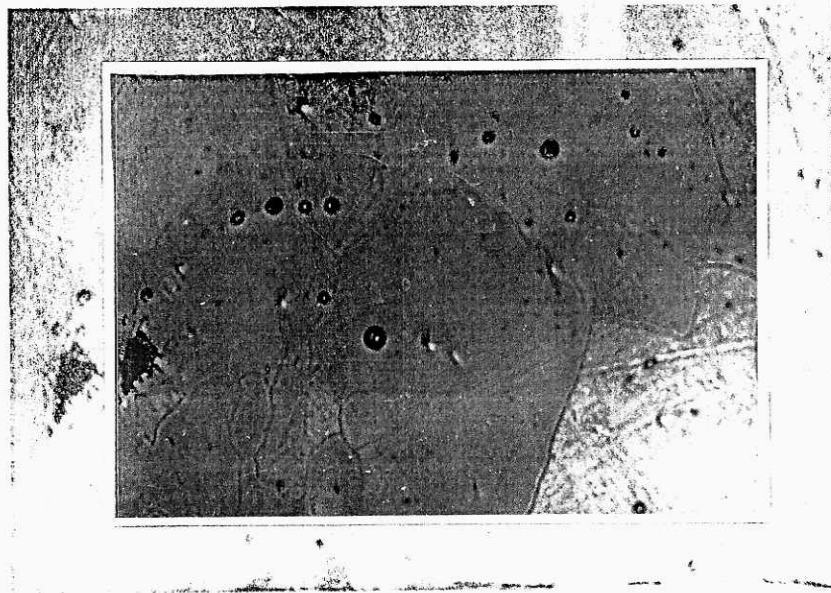


Fig. 65, Microstructure of steel sample S₁₅, with 0.003%Ce showing inclusions of type Ib, 500x.

Fig. 65 shows globular inclusions having two parts, the core inclusion in steel bright and the shell inclusion in steel dark. Commonly formed oxysulphide core and sulphide shell [309].

When high aluminum content in steel and increase of cerium additions into steel formed heterogeneous angular inclusions of type IIIb (see Fig. 66)

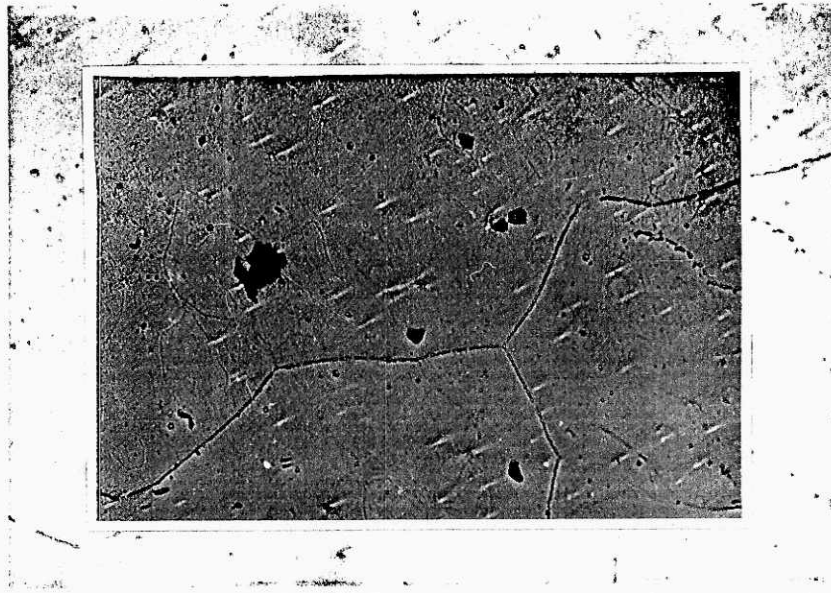


Fig. 66, Microstructure of steel sample S₂₈, with 0.004%Ce showing inclusions of type IIIb, 500x.

The increase of cerium content in steel to 0.005% appeared great amount of small-smooth globular inclusions with tendency to form inclusion cluster (see Fig.67)

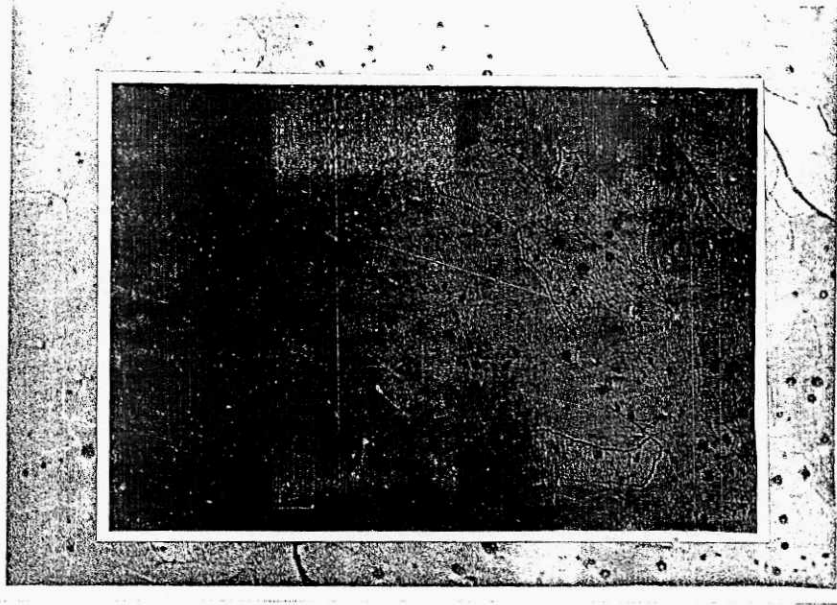


Fig. 67, Microstructure of steel sample S₅₄, with 0.005%Ce showing inclusions of type Ib and tending to form inclusion cluster 500x.

Here there are two part inclusions. This problem proved that they were cerium inclusions. Here, the cerium affected surface tension of inclusions, especially suppresses and restricts surface activity of MnS. The cerium oxides and sulphides are thermodynamically stable. The value of surface tension of cerium inclusion was very high, and therefore have not grown in size of inclusion modification. It was kinetic character.

Mainly, this kinetic character occurred to formation of great inclusion amount having small-smooth size. The part formed cluster and could be floatated into slag, the other part existed in interior grain, which occurred unclean steel.

6.3.6. SEM and EDX analytical results of inclusion in steel

In the Table 18 there were 3 series of samples. Every series took beginning sample without cerium marking S_A , S_B , S_C . The samples S_A observed globular inclusions of type I in interior grain as shown in Fig.68

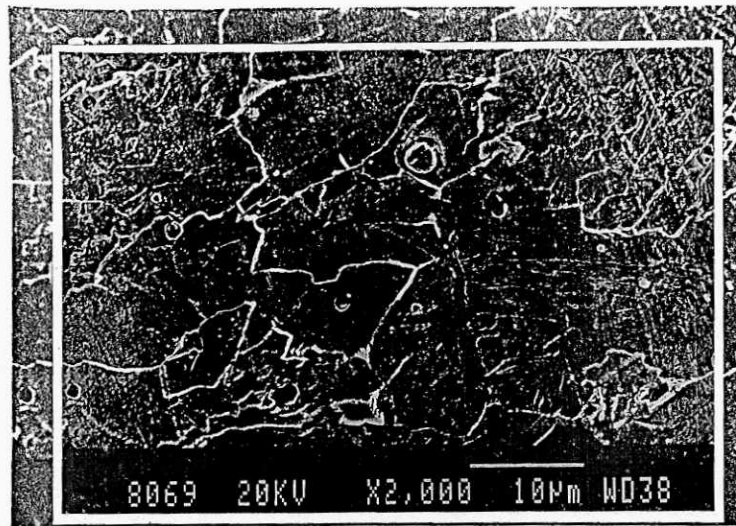


Fig. 68 SEM of steel sample S_A without cerium, showing inclusions of type I, serie A.

Fig. 68 shows that, the inclusions were two color globular.

Fig. EDX 69 was shown main composition of these inclusions of SiO_2 , besides it in heterogeneous part there were aluminum and iron.

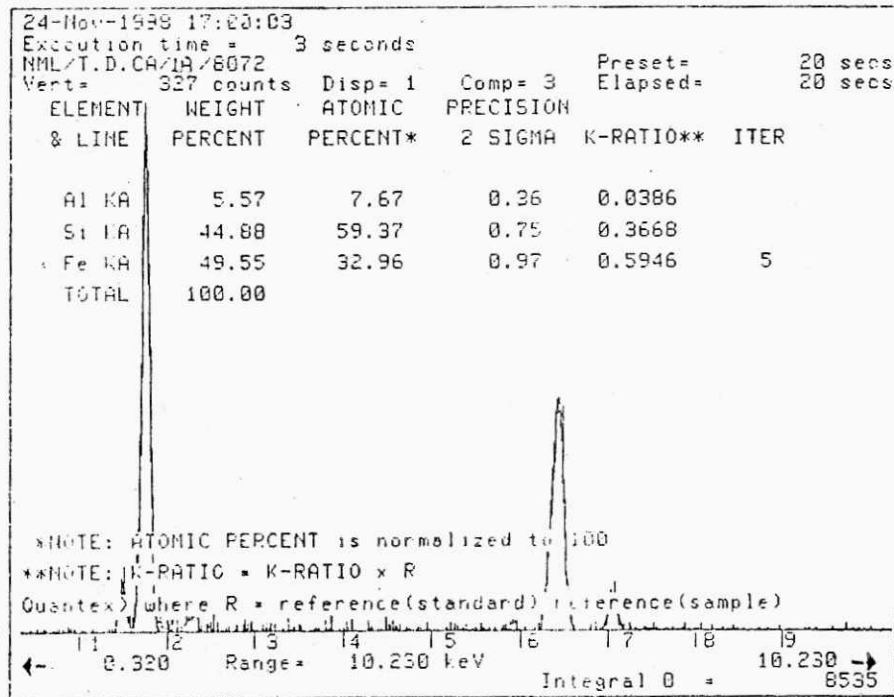


Fig. 69, Representative EDX analysis of steel sample S_A with 0.053%S, without Ce

The seri B having high percentage of sulphur of 0.063% observed also two part globular inclusions (see Fig. 70), which had main composition of manganese sulphide as shown in Fig. 71.

Fig 71 shows inclusions having mainly MnS and besides it existed amount of oxides of aluminum, silicon and iron.

The sulphur content in steel over 0.069% appeared inclusions of type II covering grain boundaries as shown in Fig.72.

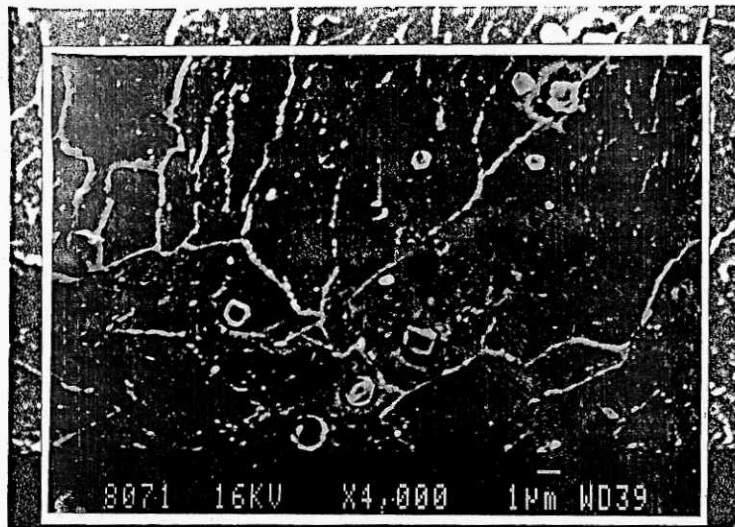


Fig. 70, SEM of steel sample S_B with 0.063%S, without cerium, showing sulphide globular inclusions, seri B.

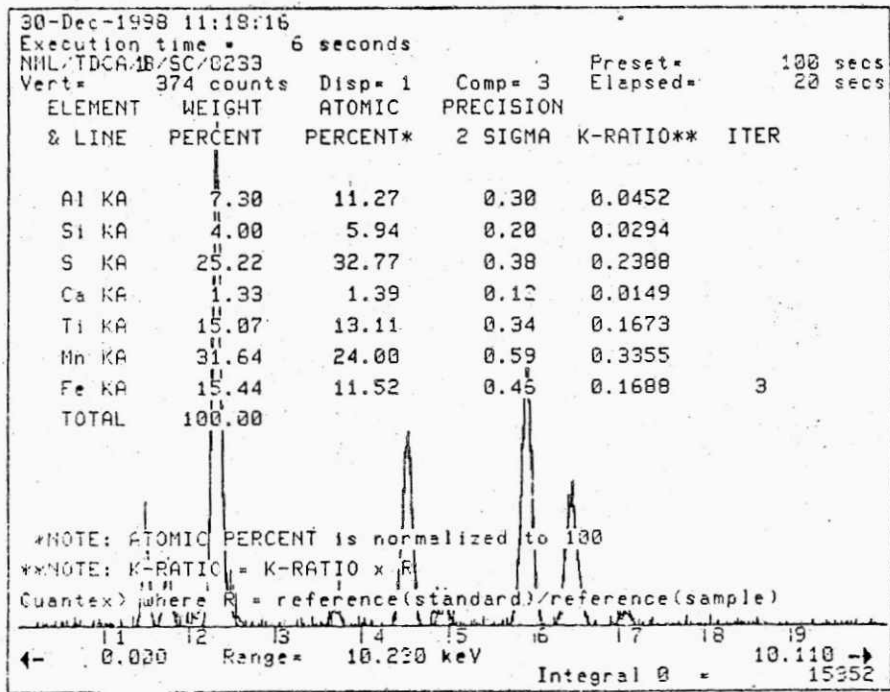
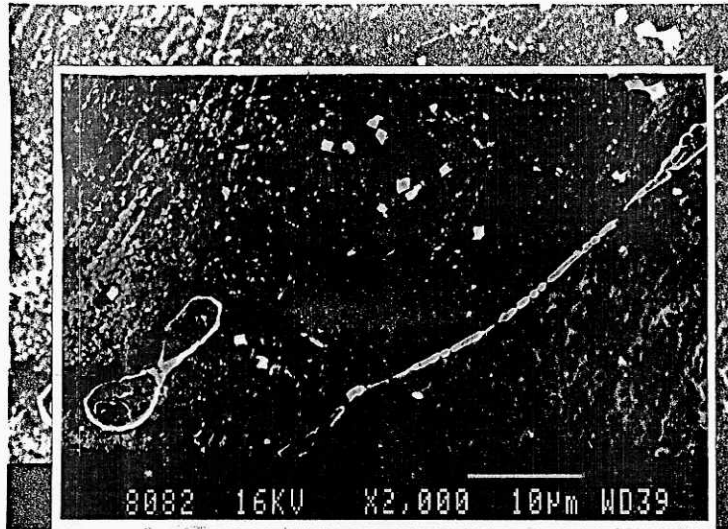


Fig. 71, EDX analysis of steel sample S_B
 of Fig. 70, without Ce, seri B.



element	wt. %	at. %
Fe	78.20	70.62
Mn	8.15	7.68
S	balance	balance

Fig. 72, SEM of steel sample S_C with 0.069%S, without cerium, showing sulphide inclusions of type II, seri C.

The main compositions of these inclusions were iron and sulphur (see Fig. 73). In the surface also appeared ribbon- stringer inclusions of type II in grain boundaries (see Fig. 74).

The inclusion composition of Fig. 74 was shown in Fig. 75.

From Fig. 75 there was know when high sulphur content in steel completely formed sulphides of type II.

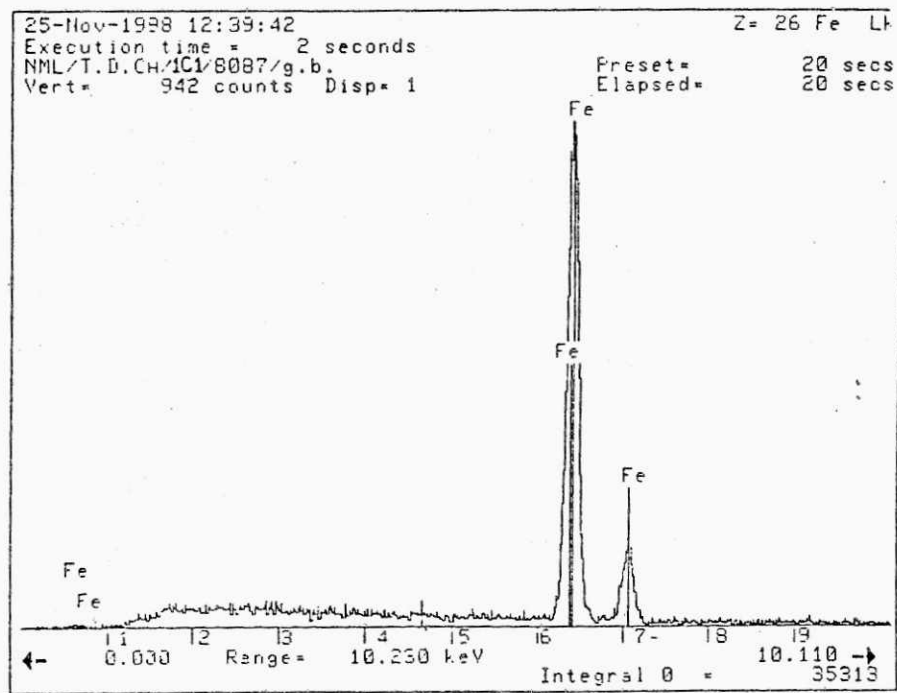


Fig. 73, EDX analysis of steel sample S_C
without Ce, seri C.

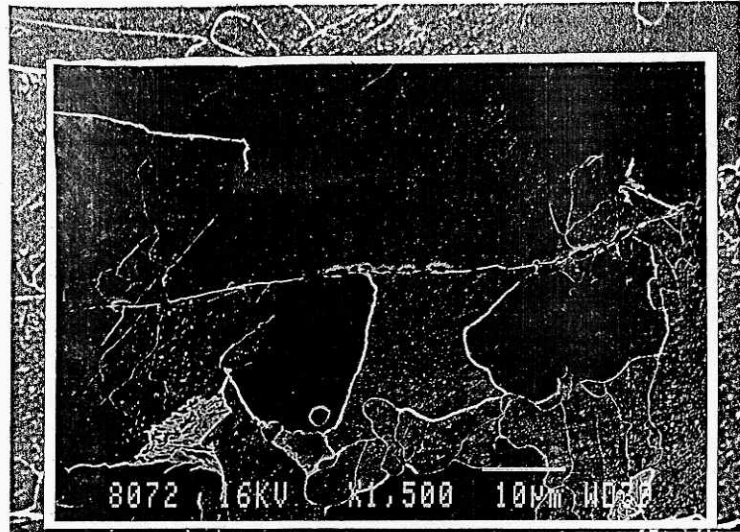


Fig. 74, SEM of steel sample S_C with 0.069%S, without cerium, showing sulphide inclusions of type II,seri C.

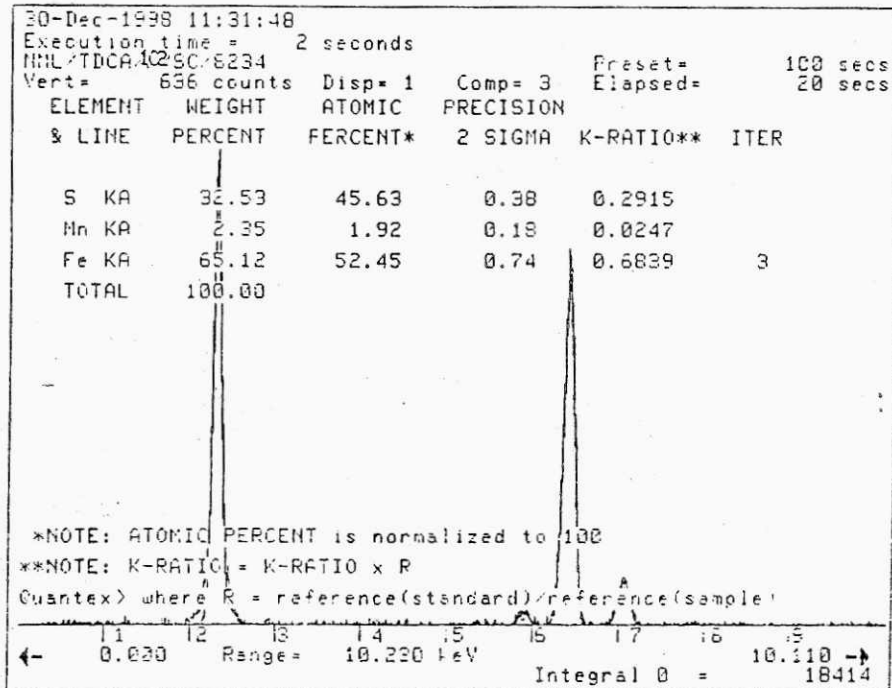
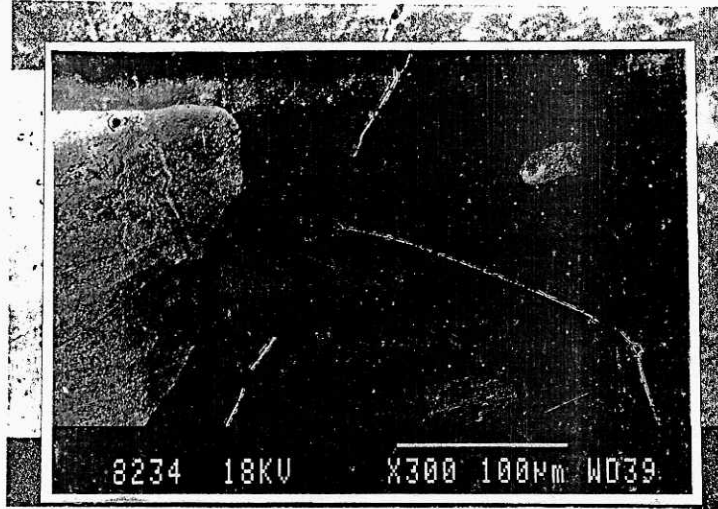


Fig. 75, EDX analysis of steel sample S_C
without Ce, seri C.

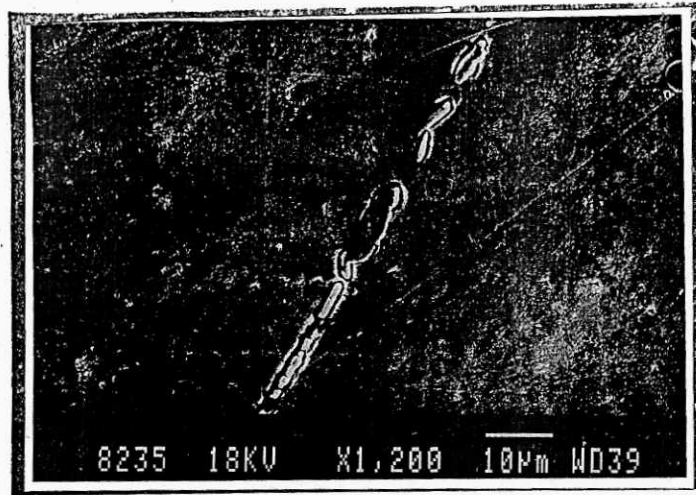
After supercooling the ribbon-stringer inclusion moved into grain (see Fig.76a,b).

The composition of inclusion in Fig. 75 shows that there were mostly manganese and iron, especially manganese presented in high content. Seri C having high inclusions of type III (see Fig.77).



element	wt.%	at.%
Fe	78.20	70.62
Mn	8.15	7.68
S	balance	balance

Fig. 76a, SEM of steel sample S_C with 0.069%S, without cerium, showing sulphide inclusions of type II, seri C,



element	wt.%	at.%
Fe	78.20	70.62
Mn	8.15	7.68
S	balance	balance

Fig. 76b, SEM of steel sample S_C with 0.069%S, without cerium, showing sulphide inclusions of type II, series C,

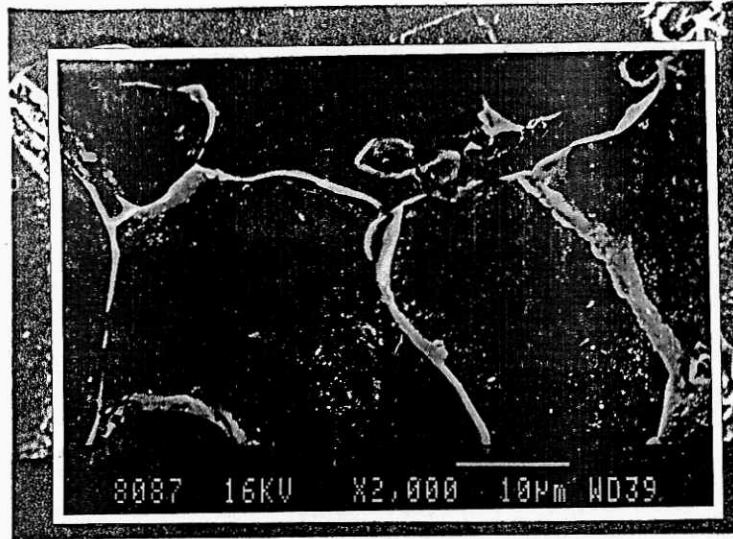


Fig. 77, SEM of steel sample S_C with 0.069%S, without cerium, showing sulphide inclusions of type III, seri C.

The composition of inclusions in Fig. 77 there was presented aluminum (see Fig. 78)

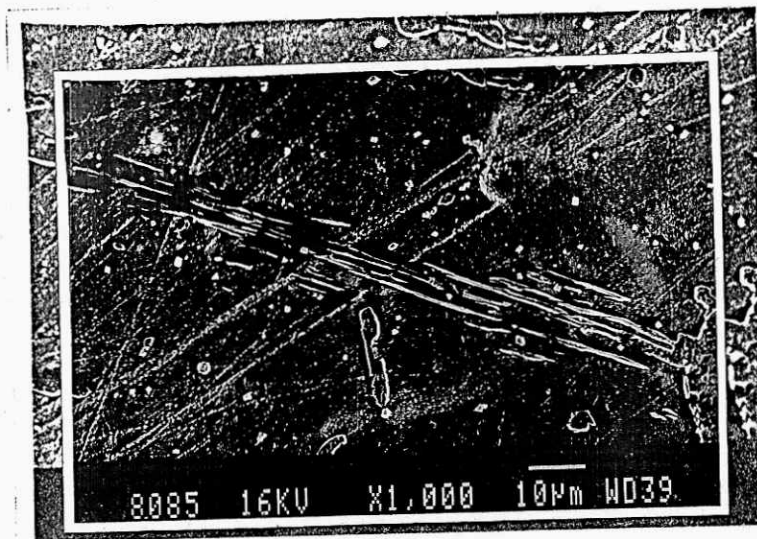


Fig. 79, SEM of steel sample S_C with 0.069%S, without cerium, showing sulphide inclusions of type III, seri C. after supercooling.

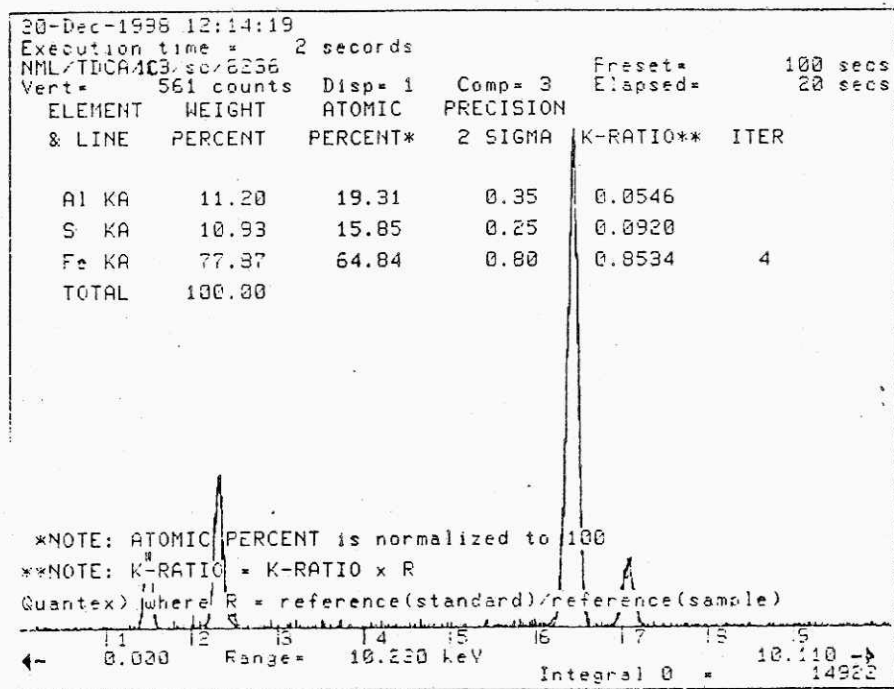


Fig. 78, EDX analysis of steel sample S_C with high aluminum without Ce, seri C.

After supercooling the inclusions of aluminum did not change (see Fig.79). When steel containing 0.003%ce formed small-smooth globular inclusions of type Ib as shown in Fig. 80. These inclusions distributed in interior grain.

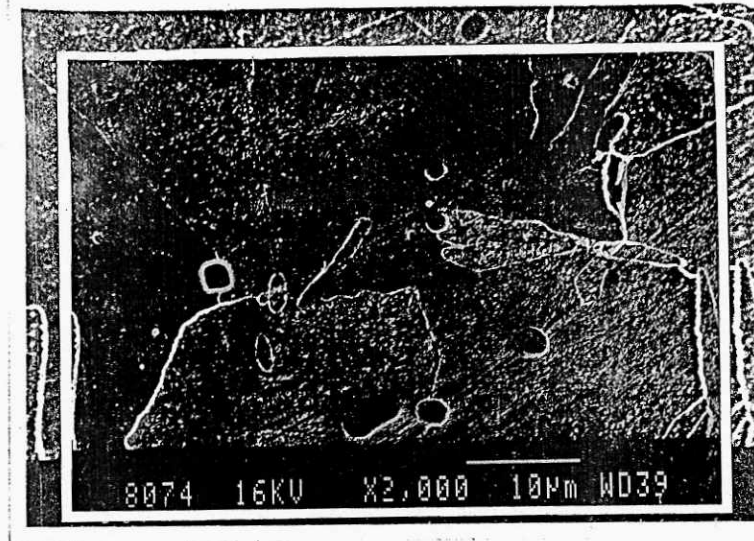


Fig. 80, SEM of steel sample S₂₅ with 0.003%Ce,
showing sulphide inclusions of type Ib.

After supercooling the grain and inclusions were refined with small forms see Fig.81.

Fig. 82 shows the composition of inclusions of fig. 81.

Here inclusions had complex composition of oxysulphides of cerium, aluminum, calcium and manganese. Especially in inclusion samples also had titanium, which perhaps there was errors of analysis, as titanium had X-ray peaks near X-ray peaks of cerium

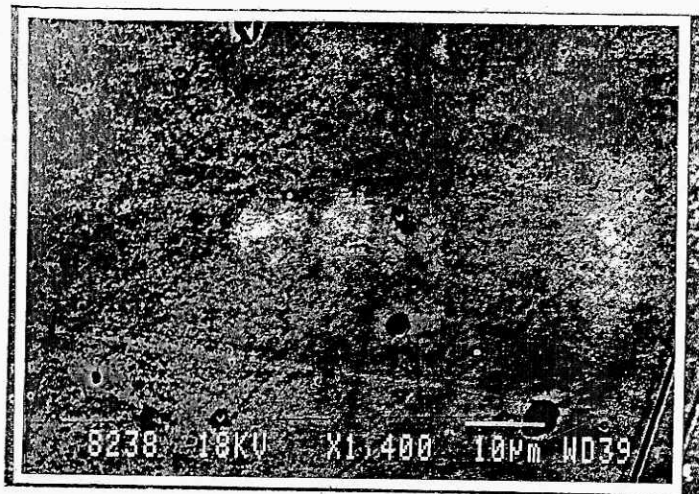


Fig. 81, SEM of steel sample S₂₅ with 0.003%Ce, , showing sulphide inclusions of type Ib.

After supercooling.

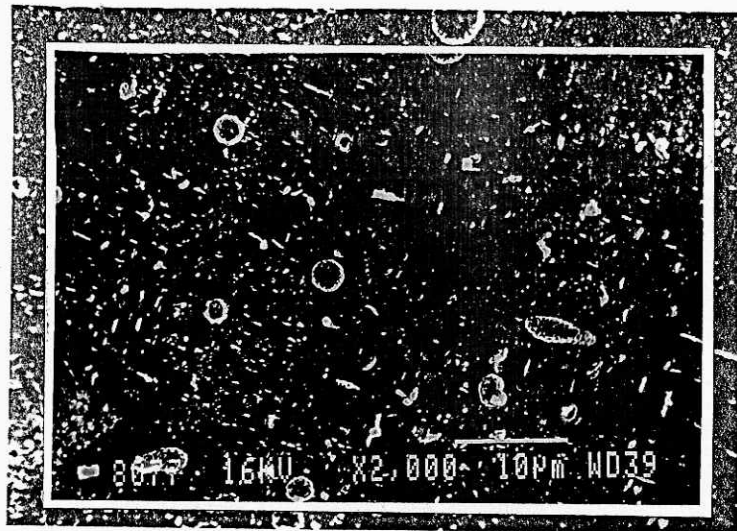


Fig. 83, SEM of steel sample S₂₆ with 0.004%Ce, showing sulphidic inclusions of type Ib.

After supercooling the crystal grain and inclusion were refined. The bean form inclusions gradually moved to globular form inclusions (see Fig. 84)

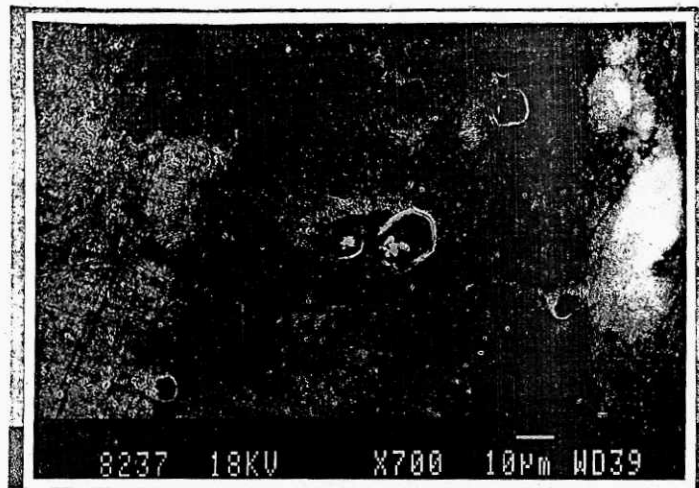


Fig. 84, SEM of steel sample S₂₆ with 0.004%Ce, after supercooling. The composition of inclusion was shown in Fig. 85.

Fig. 85 shows that here there were change of inclusion composition quantity of aluminum and cerium was higher, but titanium content was more decreased. Fig. 85 also shows that there appeared

zirconium. Here there was errors of analysis, because zirconium did not have any from pure melt bath and materials.

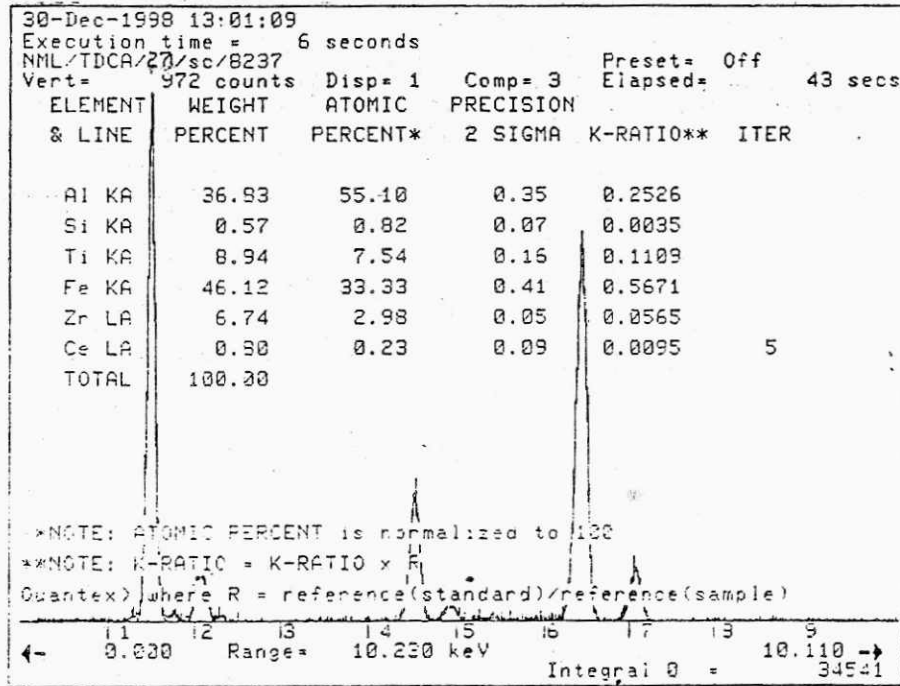
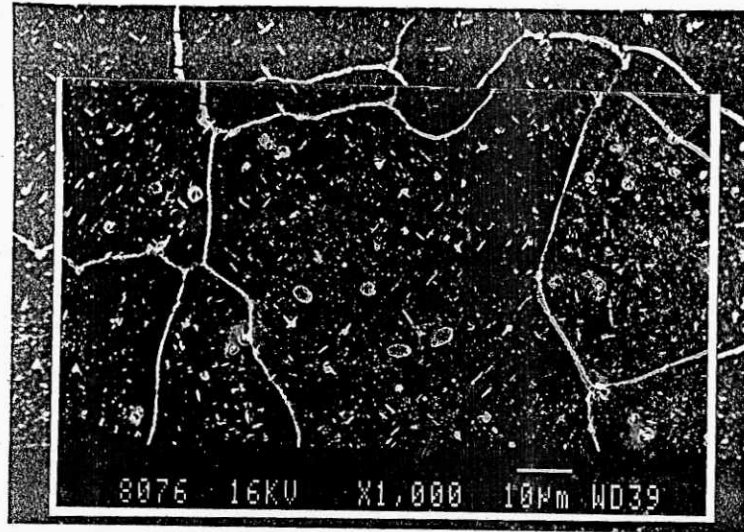


Fig. 85, EDX analysis of steel sample S₂₆ with 0.004%Ce .

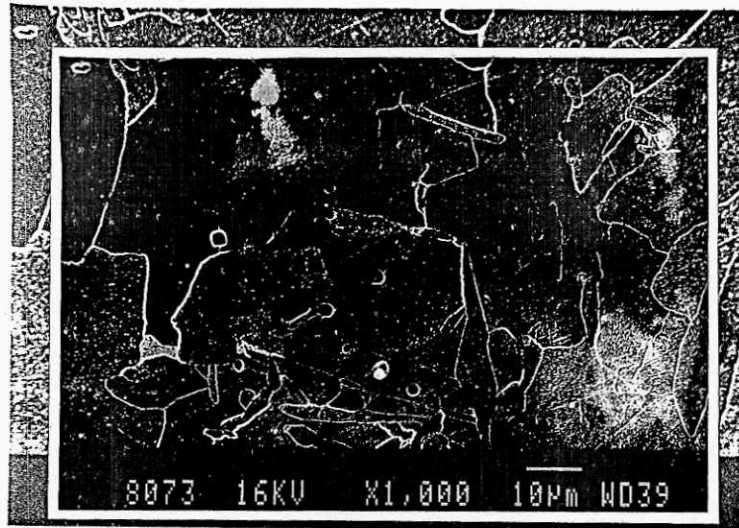
Fig. 86 shows that the cerium addition continuously increased over 2.6 kg/t, the quantity of inclusion increased moreover and the bean form inclusions separated into more small inclusions to move into clusters or spreaded them over to ribbon-stringer.



element	wt.%	at.%
Al	25.32	22.41
Si	2.17	1.92
Fe	26.24	27.42
Ce	0.18	0.17

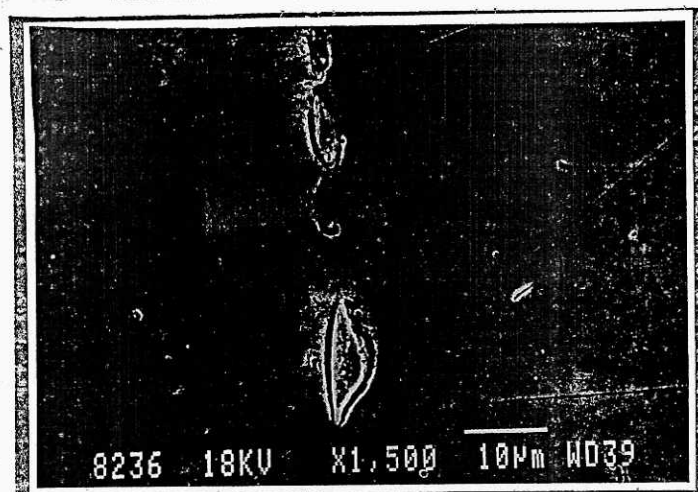
Fig. 86, SEM of steel sample S₅₄ with 0.005%Ce, showing sulphide inclusions of type Ib, tending to inclusions of type IV or II.

With aluminum content in steel over 0.05% appeared heterogeneous inclusions of type IIIb, when the cerium content was present of 0.003% in steel (see Fig.87).



element	wt.%	at.%
Al	88.72	84.21
Si	1.02	2.05
Fe	6.00	5.82
Ce	0.032	0.028

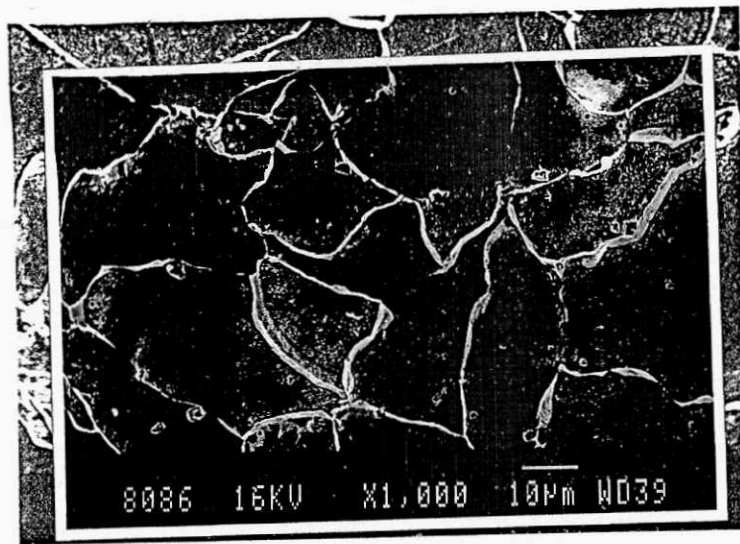
Fig. 87, SEM of steel sample S₁₅ with 0.003%Ce, and over 0.05%Al
 After supercooling the inclusion were not change their size as shown in Fig. 88.



element	wt.%	at.%
Al	85.68	83.27
Si	0.84	1.02
Fe	10.00	8.04
Ce	0.084	0.076

Fig. 88, SEM of steel sample S₅₄ with 0.005%Ce, and over 0.095%Al, after supercooling.

When the aluminum content in steel was 0.095% that not only showed angular inclusion of type IIIb but also appeared to have bold grain boundaries as shown in Fig. 89

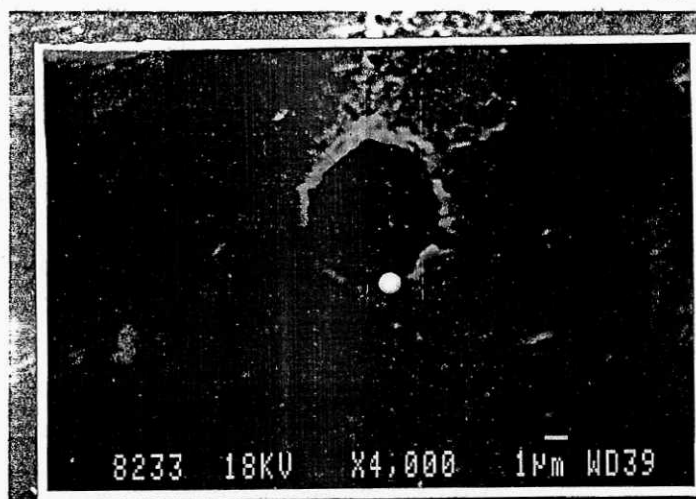


element	wt.%	at.%
Al	96.93	93.93
Si	1.09	2.11
Fe	1.98	3.96
Ce	0.028	0.037

Fig. 89, SEM of steel sample S₄₂ with 0.004% Cerium, and 0.095%Al

After supercooling the heterogeneous angular inclusions precipitated as shown in Fig.90.

Fig. 90 also shows besides coarse angular inclusions there were more small angular inclusions tending to form clusters. When cerium addition into steel increased over 4.1 kg/t and the present aluminum content of 0.125% formed more coarse angular inclusion (shown in Fig.91)



element		
Al	90.90	87.62
Si	0.90	1.60
Fe	2.81	2.90
Ce	0.08	0.062

Fig. 90, SEM of steel sample S₃₆ with 0.004%Ce, and 0.062%Al. after supercooling.

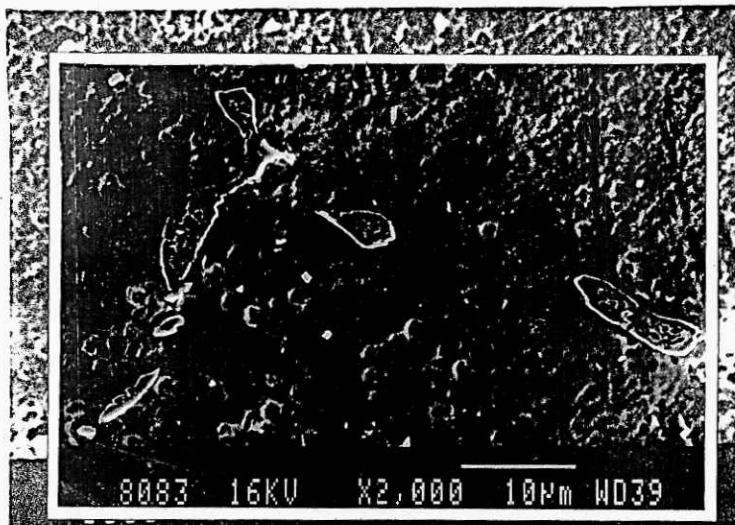


Fig. 91, SEM of steel sample S₅₇ with 0.005%Ce, and 0.125%Al.

The composition of these inclusions was shown in Fig. 92.

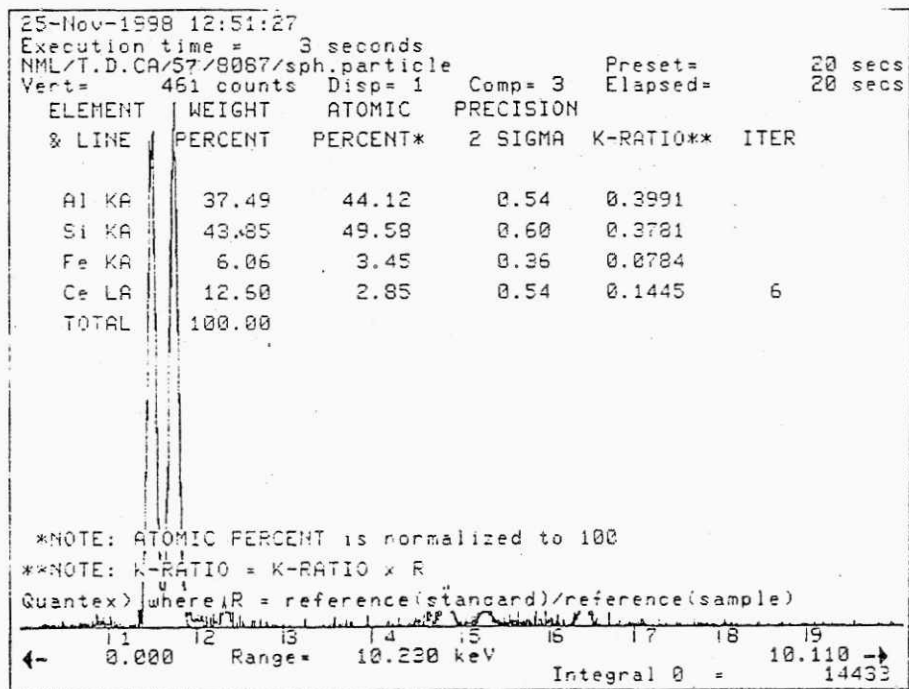
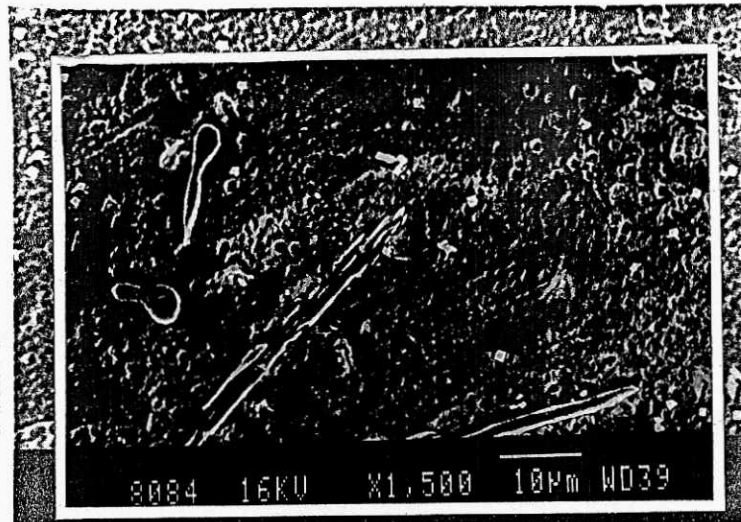


Fig. 92, EDX analysis of steel sample S₅₇ with 0.125%Al and 0.005

Fig. 92 shows that they were complex heterogeneous inclusion of cerium, aluminum and silicon having structural equations were $Ce(Al,Si)_{11}O_{18}$ or $Ce(Al,Si)O_3$ and $CeAlO_2S...$

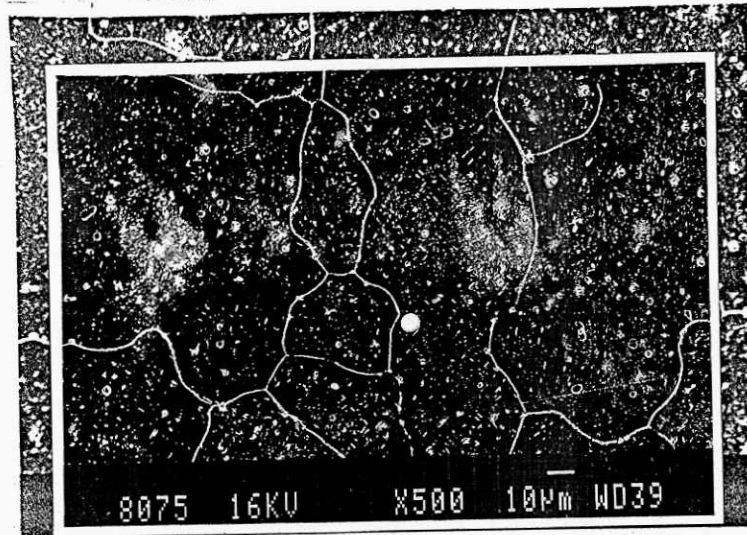
Fig. 93 also shows spreaded bean form inclusions. The main compositions of these inclusions were also cerium, aluminum and silicon with structural equation of $Ce(Al,Si)_{11}O_{18}$.



element	wt.%	at.%
Al	32.51	41.17
Si	40.10	42.20
Fe	5.42	3.20
Ce	14.72	7.20

Fig. 93, SEM of steel sample S₅₇ with 0.005%Ce, and 0.125%Al, showing spreaded bean form inclusions.

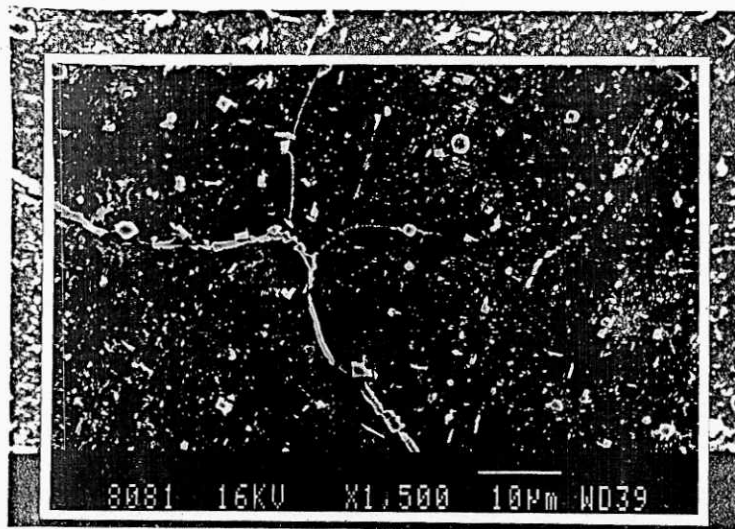
Fig. 94 shows that the cerium addition of 3.05 kg/t with 0.05%Al and residual cerium content in steel of 0.005% formed more small globular precipitated tending to form clusters of inclusions.



element	wt.%	at.%
Al	10.11	13.20
Si	1.20	2.40
Fe	15.20	13.70
Ce	22.10	18.42

Fig. 94, SEM of steel sample S₄₉ with 0.005%Ce, and 0.05%Al, showing inclusions of type IV.

When the cerium addition over 4.25 kg/t formed cluster of inclusions of type IV as shown in Fig.95



element	Al	Si	Ca	Ti	Mn	Ce	S	Fe
wt.%	8.20	0.20	0.07	4.94	20.38	25.06	28.00	13.15
at.%	13.60	0.30	0.21	5.79	20.35	22.82	26.02	10.91

Fig. 95, SEM of steel sample S₅₇ with 0.125%Ce, and 0.05%Al, cerium addition of 4.25 kg/t.

Thus the residual cerium content in steel had been analysed to 0.005%, but according to calculation and predetermination for addition amount over 4.25 kg/t formed suitable convenient cluster inclusion of type IV. The samples only analyzed cerium content to 0.005% for over 3.75 kg/t perhaps to search in side of complex inclusions. The existence of cerium in steel might be under other shape that the quantitative analytical machine DRS did not had been done; though there was controlled in the other machines DRD and ICP.

CONCLUSIONS

I. Thermodynamics of nucleation and precipitation of inclusions in molten steel was determined on the basis of thermodynamic relation for interaction coefficient as follows:

$$e^{RE}_E = \frac{\frac{1}{y} (\log K - \log K^+)}{\%RE / + \frac{x}{y} \left\{ \frac{M_{RE}}{M_E} \%E / \right\}}$$

1. Interaction coefficient of Fe-RE-O system for formation RE_2O_3 is:

$$e^{RE}_O = \frac{(\log K - \log K^+)}{3 \%RE / + 2 \left\{ \frac{M_{RE}}{M_O} \%O / \right\}}$$

2. Interaction coefficient of Fe-RE-S system for formation of RE_2S_3 is:

$$e^{RE}_S = \frac{(\log K - \log K^+)}{3 \%RE / + 2 \left\{ \frac{M_{RE}}{M_S} \%S / \right\}}$$

3. Equilibrium constant of Fe-RE-O-S system is:

$$K = \frac{k^2_o}{K^3_{os}} K_s$$

II. The mechanism and kinetics of the nucleation of RE inclusions is determined as follows:

1. Dissolution and mixing of the deoxidizer into the melt
2. Nucleation and precipitation of the inclusion phase
3. Growth of the nuclei on inclusions of an initial size distribution.
4. Floatation of the slag inclusions with concurrent growth by collision or other mechanism.
5. Assimilation of the inclusions at the metal surface or by slag or container walls.

6. The minimum energy for the nucleation of the inclusion is:

$$\Delta G^* = -\frac{16\pi\sigma^3}{3\Delta G^2}$$

7. The rate of formation of nuclei in homogeneous nucleation is:

$$I_{hom} = A \cdot \exp \frac{-\Delta G^*_{hom}}{KT}$$

8. The rate of formation of nuclei in heterogeneous nucleation is:

$$I_{het} = B \cdot f(\Theta)^{1/6} \exp \frac{-\Delta G^*_{het}}{KT}$$

9. The critical supersaturation in term of the free energy for homogeneous nucleation is: $\Delta G^{crit}_{hom} = -2.7 \cdot v \cdot \frac{\sigma^3}{KT} \cdot \log A^{\frac{1}{2}}$

10. The critical supersaturation necessary to nucleate Me_xO_y by

cooling to temperature T is:
$$\Delta G_{Me_xO_y(T)} = \Delta H^{\circ}_{Me_xO_y} \frac{T_{eq} - T}{T_{eq}}$$

11. Crystallographic consideration of nucleation potency of inclusion in supercooling is developed by:

$$\delta_{(hkl)_s}^{(hkl)_n} = \frac{\{(d / uvw)_s \cdot \cos\theta_1 - d / uvw)_n\}}{3d / uvw)_n}$$

III. Condition for inclusion precipitation is:
$$\frac{-\Delta G^{\circ}}{4.575T} > 1$$

1. Condition for inclusion precipitation of Ce_2O_3 is:

$$\frac{25.86}{-2 \log\{Ce \cdot (1 - f_s)^{-0.64}\} - 3 \log\{O \cdot (1 - 0.95 \cdot e^{0.1})\}} > P_{Ce_2O_3}$$

2. Condition for inclusion precipitation of Ce_2S_3 is:

$$\frac{16.48}{-2 \log\{Ce \cdot (1 - f_s)^{-0.64}\} - 3 \log\{S \cdot (1 - 0.97 \cdot e^{0.06})\}} > P_{Ce_2S_3}$$

3. Condition for inclusion precipitation of Ce_2O_2S is:

$$\frac{24.963}{-2 \log\{Ce \cdot (1 - f_s)^{-0.64}\} - 2 \log\{O \cdot (1 - 0.95 \cdot e^{0.1})\} - \log\{S \cdot (1 - 0.97 \cdot e^{0.08})\}}$$

4. Relationship between Ce, Al, O and S is determined as follows:

$$(1.58 \cdot Ce)^2 = \frac{(1.03 Al)^{2.05} \cdot (1.87 \cdot O)^{1.07}}{1.91 \cdot S}$$

5. Equilibrium condition between Ce oxysulphide and

oxide + oxysulphide heats is: $(1.54.Ce)^{1.81} = \frac{(1.72.O)^{23.07}}{(1.74.S)^{25.86}}$

6. Thermodynamic data of Ce inclusions precipitating in molten steel is:

for $\log K_{CeO_2} = -9.10$, $\log K_{Ce_2O_3} = -17.31$, $\log K_{CeS} = -5.54$, $\log K_{Ce_2S_3} = -11.37$ and $\log K_{Ce_2O_2S} = -16.21$.

7. Reaction paths for sequential and coupled deoxidation-desulphurization reactions are moved from RE_2O_3 field to RE_2O_2S field when the proportion between oxygen and sulphur is about 1/5. When this proportion is greater than 10, reaction path moves from RE_2O_2S field to RE_2S_3 field.

8. Mechanism of inclusion morphology precipitation is as follows: without RE addition there are conventionally inclusions as type I; randomly dispersed globular, type II; interdendritic eutectic grain boundary eutectic, type III; randomly dispersed angular. With RE addition there are precipitation and formation of inclusion of type Ib; globular oxysulphides, type IIIb; angular heterogeneous inclusion and type IV; cluster homogeneous inclusions.

IV. Elimination possibility of inclusion in molten steel is as follows:

A. Mechanism:

1. Nucleation and non-dendritic growth

2. Dendritic growth
3. Multiplication of dendrite
4. Cluster formation
5. Coalescence
6. Floatation

B. Separation possibility of RE inclusion by floatation occurs

according to equation: $\rho_{cl} = \rho \cdot \varepsilon + \rho_{incl} \cdot (1 - \varepsilon)$

and after formation of cluster size about 3000μ , then $v_{RE} \cong v_{Al_2O_3}$

V. Experimental methods have been investigated with the newest and the most believe and effective.

VI. The results of experiments are as follows:

1. When the cerium content in steel is lower than 0.003% the oxygen content increases by absorbing from furnace atmosphere and the oxygen content obviously decreases when the cerium content is over 0.003%.

2. The sulphur content in steel does not vary when the cerium content in steel is lower than 0.003% and fast reduction sulphur content with cerium content higher than 0.003%.

3. With total content of cerium and aluminum higher than 0.06% it reduced the oxygen and sulphur content substantially.

4. With Ce/S ratio higher than 0.2 it reduced the oxygen content in steel and when this ratio equals one the lowest reduction of oxygen content is 300ppm.
5. When the ratio of Al+Si/Ce is higher than 120 the oxygen content fastly is reduced in steel.
6. The increase of cerium addition increases cooling time of steel.
7. As the residual cerium content in steel increases the degree of supercooling also decreases . The lowest degree of supercooling of 400°C is obtained with 0.004%Ce.
8. The increase of cerium content increases EMF of supercooling.
9. Temperature of supercooling slowly reduces with increase of residual cerium content.
10. The weight of measuring sample no affects on degree of supercooling.
11. Without cerium in steel, the macrostructure of steel has large grain boundaries. The crystal grains form under columnar grain. The inclusions are observed in interior grain.
12. When cerium content in steel is 0.003%, the columnar zones gradually disappear and refine crystals.
13. The cerium content in steel increases to 0.004% with cerium addition of 2.5 kg/t observed the bold boundaries, the columnar grains transfer into polygonal and moves nearer to grain boundaries.
14. When cerium content increases to 0.005% with cerium addition over 3.05 kg/t, the grains crystallize smaller and appear great

quantity of small-smooth globular inclusions lying interior of the inner grain and also tend to form clusters.

15. The cerium content in steel of 0.003% precipitated inclusions of type Ib with main composition as oxysulphides of cerium, aluminum and manganese. After supercooling the inclusions lying inside grain refine infinite small.

16. The cerium content in steel of 0.004% cooling in the air without flux cover precipitated bean form inclusion inside coarse crystals. After supercooling the crystals refine into small, the inclusions move into small globular of type Ib.

17. The cerium addition into steel over 4.10 kg/t before supercooling form more bean form spreaded inclusions tending stringer, after supercooling they refine very small-smooth, but there is tendency to form cluster of these inclusions.

18. The cerium addition over 4.25 kg/t with residual content in steel of 0.005% has been precipitated heterogeneous angular inclusion of type IIIb (0.125%Al) and small-smooth clusters inclusions of type IV containing cerium and aluminum like equations of $Ce(Al,Si)_{11}O_{18}$ and $Ce(Al,Si)O_3$.

19. The cluster inclusions has compositions structure of $CeAlO_2S$.

20. With induction stirring the part of deoxidation and desulphurization product removed into slag and oxygen and sulphur content in steel reduced. The induction stirring strongly refined inclusions to small-smooth size.

REFERENCES

1. Knapp W. E. et al, Iron Age 169, (152), 129
2. Popova P.N. et al, Stal in Deustsh 7, (1967), 1113
3. Kepka M. a kol. Hutnicke listy 7, (1972), 484
4. Fischer W. A. et al, Arch. Eisenhüttenwes 44, (1973), 97
5. Kepka M. et al, Neue Hutte 18, (1973), 200
6. Lorenz L. et al, Arch. Eisenhüttenwes 44, (1973), 97
7. Buzek Z. a kol. Fiziko-chimicheskiye Osnovy Proizvodstva Stali, Moscow (1971), 209
8. McLean A. et al, Metals and Materials 8, (1974), 452
9. Reinhardt K. et al, Goldschmidt informert 4, (1974), 7
10. Wilson W.G. et al, Goldschmidt informert 4, (1974), 26
11. Wilson W. G. et al, J. Metals 26, 5, (1974), 14
12. Lorenz L. et al, Arch. Eisenhüttenwes 46, (1975), 677
13. Schurmann E. J. et al, Arch. Eisenhüttenwes 17, (1976), 1
14. Ishiguro M. et al, Transactions of ISIJ 16, (1976), 359
15. Janke D. et al, Arch. Eisenhüttenwes 49, (1978), 425
16. Samsonov G. V. The Oxide Handbook New York (1973)
17. To Duy C. Sulphur dung kim loai dat hiem trong luyen thep, Reprt ISM, Hanoi (1989)
18. To Duy c. Kandidatske Minimum Ostrava (1989)
19. Buzek Z. a kol. Hutnik 3, (1981), 91
20. Buzek Z. a kol Slevarenstvi 22, 12, (1972), 507
21. To Duy C. Kandidatska Disertacni Prace, Ostrava (1991)

22. Schindlerova V. a kol. Slevarenstvi 22, 12, (1972), 492
23. Schindlorova V. a kol. Hutnicke Listy 3, (1966), 169
24. Buzek Z. a kol. Slevarenstvi 20, 10, (1972), 409
25. To Duy C. Reviews Heavy Industry 3, (1992), 23
26. Eremenko V. I. IAN SSSR, Metally 12, (1958), 11
27. McLean A. et al, Metall. Transactions B, 19B, (1988), 383
28. Czervinka M. Report Konference FPVO Ostrava ,(1972), 156
29. Saviskij E. M. Splavy REM Izd. AN SSSR Moskva (1962)
30. Kepka M. Ovlivnovani Cistoty Oceli, Studie CSAV (1986)
31. Myslivec T. Fizikalni Chemie Zaklady Ocelarstvi, Praha (1971)
32. Volny O. Kandidatska Disertacni Prace VSB, Ostrava (1981)
33. Mohyla M. a kol. Vyzkumna Prace VSB, Ostrava (1988)
34. Elliot J. F. Geiser M. Thermochemistry for Steelmaking I, (1960)
35. Buzek Z. Hutnicke Aktuality 1&2 VUHZ, Dobra (1979)
36. Waudby P. E. et al, International Metals Reviews, Reviews 229, 2, (1978), 74
37. Luyckx L. et al, AIME Electric furnace Conf. 31, (1973), 175
38. Li H. et al, Metall. Transactions B, 19B, (1988), 383
39. Nuri Y. et al, Transactions ISIJ 22, (1982) 399
40. Nuri Y. et al, Transactions ISIJ 22, (1982) 408
41. Vahed A. et al, Metall. Transactions B, 7B, (1976), 375
42. Lu W. K. eta al, Iron and Steelmaking 1, 4, (1974), 228
43. Lu W. K. et al, Metals and Materials 10, (1974), 452
44. Dong Y. et al, Acta Metyallurgica Sinica 22, 2, (1986), 14

45. Braun M.P. et al, Russian Casting Production 98, (1966), 417
46. Ohashi T. et al, Transactions ISIJ, 17, (1977), 262
47. Wilson W. G. Proc. at Conf. on " Inclusion and their effects on Steel properties" 17-19, Sept. University of Leeds (1974)
48. Turkdogan E. F. Transactions AIME 233, (1965), 2100
49. Staffan Malm Scandinavian J. Metallurgy (1976), 278
50. Janke D. et al, Arch. Eisenhüttenwes 46, (1975), 755
51. Yingsheng Y. et al, J. Metals, 5, (1988), 26
To Duy C. Effect of REM on mechanical properties of steel, Report ISM, Hanoi (1987)
52. Buzek Z. Hutnicke Aktuality 7, (1978)
53. Buzek Z. a kol. Hutnicke Listy 10, (1977), 718
54. Turkdogan E.T. Arch. Eisenhüttenwes 54, (1983), 45
55. Volny O. a kol, Vyzkumna Prace VUHZ, Dobra, (1988)
56. Buzek Z. Sbornik Konf. VEOI Ostrava (1973) 77
57. Buzek Z. Hutnicke Aktuality 7, (1988)
58. Buzek Z. a kol. Hutnicke Listy 11, (1984), 767
59. Kirshenbaum A. D. et. al, Transactions AIME 224, (1962), 816
60. Kulikov I. S. Raskislenije Metalov, Metallurgija Moskva (1975)
61. Keller H. et. al, Arch. Eisenhüttenwes 46 , (1975), 331
62. Averin N. N. Metallurgiczeskije metody povyscenija kaczestva Stali 33, Moskva (1979)
63. Samsonov G.V. The Oxide Handbook New York (1973)
64. Stulen F. B. et. al, The Iron and Steel Institute, London, (1956), 439

65. Cummings H. N. et. al, Proceedings of ASTM, 58, (1958), 505
66. DuckWorth W.E. Metallurgia 69, (1964), 53
67. Heiser F.A. et. al, Transactions AIME 93, (1971), 211
68. Levin E. M. et. al, The American Ceramic Society Ohio, (1964),
123
69. Philbrook W.O. et. al, International Materials Reviews, Review
220, (1977), 187
70. Novotny J. Interface Segregation and related processes in materials,
Trans. Tech. Publ. Switzeland (1991), 161
71. Kubaschewski O. Proceedings of Metall. Chemistry Symposium,
London 14-16 July, (1971), 263
72. Hume-Rothary W. et. al, Metallurgical Equilibrium diagrams,
London, (1952), 24
73. Turkdogan E.T. BOF Steelmaking 2, (1975), 4
74. El Gammal et. al, Iron Steel Institute -Japan, 2, (1974), 125
75. Sims C. E. Transactions AIME 215, (1959), 376
76. Parma V. a kol. Vyzkumna Zprava UTHP CSAV, Ostrava (1982)
77. Lanskaja K.A. a kol. Stal 55, 5, (1985), 66
78. Kinne G. i kol. Izv. VUZ czernaja Metallurgija 5, 9, (1962), 92
79. Kinne G. i kol. Izv. VUZ czernaja Metallurgija 6, 5, (1963), 65
80. Jacquemot A. et. al, Report IRSID PCM. RP 63, Aout. (1973)
81. Ishikawa R. et. al, Bulleten Res. Inst. Min. Dress. Metallurgy
Tohoku University 29, (1973), 193
82. Richerd J.J. Mem. Sci. Rev. Metallurgy 59, (1962), 527

83. Hitchon J. W. et. al Report IRSID, (1966)
84. Fruehan R.J. Metall. Transactions B 5B , (1974), 345
85. Buzek Z. Proceedings of Inter. symposium on Metall. Chemistry
University of Sheffield, England, July (1971)
86. Teplitskij E.B. i kol. Metallurg, 4, (1987), 30
87. Ishiguro M. et. al, Transactions Iron Steel Institute -Japan, 2,
(1974), 125 16 , (1976), 359
88. Viskarev A. F. i kol. Izv. VUZ czernaja Metallurgija 1, (1987), 30
89. Qiyong H. et. al Metall. Transactions B 21B, 4, (1990), 295
90. Gschneidner K.A.N. et. al, thermochemistry of the rare earths,
Report 6, Iowa, (1973)
91. Chipman J. Basic Open Hearth Steelmaking 3rd Ed. Ed. by
G. Derge New york (1964) , 640
92. Wilson W. G. et. al, Metal. Progress 104, (1975), 75
93. To Duy C. Journal of Science and Technology 32, 5 , (1994), 45
94. Buzek Z. Sbornik VSB 3, (1965), 435
95. Buzek Z. Sbornik VSB 3, (1965), 409
96. Langenberg F.C. et. al, Transactions AIME 212, (1958), 290
97. Singleton R.H. Transactions AIME 215, (19), 1987
98. Narita T. et. al, Tetsu-to-Hagane 50, (1964), 2011
99. Qiyong H. et. al, Metall. Transactions B 16B , (1985), 785
100. Kusakawa T. et. al, Tetsu-to-Hagane 51, (1965), 1987
101. Turkdogan E.T. et. al, Proceedings of Inter. symposium 7-8 Nov.
(1974), 1

102. Ejima A. et. al, Transactions ISIJ 17 , (1977),349
103. Sanbongi K. et. al, Transactions ISIJ 19 , (1979),1
104. Wang C. et. al, Acta Metallurgica Sinica 16 , (1980),83
105. Prosvirin K.S. i kol. Izv. VUZ czernaja Metallurgija 1 , (1986),1
106. Qiyong H. et. al, Metall. Transactions B 19B , (1988),409
107. To Duy C. Journal of Science and Technology 32,2, (1994),23
108. Malm S. Scandinavian J. Metallurgy 5 , (1976),248
109. Kracenko N. F. i kol. Izv. ANSSSR Metally 3 , (1966), 3
110. Luyckx L. et. al, Metallurgical Transactions 1 12, (198),3441
111. Maninovska J.N. Stal 56, 4, (1986), 78
112. Iskovic G. M. Stal 2, 5, (1977), 125
113. Fruehan R.J. et. al, Metall. Transactions B 10B , (1979),143
114. Buzek Z. Hutnicke Aktuality VUHZ, Dobra, 1-2 , (1979)
115. Iskovic G.M. Raskislenie Stali i modifitsirovanie metaliczeskich
vkluczenij, M. Metallurgija (1981), 296
116. Akila R. et. al, Metall. Transactions B 19B , (1987),163
117. Kreszanovskij N.S. modifitsirovanie Stali, Moskva (1970)
118. Wilson W. G. et. al Metal. Progress 104, 7, (1975),75
119. Wilson W. G. et. al Goldschmidt 4, 31, (1977), 26
120. Samarin A. M. et. al Neue Hutte 7, (1962), 213
121. Plockinger E. The Iron and Steel Institute, London 51, (1963),
122. Plockinger E. The Iron and Steel Institute, London 64, (1963),
123. Torssell K. Jernkonterets annaler, 151, (1967), 890

124. Turkdogan E. I. The Iron and Steel Institute, London
153, (1973),
125. Gatellier G. et. al, The Iron and Steel Institute, London 191,
(1973),
126. Pomey G. et. al, The Iron and Steel Institute, London
1, (1972),
127. Miyashita Y. et. al, Proceedings of Second Japan-USSR Joint
Symposium on physico-chemistry of Metallurgy
Tokyo (1969), 101
128. Lindborg U. et. al, Transactions AIME 242, (1968), 94
129. Matthew P.M. et. al Arch. Eisenhüttenwes 45, (1974),569
130. Turkdogan E.T. Iron Steel Institute -Japan, 204, (1966), 914
131. Sigworth G. K. et. al, Canadian Metallurgy 11, (1972), 337
132. Lacmann R. Kinetic Metallurgischer Vorgängebeider
Stahlherstellung, Dusseldorf, Verlag Stahleisen (1972), 381
133. Turpin M. et. al, Iron Steel Institute -Japan, 204 , (1966), 217
134. Forward G. et. al Proceedings of Conf. on AIME Electric arc
furnaces Stell 24, (1966). 16
135. Miyashita Y. Transactions ISIJ 7 , (1967), 1
136. Kozabevitch P. et. al, The Iron and Steel Institute, London 42,
(1972),
137. Chipman J. Transactions AIME 224, (1962), 1288
138. Schenck H. et. al Arch. Eisenhüttenwes 41, (1970),131
139. Gatellier C. et. al, Reviews of Metallurgy 66, (1969), 673

140. Cahn J. W. et. al, J. Chem. Physics, 28(1958), 258
141. Volmer M. et. al, Z. electrochemistry 35, (1959), 555
142. Tiller W. A. et. al, Acta Metallurgy 17, (1969), 483
143. Turnbull D. et. al, Industrial Eng. Chemie 44, (1952), 1292
144. Turnbull D. et. al, J. Chem. Physics 17, (1949), 71
145. Elliot J. et. al, Chemistry for Steelmaking II, (1963)
146. Turnbull D. et. al, J. Chem. Physics 20, (1952), 411,483
147. Bramfitt B. L. Metallurgical Transactions 1 , (1970), 1987
148. Sundquist B.E. et. al Transactions AIME 221, (1961), 607
149. Pound G. M. Liquid Metals and Solidification ASM (1958), 87
150. Tiller W. a. et. al, Acta Metallurgy 17, (1969), 483
151. Narita K. Tetsu-to-Hagane 53, (1967), 1024
152. Narita K. Tetsu-to-Hagane 52, (1966), 1098
153. Turkdogan E.T. Chem. Metallurgy of Iron and Steel The Iron and Steel Institute, London, (19), (1971), 153
154. Forward G. et. al, Metallurgical Transactions 1 , (1970),2889
155. Scheil E. Z. Metalik 34, (1942), 70
156. Pfann W. G. J. Metals 4 , (1952),747
157. Lindblom B. E. Jarnkonforets Annaler 152, (1968), 53
158. Hume-Pothery W. et. al, J.The Iron and Steel Institute, London, 202, (1964), 534
159. Hausen M. Constitution of binary alloys 2nd Ed. Mc. Graw-Hill New York (1958)
160. Keqiu H. et. al, Steel Research 67 , (1996),268

161. Faulkner R.G. International Materials Reviews, Review 41, 5, (1996), 198
162. Sigworth G.K. et. al J. F. Met. Sci. 8, (1974), 298
163. Tanabe J. et. al, Metall. Transactions B 26B, (1995), 95
164. Suito H., Iron Steel Institute Japan - International 31, (1991), 1381
165. Tanabe J. et. al, Steel Research 66, (1995), 146
166. Suito H. et. al, Steel Research 63, (1992), 419
167. Lee K.R. et. al, Metall. Transactions B 27B, (1996), 423
168. Li G. et. al, Metall. Transactions B 27B, (1996), 96
169. Schindlerova V. a kol. Hutnicke Listy 5, (1970), 316
170. Povolockij D.J. a kol. Izv. VUZ czernaja Metallurgija 10, (1969), 51
171. Cistjakoc S. L. a kol, Stal 12, (1969), 1134
172. Javojskij V. I. i kol. Nemetalicheskiye vkluchenija i svojstva Stali, M. Metallurgija (1980), 176
173. Lunev V.V. i kol. Vlijanie kompleksnovo raskislenija na svojstva Stali, M. Metallurgija (1982), 32
174. Skok Jo.Ja. i kol. Vlijanie kompleksnovo raskislenija na svojstva Stali, M. Metallurgija (1982), 97
175. Yuanchi D. et. al, Steel Research 68, (1997), 388
176. Feng X. Journal of Chinese Rare Earth Soc. 5, 4, (1987), 33
177. Wilson W. G. AIME Electric furnace Conf. 31, (1973), 154
178. Wilson W. G. et. al, J. Metals 9, (1985), 36

179. Tiurin A. G. i kol Izv. VUZ czernaja Metallurgija 14 , (1985),175
180. Henderson W. et. al, AIME Electric Conf. 31, (1973), 162
181. Zhao S. et. al, Scandinavian J. Metallurgy14 , (1985),175
182. VanEeghem J.I. Slevarenstvi 8-9 , (1963),360
183. Kepka M. Hutnicke Listy 8, (1976),575
184. Cizner J. Slevarenstvi 6 , (1979),230
185. Buzek Z. Sbornik Konf. VEO III Ostrava (1975),II-1
186. Fremunt P. Slevarenstvi 1 , (1976),11
187. Iskovic G.M. Stal 12, 5, (1976), 1082
188. Rountree G. et. al, Journal of ISI , 211, (1973),83
189. Hilty D.C. et. al, AIME Electric Conf. 11, (1953), 121
190. Crafts W. et. al, Transactions AIME194 ,1, (1952),1307
191. Volny O. Vyzkumna Prace VUHZ, Dobra 5(1985), 25
192. Liu S. et. al, Acta Metallurgica Sinica 20 ,5, (1984),322
193. Weiss. Stahl Und Eisen 10, (1974), 477
194. Matrasov J.I. i kol. Metallov i termich. obrabotka Metallov
6, (1978,56
195. Gurasev K.N. i kol. Litejnoje Proizvodstvo 3 (1970), 35
196. Sidorenko N. F. i kol. Litejnoje Proizvodstvo 3 (1970), 28
197. Gladich A.N. i kol. Metallov i termich. obrabotka Metallov
3, (1970) 31
198. Kawamura K. et. al, Transactions ISIJ 18 , (1978),212
199. Paul S. K. et. al, Metall.TransactionsB 13B , (1982),185
200. Brainen I. E. i kol. Metallov i termich. obrabotka Metallov,

- 10, (1968), 53
201. Marjanovskaja T.S. i kol. Metallov i termich. obrabotka Metallov
7, (1968), 65
202. Reinhardt K. Goldschmidt 4, (1974), 7
203. Sorkin N.A. i kol. Stal 57 ,8 , (1986),74
204. Jufeng Qiu, Acta Metallurgica Sinica 20 ,2, (1984),A92
205. Knight R.F. et. al, Metals Technology 11, (1984), 272
206. Landova S. Hutnicke Aktuality VUHZ, Dobra, 6 , (1987),28
207. Yishi Yang et. al, Acta Metallurgica Sinica 19 ,2, (1983),A118
208. Graham M. J. et. al, Metall.TransactionsA 14A , (1983),2553
209. Gicia C.I. et. al, J. Metals 37 ,9, (198 5),22
210. Lopez H. F. Metall.Transactions 18A , (1977),1971
211. McKimpson M. et. al, Metall.Transactions 12A , (1981),825
212. Piskho R. et. al, Metall.Transactions 10A , (1979), 887
213. Parthasarathy T.a. et al, Metall.Transactions 15A , (1984),2021
214. Pridancev M.V. i kol. Izv.ANSSSR Metally 3 , (1974), 136
215. Ipatov V.A. i kol. Izv.ANSSSR Metally 4 , (1977), 131
216. Flemings M.C. International Materials Reviews,
Review 9, (1977),201
217. Iyengar R.K. et. al, Metall.TransactionsB 3B , (1972),1823
218. Knuppel V.H. et. al, Stahl und Eisen 85, (1965), 675
219. Kozakevitch P. et. al, Reviews Metallurgy 65, (1968), 589
220. Iyengar R.K. et. al, " Kinetic Metallurgisther Vorgange bei der
Stahlherstellung - Dusseldorf Verlag Stahleisen (1972), 219

221. Linder S. Scandinavian J. Metallurgy 5 , (1974),137
222. Rege R.A. et. al Metallurgical Transactions 1 , (1970),2652
223. Crussard C. The Iron and Steel Institute, London, 66 (1963),
224. Ham F. S. J. Physic-Chemistry 6, (1958), 335
225. Takamura J. et. al, Proceedings of 6th Inter. Iron & Steel Congress 1 ISIJ,Tokyo (1990), 605
226. Ohnaka I. Transactions ISIJ 24 , (1984), 2101
227. Goto H. et. al, Iron Steel Institute Japan - International 35, (1995), 286
228. Goto H. et. al, Iron Steel Institute Japan - International 34, (1994), 414
229. Ogibayoshi S. et. al, Proceedings of 6th Inter. Iron & Steel Congress 1, Tokyo (1996), 612
230. Ohnaka I. Tetsu-to-Hagane 70, (1984), 913
231. Sawai T. et. al, Proceedings of 6th Inter. Iron & Steel Congress 1, Tokyo (1996), 605
232. Goto H. et. al, Iron Steel Institute Japan - International 35, (1995), 708
233. Fischer W. A. et. al, Arch. Eisenhüttenwes 31 , (1960),365
234. Veshima Y. et. al, Metall.TransactionsB 17B , (1986),845
235. Kawashita Y. et. al, Iron Steel Institute Japan - International 35, (1995), 1468
236. Ouchi C. et. al, Tetsu-to-Hagane 69, (1983), A293
237. Bester H. et. al, Arch. Eisenhüttenwes 43, (1972),207

238. Suzuki K. et. al, Iron Steel Institute Japan - International
35, (1995), 34
239. Coleman T. H. et. al, Mater. Sci. Technology
1, (1985), 80
240. Turkdogan E.T. Physic-Chemistry of high temperature technology,
Academic Press. New York (1980), 8
241. Bogdandy L. et. al, Arch. Eisenhüttenwes 34, (1963),235
242. Kojima Y. et. al, Tetsu-to-Hagane 53, (1968), 589
243. Oei H. Tetsu-to-Hagane 59, (1973), 1078
244. Bramfitt B.L. Metall.Transactions1 , (198 4),1970
245. Akselrod A. Je. i kol. Izv. VUZ czernaja Metallurgija 30,
12 , (198 6),59
246. Eevsiev P.P. i kol. . Metallov i termich. obrabotka Metallov
9, (1985), 30
247. Kepka M. Hutnicke Listy 3 , (1977),171
248. Ohashi T. et. al Transactions ISIJ 17 , (1977),263
249. Kepka M. Hutnik 10 , (1973), 370
250. Kepka M. Hutnik 1 , (1972), 2
251. Popova N.M. i kol. . Metallov i termich. obrabotka Metallov
2, (1966), 18
252. Popova N.M. i kol. . Metallov i termich. obrabotka Metallov
8-9, (1983), 34
253. Sloman H.A. et. al, Journal of Iron Steel Institute 165, (1950), 81
254. Asano K. et. al, Tetsu-to-Hagane 57, (1974), 1943

255. Kuczynski K. et. al, Kinetic of high temperature process Ed. Technology Press and John Wiley Boston, Mass163, (1959)
256. Coble R. C. et. al J. American Ceramic Soc. 41, (1958), 55
257. Kingery W. D. et. al J. Appl. Physics 26, (1955), 1205
258. Myers M. et. al, Metall. TransactionsB 3B , (1972), 1205
259. Hagen K. et. al, Stahl und Eisen 95, (1975), 398
260. Perry J. H. Chemical Engineer's Hanbook McGrawHill Book Co. (1950)
261. Asano K. et. al, Tetsu-to-Hagane 57, (1971), 1943
262. Mori H. et. al, Tetsu-to-Hagane 52, (1966), 419
263. Romanov A.A. Riz. Chim. Teplofiz. prots. krystal. Stal slikov (1967), 133
264. Emi T. et. al Physico Chimie et siderurgie Versailles (1978)
265. Takenouchi T. et. al, Transactions ISIJ 18 , (1978),344
266. Emi T. et. al, NOHBOS Conf. AIME Chicago 16-20 April (1978)
267. Haida O. Nakanishi K. et. al, Scaninject II 2nd International Conf. on Injection Metallurgy Lulea Sweden (1980)
268. Gruner H. et. al, Stahl und Eisen 99, (1979), 725
269. Trivelius B. et. al, Iron and Steelmaker Nov. (1979), 38
270. Utockin Ju. I. Izv. VUZ czernaja Metallurgija 7 , (1984),150
271. Mari H. et. al, Tetsu-to-Hagane 52, (1966),419
272. Tadayoshi T. et. al, Transactions ISIJ28 , (1988),B13
273. Gasik M. I. i kol. Stal 54 ,1 , (1966),28

274. Zavjalov A.S. Masinostrojitelnuje Stali s redkomelnymi prisadami.
Masinostrojitelnije Petrograd (1969)
275. Powell G. I.F. et. al, J. Metals 93 , (1964),505
276. Kolm A. Mem.Sci. Rev. Metals 59,
(1962), 713
277. Ohashi T. et. al, Tetsu-to-Hagane 58, (1972),344
278. Janke D. et. al, Arch. Eisenhüttenwes , (1977),311
279. Qiyong H. et. al, Proceedings of Sino-Japanese Symposium on
steelmaking, The Chinese Society of Metals, Beijing Thina
(1981), 25
280. Harimaya S. et. al, Report of 19th Committe of Japan Society for
the promotion of Science, 9845, (1973)
281. Suito H. et. al, Steel Research 63 , (1992),419
282. Inoue R. et. al, Mater. Trans. Japan Institue of Metals 32,
(1991), 1164
283. Ejima A. et. al, Tetsu-to-Hagane 61, (1975),2784
284. Nuri Y. et. al, Tetsu-to-Hagane 61, (1975),507
- 285., Qiyong H. et. al, First Sino-America Bilateral Metallurgical Conf.
Beijing (1981), 192
286. Qiyong H. Proceedings of Sino-Japanese Symposium on
steelmaking, The Chinese Society of Metals, Beijing Thina
(1981), 15
287. Kawamura K. et. al, Tetsu-to-Hagane 57, (1971),158
- 288.Kammori O. et. al, Tetsu-to-Hagane 57, (1971),158

289. Rayback R.M. et. al, Proceedings of Conf. Analyt. Chem. Appl. Spectroscopie (1965), 24
290. Soda H. et. al, Trans. Japan Institute of Metals 18, (1977), 445
291. Schada J. et. al, Proceedings of the TMS-AIME Hume Rothery Symposium on Undercooling alloy Phase, new Orleans. LA, March 2- 6, (1986), 233
292. Rayleigh , Theory of Sound, Mac Millan and Co. 2, (1984), 371
293. Keene B. J. International Materials Reviews, Review 38, 4 ,(1993),157
294. Ogino K. et. al, Transactions ISIJ 23, (1983),234
295. Xue X.M. et. al, J. Mater. Science 28, (1993), 1317
296. Jimbo I. et. al, Iron Steel Institute Japan - International 32, (1992), 26
297. Keene B. J. International Materials Reviews, Review 33, 4 ,(1988),1
298. Kharlashin P.S. Izv. VUZ czernaja Metallurgija 7 , (1991),1
299. Nogi K. et. al, Metall. Transactions B 17B , (1986),163
300. Lee H. et. al, Steel Research 64, (1993),191
301. Xue X.M. et. al, Metall. 27 B , (1996),71
302. Allen B.C. In "liquid Metals Chemistry and Physics"
Ed. S.Z. Beer New York, (1972)

303. McLean A. Significance of Reoxidation in Steelmaking ,
Proceedings of Inter. Symposium on “ Mordern development in
Steelmaking “Jamshedpur, India 16-18 Feb. (1981), 8.2.1
304. McLean A. et. al, Microalloying 75, Proceedings of Union
Carbide Corp. 215, (1977)
305. To Duy C. Effect of REM injection and gas stirring on Cleanlines:
of pipeline steel. Report ISM, Hanoi (1997)
306. To Duy C. “The use of REM for modification of non-metallic
inclusion in silicon steel.” Proceedings of Inter. Symposium in
Materals Processing , Bangalore India 14-17 Nov. (1998), 43
307. To Duy C. Non- metallic inclusions in carbon steels. Report ISM.,
Hanoi (1996)
308. To Duy C. Proceedings of th 6th Asian Foundry Congress ,
on “Asian Foundries - Challenges & Opportunities”
Calcutta 23-26 Jan. (1999), 174

APPENDIX

List of symbols

- a_{Me} : activity of metal
- a_E : activity of non-metal
- A : frequency factor $\text{cm}^{-3} \cdot \text{s}^{-1}$
- C_l : liquid composition in equilibrium with solid C_s
at.%, wt.%
- C : the dependent components (eq. 19)
- $\text{Cos}\theta$: cosinus of angle of the nucleus
- c : concentration of oxygen in liquid steel g.atmO.cm^{-3}
(eq. 113)
- c_o : concentration of oxygen for initial uniform g.atmO.cm^{-3}
(eq. 113)
- c_m : concentration of oxygen for distance m g.atmO.cm^{-3}
(eq. 113)
- c_s : concentration of oxygen for distance s g.atmO.cm^{-3}
(eq. 113)
- $\delta_{(hkl)n}^{(hkl)s}$: Bramfitt crystallographic plane
- e_{Me}^E : interaction parameter expressing influence of element E on
metal Me

- E_o : concentration of solute in charge at.% (eq.94)
- ε : ratio of molten steel in cluster (eq.127)
- E : electromotive force, mV (eq.129)
- f_{Me} : activity coefficient of metal,
- f_E : activity coefficient of non-metal,
- F : the variability on degree of freedom
- ΔF : driving force for phase change $J.mol^{-1}$
- f_s : fraction of the original volume
- g : acceleration due to gravity, $g.cm^{-2}$ (eq.120)
- ΔG : Gibbs free energy $J. mol^{-1}$
- ΔG^* : work of activation energy $J. mol^{-1}$
- ΔG^*_{hom} : min work of activation energy of homogeneous nucleus
 $J. mol^{-1}$
- ΔG^*_{het} : min work of activation energy of heterogeneous nucleus
 $J. mol^{-1}$

- ΔG^a : free energy of activation for diffusion of atoms $J. mol^{-1}$
- ΔG^a_{crit} : critical free energy of activation for homogeneous nucleus $J. mol^{-1}$
- ΔH : entelpi , $J. mol^{-1}$
- I_{het} : number of nuclei per unit of surface , cm^{-2}
- ρ_L : density of liquid, $g.cm^{-3}$ (eq.120)
- ρ_i : density of inclusion, $g.cm^{-3}$ (eq.120)
- ρ_{cl} : density of cluster, $g.cm^{-3}$ (eq.127)
- ρ_{incl} : density of inclusion, $g.cm^{-3}$ (eq.127)
- K_E : equilibrium constant of reaction
- K_S : corresponding product for the supersaturated solution
- K : thermodynamic solubility product
- k : equilibrium partition coefficient between solid phase and liquid phases (eq.92)
- $\log K$: logarithm of equilibrium constant of reaction
- Me_xO_y : oxide of metal

- M_e^{\sim} : the solute concentration in the liquid
 M_e^0 : the original solute concentration
 m : mass of the droplet, g (eq.130)
 η : liquid viscosity of metal, $\text{g.cm}^{-1}.\text{s}^{-1}$
 p : the coexisting phase (eq.19)
 p_{total} : critical gas pressure, atm (eq.123)
 p_A : atmospheric pressure, atm (eq.123)
 p_F : ferrostatic pressure, atm (eq.123)
 $p_{\text{H}_2}, p_{\text{N}_2}, p_{\text{CO}}$: pressure of H_2 , N_2 and CO , atm (eq.125)
 O : oxygen
 Q : energy of reaction, J.mol^{-1}
 RE : rare earth metals
 R : the gas constant, $8.3143 \text{ J.K}^{-1}\text{mol}^{-1}$
 r : the particle radius (eq.61), m
 r_0 : the radius of spherical diffusion zone, m
 r_i : instantaneous radius of growing inclusion (eq.114), m

- r : the radius of inclusion in molten steel ,m (eq.120)
- r : the bubble radius, m (eq.123)
- ΔS : the entropy of system, $J.K^{-1}mol^{-1}$
- s : amount of solute remaining in the liquid, g
- s_0 : total amount of solute, g
- T : temperature of reactions $^{\circ}K$
- T_{eq} : temperature of supersaturation of reactions $^{\circ}K$
- t : time, min
- τ : surface tension measuring by levitated droplet (eq.130)
 $J.m^{-2}$
- v : the molar volume of new phase , $m^3 mol^{-1}$
- v : velocity of floatation of inclusion, ms^{-1}
- w : work to form a spherical nucleus (eq.61)
- w : cylindrical volume (eq.121)
- w : oscillation frequency of the droplet, s^{-1} (eq.130)
- Z : diffusion zone

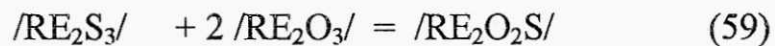
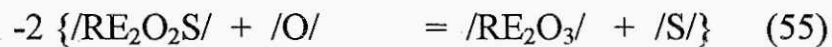
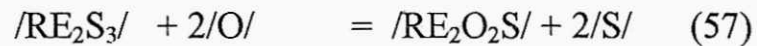
- θ : angle at phase of nucleus on the substrate
- σ : interfacial tension of liquid (eq.61) J.m^{-2}
- σ_{LS} : interfacial tension between molten iron and catalyzer
(eq.61) J.m^{-2}
- σ_{SC} : interfacial tension between solid iron crystal and substrate
 J.m^{-2}
- σ_{SL} : interfacial tension between substrate and liquid iron
 J.m^{-2}

DECLARATION

I hereby declare:

That I have studied and achieved the results of this work at National Metallurgical Laboratory, Jamshedpur - India completely based on my individual independent intellectual inputs.

That the following equations are mine and they are not like of any other previous author:



That the table 10 of thermodynamic data of RE inclusions precipitation in molten steel at 1600°C is mine, which is not like of any other previous author.

That the following models/schema are mine, they are not like of any other previous author;

1. Model-schema of Fig. 21; modification of inclusions with convenient RE.

2. Model-schema of Fig. 22; modification of unfavourable inclusions with RE addition.

That the conclusion point of III/8 is mine, " Mechanism of inclusion morphology precipitation is as follows : without RE addition there are conventional inclusions as type I; randomly dispersed globular, as type II ; interdendritic eutectic - grain boundary eutectic, as type III; randomly

dispersed angular. With RE addition there are precipitation and formation of inclusion of type Ib; globular oxysulphides, of type IIIb; angular heterogeneous inclusions and of type IV; cluster homogeneous inclusions.”

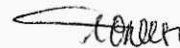
That the conclusion point IV/20 is mine, “With induction stirring the part of deoxidation and desulphurization product removed into slag and oxygen and sulphur content in steel reduced. The induction stirring strongly refined inclusions to small-smooth size.”

I further declare that to the best of my knowledge and belief, the particulars of the equations, tables, model-schema, figure, photos and rule conclusions given in the work are correct being output of my research work and I hold intellectual property right of the same.

National Metallurgical Laboratory
Jamshedpur 831007-India

Feb. 22 1999

The author



Ph.D. TO DUY CA